Aerospace Engineering Department
Middle East Technical University

HECTOR
Candidate Engines for a Supersonic Business Jet

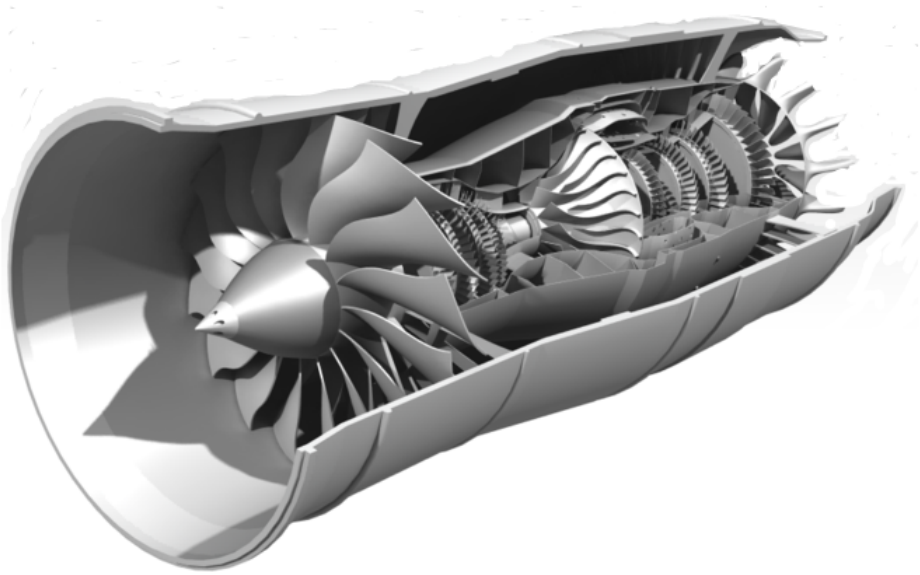

Team Members
Berkay Keleş
Furkan Göktürk Öztiryaki
Melisa Başak
Mert Durmaz
Ülkü Ünver

Advisor
Asst.Prof. Sıtkı Uslu

15.05.2020

Signatures

Faculty Advisor
Asst. Prof. Sıtkı USLU
Middle East Technical University
AIAA Member Number: 506268

Team Member
Melisa Başak
Middle East Technical University
Department of Aerospace Engineering
AIAA Member Number: 1109551

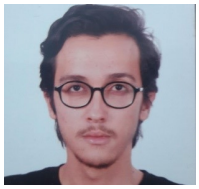

Team Member
Mert Durmaz
Middle East Technical University
Department of Aerospace Engineering
AIAA Member Number: 1109553

Team Member
Furkan Göktürk Öztiryaki
Middle East Technical University
Department of Aerospace Engineering
AIAA Member Number: 1109519

Team Member
Ülkü Ünver
Middle East Technical University
Department of Aerospace Engineering
AIAA Member Number: 1109555

Team Member
Berkay Keleş
Middle East Technical University
Department of Aerospace Engineering
AIAA Member Number: 1109546

Abstract

The HECTOR is a two-spool, mixed flow, low bypass ratio turbofan engine designed as a candidate for a supersonic business jet. The HECTOR is capable of achieving both subsonic cruise at Mach 0.98, transonic cruise at 1.15 and supersonic cruise at Mach 2.1 up to Mach 3. Since lighter weight, lower take-off noise, reduced emissions at high altitudes and affordable fares are demanded, the HECTOR is designed in such a way that it satisfies general improvements given by Request of Proposal. Besides, for the highest operating performance, reducing the rate of total fuel consumption is considered throughout the design point and off-design engine missions.

Table 1

Engine Component	**Improvement and Technology**
Inlet System	2 Ramp External Compression Supersonic Inlet
Transonic Fan	Carbon Fiber Rain-Forced Polymer with Ti-6Al-4V Leading Edges
High-Pressure Compressor	Ti-45Al-8Nb Compressor Blades
Combustion System	Hybrid Diffuser Lean Direct Injection (LDI) Combustor Convective Film Cooling via SiC/CMC with Pedestal Liner
High-Pressure Turbine	T-238 5^{th} Generation Single Crystal Super Alloy
Low-Pressure Turbine	Ti-45Al-8Nb PST Single Crystal
Mixer	Force Flow Lobed Mixer with Chevrons
Exhaust System	Fully Variable Convergent-Divergent Nozzle

Contents

List of Tables

List of Figures

Nomenclature

- A - Cross-Sectional-Area
- AC - Inlet Capture Area
- ALR - Air-Liquid Ratio
- AR - Aspect Ratio
- AIAA - American Institue of Aeronautics and Astronautics
- APU - Auxilary Power Unit
- BPR - By-Pass Ratio
- CAD - Computer-Aided Design
- CC - Combustion Chamber
- CD - Convergent - Divergent
- CFD - Computational Fluid Dynamics
- CFRP - Carbon Fiber Reinforced Polymer
- CRV - Central Recirculation Vortex
- CMC - Ceramic Matrix Composite
- CMV - Chrome Molybdenum Vanadium
- CO - Carbon Monoxide
- CLP - Combustion Loading Parameter
- FAA - Federal Aviation Administration
- FAR - Fuel-Air Ratio
- FADEC - Full Authority Digital Engine Control
- FOD - Foreign Object Damage
- FPR - Fan Pressure Ratio
- HPC - High Pressure Compressor
- HPT - High Pressure Turbine
- HTS - High Thermal Stability
- IGV - Inlet Guide Vane
- L/D - Lift to Drag Ratio
- LDI - Lean Direct Injection
- LPC - Low Pressure Compressor
- LPP - Lean, Pre-mixed, Pre-vaporized
- LPT - Low Pressure Turbine

- M - Mach Number
- MATLAB - Matrix Laboratory
- MFP - Mass Flow Parameter
- NASA - National Aeronautics and Space Administration
- NGV - Nozzle Guide Vane
- NOx - Nitric Oxides
- OPR - Overall Pressure Ratio
- PRF - Pressure Recovery Factor
- PF - Pattern Factor
- PM - Powder Metallurgy
- RES - Residence Time
- RFP - Request For Proposal
- RQL - Rich-burn quick-Quench Lean-burn
- SiC - Silicon Carbide
- SLS - Sea Level Static
- TBC - Thermal Barrier Coating
- TET - Turbine Entry Temperature
- TO - Take-Off
- TPR - Total Pressure Recovery
- TRL - Technology Readiness Level
- TSFC - Thrust Specific Fuel Consumption
- W - Weight

Acknowledgements

The authors wish to thank the following individuals who were instrumental in the success of this engine design:

- Asst. Prof. Sıtkı Uslu for his impeccable guidance and support,
- Asst. Prof. Anna Prach for her assistance in regards to any aids about the project,
- Dr. Joachim Kurzke for his aids on GasTurb,
- Dr. Andrew J. Yatsko for his assistance in regards to any technical questions about the RFP,
- Assoc. Prof. Dr. Volkan Esat for allowing us to use his lecture notes in the analyses of shaft design and lubrication,
- All the teachers, students and facilities who have aided.

Scientia Dux Vitae Certissimus

"Everyone else is thinking slower, if you go faster,

and I think you need to go at least Mach 2.0 for this to work"

-Blake Scholl

1. Introduction

AIAA Undergraduate Team Engine Design Competition 2019/20 Project "Candidate Engines for a Supersonic Business Jet" is about preliminary design of the mixed flow, two spool, low-bypass ratio turbofan engine. As per the Request of Proposal (RFP), the HECTOR is designated as a candidate engine for the supersonic business jet capable of replacing the baseline engine given in the RFP.

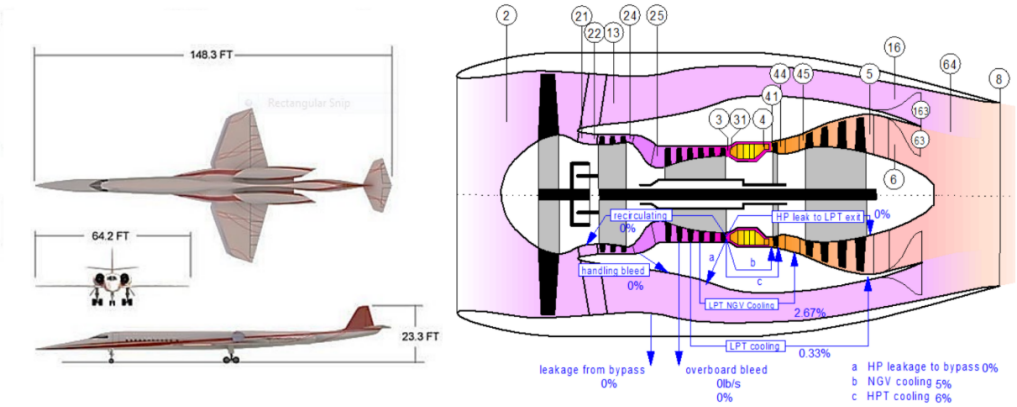

Figure 1.1: Supersonic Business Jet Layout with the Baseline Engine

Table 1.1: General Characteristics of the Baseline Engine

General Characteristics	
Crew	2
Capacity	8-12 passengers
Length	135.6 ft (41.33 m)
Wing Span	64.2 ft (19.57 m)
Height	21.2 ft (6.46 m)
Wing Area	1,200 ft^2 (111.5 m^2)
Maximum Take-off Weight	146,000 lbm (40,823 kg)
Power Plant	2 × low bypass ratio turbofans; 21,700 lbf (96.53 kN) each

In the RFP, the base engine has a plan form which is similar in wing and tail shape and arrangement to the F-104 Starfighter. In performance calculations, this information is taken into account. Also, the supersonic business jet layout with the baseline engine are given in the Figure 1.1. The general characteristics and performance specifications of the supersonic business jet is given in the Table 1.1 and 1.2, respectively. Besides, design features of the baseline engine given in the RFP are stated in the Table 1.3. Although these features are tabulated based on the RFP, they will be changed and improved with respect to the mission requirements at the upcoming chapters.

Table 1.2: Performance Specifications of the Baseline Engine

Performance Specifications	
Maximum Speed	Mach 3.0
Cruise Speed	Mach 2.1 at 40,000 ft
Range	At Mach 0.95 ; 4600 nm
Service Ceiling	51,000 ft

Subsequent chapters demonstrate the cycle analysis and optimization of the HECTOR engine at design and off-design conditions. The new aircraft engine's supersonic cruise performance results are compared with the baseline engine and requirements stated in the RFP. Furthermore, a detailed engine component design is also presented, which demonstrates and provides justification for the use of advanced technologies in the design of the HECTOR engine. Afterwards, the installed performance of the engine is checked using GasTurb and AxSTREAM tools. Moreover, the exhaust system design is carried out using Method of Characteristics. In addition, a detailed structural analysis, such as material choice, shaft design and detailed CAD models of the components are presented. Finally, investigation of the technologies to reduce noise, and the subsystems to be used, anti-icing, secondary power, engine control system, fuel and lubrication system including shaft lubrication analysis are illustrated.

Table 1.3: Design Features of the Baseline Engine

Design Features of the Baseline Engine	
Engine Type	Axial, turbofan
Number of Fan/Booster/Compressor Stage	2, 6, 7
Number of HP/LP Turbine Stages	1, 3
Combustor Type	Annular
Maximum Net Thrust at Sea Level	21,700 lbf
Specific Fuel Consumption at Max. Power	0.519 lbm/hr/lbf
Overall Pressure Ratio at Max. Power	21.0
Max. Envelope Diameter	49.2 inches
Max. Envelope Length	154.1 inches
Dry Weight Less Tail-Pipe	4.515 lbm

2. State of Art

A comprehensive review of the literature was carried out to set a baseline by investigating similar aircraft that have a low bypass ratio turbofan engine installed and can produce the thrust required to achieve supersonic cruise.

Table 2.1: Similar Engine Specifications

Engine	Number of Spool	Max. Thrust [lbf]	SFC (w/o ab) [lb/lbfhr]	BPR	OPR	TET [K]	Weight [lb]	Length [in]	Diameter [in]
Kuznetsov NK-144	Dual	28,660	1.81	0.60	14.2	-	-	204.72	59.05
Pratt & Whitney F135-600	Dual	27,000	0.886	0.56	28	2260	-	369	46
Soloviev D-30KP-2	Dual	26,460	1.57	2.24	20	1427	5820	214.5	57
General Electric YF120	Dual	23,500	-	0.32	-	-	4100	166.8	42

Table 2.2: Similar Supersonic Transportation Aircraft and Specifications

Supersonic Transport	**Cruise Mach**	**Range (nmi)**	**MTOW (lb)**	**Total Thrust (lbf)**	**T/W**
Aerion AS2	1.4	4,200	133,000	54,000	0.406
Boom Overture	2.2	4,500	170,000	45,000-60,000	0.26-0.35
Spike S512	1.6	6,200	115,000	40,000	0.34
Aerion SBJ	1.6	4,800	90,000	39,200	0.44
Concorde	2.04	40,000	408,000	152,000	0,373

The design characteristics such as OPR, BPR, thrust and engine weight of such engines are shown in Table 2.1. The HECTOR engine will be designed in the light of these information while considering the promising technological developments.

3. Cycle Analysis

This chapter describes the basic structure of the HECTOR engine and documents the cycle analysis program that was used to aid in the design of the low bypass ratio turbofan. The optimal cycle design is presented in this chapter.

3.1 Advanced Engine Cycle Concepts for HECTOR

This section includes the first step in the development of the optimal cycle design for the HECTOR engine by considering several different, but promising, cycle concepts and determines which cycle concept will provide the optimal combination of performance, complexity, technology readiness level (TRL), and cost.

3.1.1 Variable Bypass Technology

Bypass ratio (BPR) is defined as the ratio of the mass flow rate passing through the bypass channel to the mass flow rate in the core stream of the turbofan engine. In turbofan engines, mass flow is separated into two, "Primary Flow/Hot Stream" which passes through the engine core, and the airflow which splits through the bypass channels without entering the core is called as "Secondary Flow/Cold Stream".

It is possible to classify a turbofan engine as a low, medium, high, or ultra-high bypass depending on its bypass ratio. This classification process is as follows.

- Low-Bypass Turbofan Engine BPR < 2
- Medium-Bypass Turbofan Engine $2 \leq$ BPR < 5
- High-Bypass Turbofan Engine $5 \leq$ BPR < 9
- Ultra-High-Bypass Turbofan Engine BPR≥ 9

To fulfill both subsonic and supersonic flight conditions, a variable cycle engine is used since it combines the high specific thrust of the turbojet with the low specific fuel consumption and noise of the turbofan. By reviewing the literature, variable cycle engine configurations, such as F120 as indicated at the State of Art section of the report, has successfully achieved the flight in YF22 and YF23 aircraft prototypes [23].

During supersonic cruise, it is possible to produce different ranges of thrust without varying the mass flow rate in the variable bypass cycle engines. This situation provides optimum flow condition at the intake while the engine operates with an appropriate pressure recovery for supersonic flight without creating spillage drag [23].

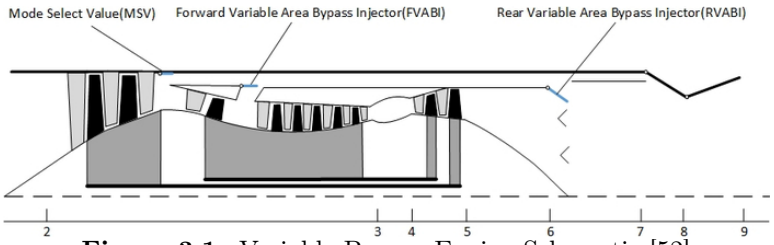

Figure 3.1: Variable Bypass Engine Schematic [52]

3.1.2 Afterburner Investigation

In the first step of developing the HECTOR, different but promising design concepts are considered by taking into account optimal combination of performance, complexity and existing technology with maintenance cost. Besides, since the main goals of this project are minimizing fuel consumption, reducing engine total weight and size, several designs in the literature are also considered such as Concorde. The Concorde is a passenger transport aircraft utilizing afterburner technology specifically for the take-off. Since the engine of the Concorde and the HECTOR have similar mission requirements and both are used for transportation, augmentation of afterburner technology is investigated.

By implementing an afterburner, one of the goals of this project, which is creating required thrust while reducing the fan and the engine size, can be achieved. However, as it is well known, using and afterburner will increase the specific fuel consumption. This increase carries fuel consumption to unacceptable levels, and makes the HECTOR engine inherently inefficient. Also, not using an afterburner in the HECTOR engine implies that there will be less noise generation.

3.1.3 Nozzle Investigation

The main purpose of the exhaust nozzle is to increase the velocity of the exhaust gas. The rise in the kinetic energy of the gas, results in higher thrust values. When the exit and ambient pressure are equal, the maximum uninstalled thrust can be obtained. Also, the expansion process is controlled by the pressure ratio over the nozzle. The list below states the possible operating functions and design criteria of the nozzle for the modern jet engines [32].

- The flow accelerate to higher velocities with minimum pressure loss
- Nozzle exit and atmospheric pressure are kept close as possible
- Permit mixing of core and bypass streams of turbofan when desired

- Thrust reversing when desired
- Cooling of walls allowed
- Suppressing noise formation
- Achieve all listed items with minimal cost and weight [32, 48]

In preliminary design of the HECTOR engine, it is important to size the nozzle appropriately to meet the requirements stated in the RFP while obtaining a high efficiency in supersonic cruise condition along with a noise attenuation. Besides, considering all on-design and off-design performance requirements, which must be achieved with low noise levels, the best choice for the HECTOR engine is to deploy a fully-variable converging-diverging (Con-Di) nozzle with noise attenuation for optimum performance in both subsonic and supersonic flight.

As divergent flaps move, area ratio is altered to ideally expand the flow. Furthermore, this nozzle concept provides an ideal performance in producing the required thrust without the implementation of an afterburner. Hence, selection of Con-Di nozzle has been done. Comparison and drawbacks of the performance resulted in selection of Con-Di nozzle is explained deeply in the exhaust system design part.

3.2 Engine Components and Diagrams

The HECTOR engine is designed as a low bypass, 2-spool mixed flow axial turbofan engine. For the main components, the HECTOR engine consists of air intake system, 2 stage fan, 7 stage high pressure compressor (HPC), combustion chamber and fuel atomizing system, 1 stage high pressure turbine (HPT), 3 stage low pressure turbine (LPT), mixer and exhaust system. In addition to these main systems and components, engine auxiliary systems such as lubrication system, anti-icing system, auxiliary power unit (APU) and starting system are fully developed. The HECTOR engine is designed to be installed in a supersonic business jet. Besides, the HECTOR engine has superior performance characteristics over the existing low bypass ratio turbofan engines. The reason behind this superiority can be explained by having better cruise capabilities, and flying without an afterburner installation, which remarkably reduces fuel consumption, and the reduced weight of the engine.

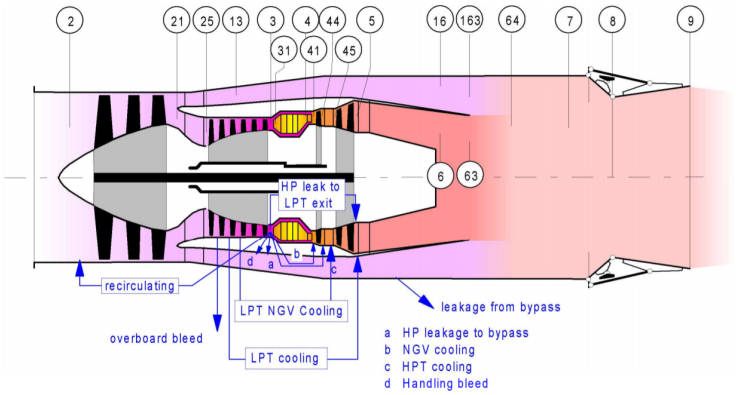

Figure 3.2: Station Numbers for the HECTOR *A Mixed-Flow Turbofan Engine*

3.3 Baseline Engine Cycle Analysis and Validation

This section of the preliminary design briefly describes the on-design and off-design performance analysis and validation of the baseline engine given in the RFP reproduced with GasTurb 13.

3.3.1 On-Design Analysis of Baseline Engine: Simulation Validation

Station	W lb/s	T R	P psia	WRstd lb/s
amb		518,67	14,696	
2	479,001	518,67	14,696	479,000
13	301,594	650,06	29,392	168,819
21	177,408	623,79	26,453	108,087
22	177,408	623,79	26,453	108,087
24	177,408	853,05	74,068	45,142
25	177,408	853,05	72,586	46,063
3	172,086	1312,60	308,493	13,041
31	152,571	1312,60	308,493	
4	155,431	2492,00	293,068	17,084
41	164,301	2432,72	293,068	17,843
43	164,301	1997,56	117,720	
44	174,946	1958,22	117,720	
45	179,677	1937,77	114,225	44,682
49	179,677	1453,88	32,263	
5	180,268	1453,02	32,263	137,438
6	180,268	1453,02	31,940	
16	301,594	650,06	28,657	
64	481,862	962,79	29,778	
8	481,862	962,79	29,778	323,998
Bleed	0,000	1312,60	308,493	

Efficiencies:	isentr	polytr	RNI	P/P
Outer LPC	0,8622	0,8749	1,000	2,000
Inner LPC	0,9000	0,9079	1,000	1,800
IP Compressor	0,9197	0,9303	1,445	2,800
HP Compressor	0,9010	0,9180	2,730	4,250
Burner	0,9995			0,950
HP Turbine	0,9219	0,9136	3,271	2,490
LP Turbine	0,9268	0,9151	1,654	3,540
Mixer	0,6000			

HP Spool mech Eff 0,9800 Nom Spd 14372 rpm
LP Spool mech Eff 0,9900 Nom Spd 6482 rpm
P22/P21=1,0000 P25/P24=0,9800 P45/P44=0,9703

hum [%]	war0	FHV	Fuel
0,0	0,00000	18552,4	Generic

FN	=	21699,31 lb
TSFC	=	0,4745 lb/(lb*h)
WF	=	2,8601 lb/s
s NOX	=	0,5982
Core Eff	=	0,4370
Prop Eff	=	0,0000
BPR	=	1,7000
P2/P1	=	1,0000
P3/P2	=	20,99
P5/P2	=	2,1953
P16/P13	=	0,9750
P16/P6	=	0,89722
P16/P2	=	1,95000
P6/P5	=	0,99000
P63/P6	=	1,00000
P163/P16	=	1,00000
XM63	=	0,56095
XM163	=	0,37698
XM64	=	0,46030
A64	=	1352,51 in²
WBld/W2	=	0,00000
A8	=	987,26 in²
CD8	=	0,96000
XM8	=	1,00000
PWX	=	100,0 hp
WBLD/W22	=	0,00000
Wreci/W25	=	0,00000
Loading	=	100,00 %
e444 th	=	0,89002
WBLD/W25	=	0,00000
WCHN/W25	=	0,05000
WCHR/W25	=	0,06000
WCLN/W25	=	0,02667
WCLR/W25	=	0,00333
WLkBy/W25	=	0,00000

Figure 3.3: Baseline Engine Performance at Sea Level

As per the RFP, the design point for the baseline engine includes a required takeoff thrust of 21,700 lbf at standard sea-level conditions at 27 °F. Figure 3.3 represents the baseline engine performance characteristics at the sea-level condition. Validation of the exact cycle parameters provided by the RFP for the takeoff condition is done by using the gas turbine engine simulation software GasTurb 13.

3.3.2 Off-Design Analysis of Baseline Engine: Simulation Validation

As stated in the RFP, the aircraft should takeoff at 27°F and standard sea level conditions. Since the desired cruise altitude is given as 40,000 feet, and it is required to achieve flight with various Mach numbers which are 0.98, 1.15, 2.1 and 2.4, the engine should satisfy both subsonic and supersonic cruise at this specified altitude. By using GasTurb 13, off-design analysis is done from the "Mission" tool for the baseline engine. To generate required thrust at the takeoff design point and specified Mach numbers, the altitude is kept constant to observe the effects of flight Mach number in the key parameters such as specific fuel consumption (TSFC), overall pressure ratio (OPR) and turbine inlet temperature (TET).

Table 3.1: Baseline Engine Performance at Off-Design Conditions

Altitude : 40,000 ft				
Mach	0.98	1.15	2.1	2.4
F_n **(lbf)**	5040.35	5253.23	3568.33	1360.59
TSFC (lbm/hr/lbf)	0.7820	0.8218	1.7135	5.0820
T_{t4} **(R°)**	2542.84	2528.32	2505.82	2506.63
OPR	22.48	20,47	8,19	6,22

3.4 HECTOR Cycle Analysis : New Engine Optimization

Having established the parametric cycle analysis of the baseline engine by using the GasTurb 13, the following procedure is used in the preliminary design of the HECTOR engine. For an engine which has supersonic flight capabilities, rather than takeoff, design point should be considered as top-of-climb, in essence, beginning of the cruise. Since the design point for the takeoff is given in the RFP, "In-Flight Thrust Requirements" graph is extended, using drag estimation and is given in the Figure 3.4, to find the required thrust to carry out both subsonic and supersonic cruise missions. Besides, as demanded in the RFP, the HECTOR engine will successfully achieve supersonic cruise with 2.1 Mach at 40,000 feet altitude where the design point criteria is authenticated.

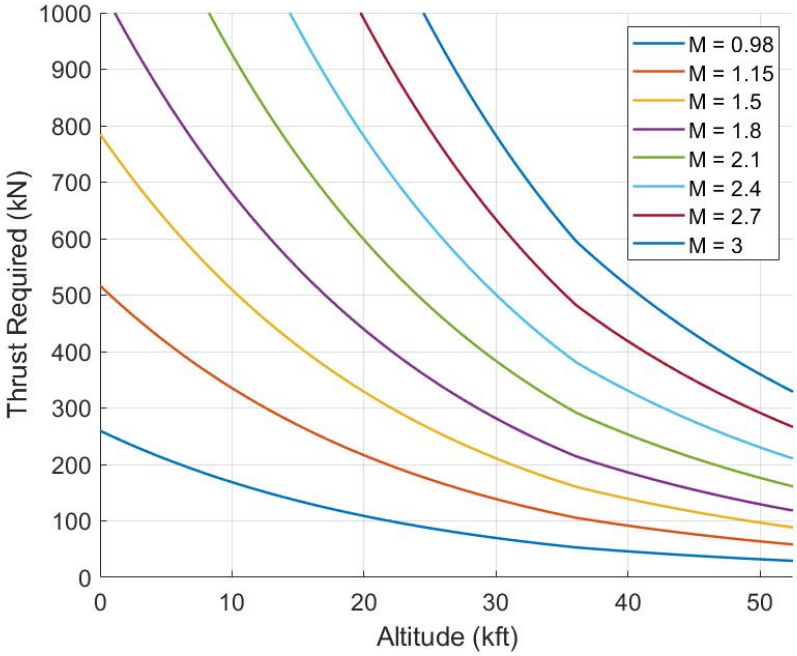

Figure 3.4: In-Flight Thrust Requirements

The design point optimization of the HECTOR engine targets to reduce specific fuel consumption throughout the flight envelope. Furthermore, for the sake of reducing the weight of the power plant, the HECTOR engine is designed using advanced materials and manufacturing techniques considering the promising technological developments. Another important design limitation is the maximum turbine inlet temperature, which is given as 2840°R in the RFP. In order to not exceed NOx emission standards, the upper limit for the TET is kept as 2840°R since it is known that the NOx emission increases exponentially with increasing TET. In addition, if technological constraints are considered, ceramic-matrix-composite (CMC) materials, which can withstand temperatures up to 3330 °R without the use of any cooling methods, has been tested by GE Aviation to overcome the TET restriction and might be considered as a breakthrough in

jet propulsion industry [2]. By implementing this technology into the HECTOR engine, maximum turbine inlet temperature might be extended to a certain limit to operate safely at higher thrust values, if demanded. Although extending the limits of TET has many advantages, some drawbacks exist such as increasing TSFC, and the cost.

The next section underlines how to minimize the specific fuel consumption of the HECTOR engine by deploying the "Optimization" tool in the GasTurb 13 to determine the best combination of the 4 main design parameters, which are bypass ratio, fan pressure ratio, turbine entry temperature, and overall pressure ratio, to meet the desired constraints and satisfying the required thrust.

3.4.1 On-Design Analysis of HECTOR: Simulation Validation

The on-design condition for a supersonic jet is defined as “top-of-climb”, which is at Mach 2.1 and 40,000 feet. As a rule, engines with supersonic capacities are regularly designed for "top-of-climb" conditions, instead of at take-off, and the HECTOR engine follows this training. To begin the analyses, a few constraints and assumptions were made. First, the fan diameter of the new engine is limited to 49” by the existing engine envelope. This limits the cross-sectional area at the engine face (station 2), thus, limiting the corrected mass flow rate at the engine face with a reasonable axial Mach number, i.e., 0.5-0.6. For this reason, the corrected mass flow rate at all flight conditions (on-design and off-design points) was held below 487 lbm/s to ensure that the fan diameter did not exceed the 49” limit.

A pre-analysis will guide to determine the preferred scope of the main design parameters before making a more in depth one. Firstly, the turbine entry temperature of the baseline engine is 2492°R and the limit given RFP is 2840°R. So, it may be chosen between this range. The core thermal efficiency of the baseline engine is too low and it cannot perform the limit of performance requirement at cruise. For this reason, the turbine entry temperature was chosen as the limit (2840°R). With a basic determination of TET, the most efficient OPR for the lowest TSFC can be found.

According to the RFP, the required thrust for a supersonic cruise is around 28,560 lb, which may require a lower BPR with mixed exhaust to get a higher exhaust velocity. The BPR may be chosen to be below 0.7 since the HECTOR engine is expected to be able to operate at Mach 3.0. However, as BPR decreases, TSFC increases, which is not desired. So, the optimum point for OPR can be found for the lowest TSFC. The OPR of the baseline engine at sea level is 21. In our case, it may be increased to be between 30-35. Taking into account that OPR decreases at higher elevations, the OPR at on-design may be selected to be between 20-25. Furthermore,to ensure that the number of fan stages is not greater than 2 to get a low engine weight, and the single-stage fan pressure ratio is not more than 1.7 to provide a high fan efficiency, the FPR is limited to less than 2.89.

From here, the optimization program featured in GasTurb 13 is used to address the impact of the bypass ratio, fan pressure ratio, HPC pressure ratio, and burner exit temperature on TSFC. Some of the most critical trade studies to determine the optimal parameters for the on-design condition of the HECTOR engine are shown in Figure 3.5. The black square shown in the carpet plots of Figure 3.5 represents the result of the overall optimization.

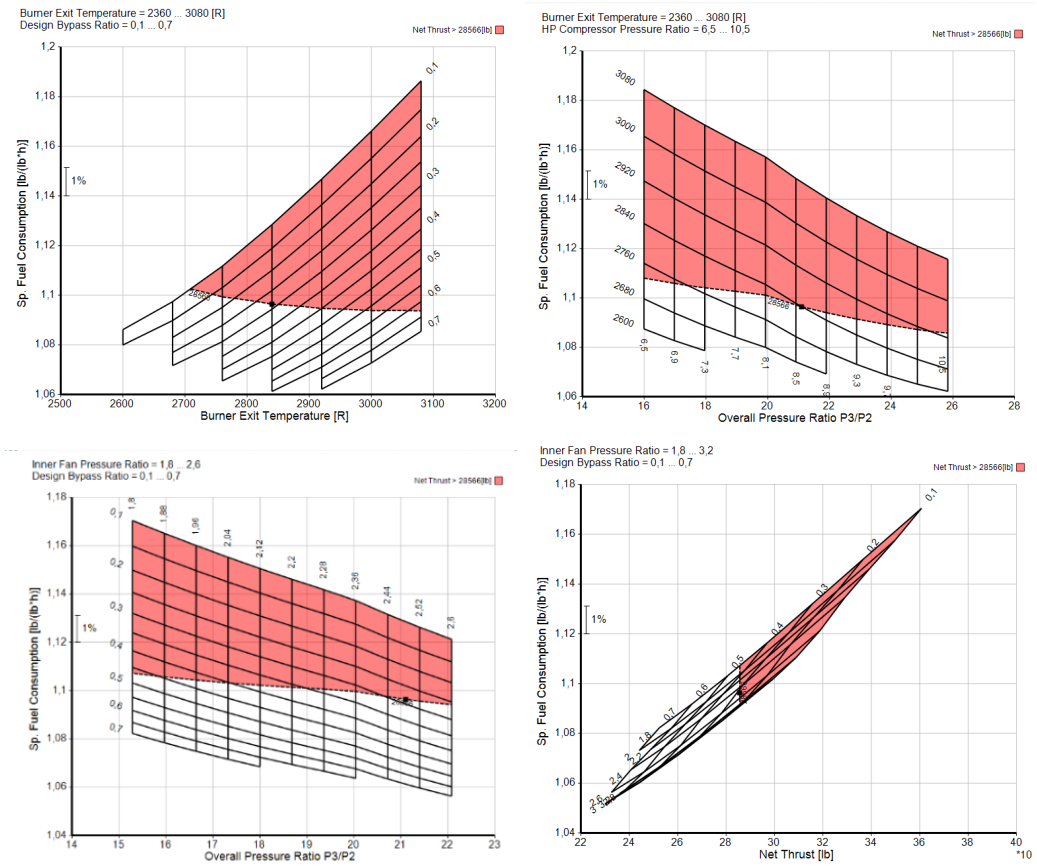

Figure 3.5: Parametric Studies of Cruise TET, BPR, FPR, OPR, and TSFC for the HECTOR

The optimum point of the TSFC for design point was selected as 1.0964 lb/lbf-hr, as well as a bypass ratio of 0.286 and a turbine entry temperature of 2840 R. According to the results from parametric studies, the selected design parameters provide a high performance and efficiency. Optimized performance of the HECTOR engine at supersonic cruise are described in Figure 3.6.

Station	W lb/s	T R	P psia	WRstd lb/s
amb		389,97	2,720	
1	692,717	733,50	24,894	
2	692,717	733,50	24,894	486,300
13	154,104	1029,56	74,270	42,962
21	538,613	973,43	61,869	175,271
25	538,613	973,43	61,250	177,041
3	527,841	1829,49	525,390	27,729
31	514,375	1829,49	525,390	
4	523,076	2840,00	499,120	36,039
41	528,462	2830,27	499,120	36,347
43	528,462	2062,50	110,916	
44	533,848	2060,24	110,916	
45	542,825	2043,66	109,807	144,207
49	542,825	1757,78	55,148	
5	544,620	1755,35	55,148	266,993
6	544,620	1755,35	54,045	
16	154,104	1029,56	72,413	
64	698,724	1603,54	55,999	
8	698,724	1603,54	55,999	322,414
Bleed	2,693	1829,49	525,390	

Efficiencies:	isentr	polytr	RNI	P/P
Outer LPC	0,8841	0,9000	1,121	2,983
Inner LPC	0,8868	0,9000	1,121	2,485
HP Compressor	0,8698	0,9000	1,969	8,578
Burner	0,9995			0,950
HP Turbine	0,9152	0,9000	4,687	4,500
LP Turbine	0,9074	0,9000	1,496	1,991
Mixer	0,6000			

HP Spool mech Eff 0,9900 Nom Spd 12000 rpm
LP Spool mech Eff 0,9800 Nom Spd 8000 rpm

P2/P1= 1,0000 P25/P21=0,9900 P45/P44= 0,9900
Con-Di Nozzle:
A9*(Ps9-Pamb) 5229,912

FN	=	28567,02 lb
TSFC	=	1,0964 lb/(lb*h)
WF Burner	=	8,70016 lb/s
s NOX	=	3,2428
BPR	=	0,2861
Core Eff	=	0,6504
Prop Eff	=	0,7581
P3/P2	=	21,105
P16/P6	=	1,33987
A63	=	1229,58 in²
A163	=	134,27 in²
A64	=	1363,86 in²
XM63	=	0,42530
XM163	=	0,79292
XM64	=	0,46030
P63/P6	=	1,00000
P163/P16	=	1,00000
A8	=	1003,25 in²
CD8	=	0,95000
Ang8	=	25,00 °
P8/Pamb	=	20,58780
WLkBy/W25	=	0,00000
WCHN/W25	=	0,01000
WCHR/W25	=	0,01000
Loading	=	100,00 %
WCLN/W25	=	0,01667
WCLR/W25	=	0,00333
WBHD/W21	=	0,00000
far7	=	0,01261
WBLD/W25	=	0,00500
PWX	=	100,0 hp
P16/P13	=	0,9750
P6/P5	=	0,9800
A9/A8	=	2,00000
CFGid	=	0,98252

Figure 3.6: The HECTOR Engine Performance at Supersonic Cruise

3.4.2 Off-Design Analysis of HECTOR: Simulation Validation

With the cycle parameters at the on-design point of supersonic cruise determined, it is important to evaluate the performance of the HECTOR engine at major off-design conditions too. The RFP states that the supersonic business jet must takeoff at 27°F over the standard sea-level static day (i.e., hot day), fly supersonic at Mach 2.1, at Mach 2.4 over water and 40,000 feet, and Mach 3.0 should be achievable. The aircraft in question can also fly subsonic at Mach 0.98. Besides, it will cruise at Mach 1.15 overland without producing a sonic boom on the ground. To conduct the off-design analysis, a series of mission points were defined in GasTurb 13, corresponding to the five above-listed flight conditions. For the HECTOR at off-design conditions, the objective was to acquire the necessary thrust while accomplishing improved fuel efficiency from the baseline engine model.

As per the RFP, it is stated that the new aircraft must cruise at Mach 1.15 over land, without producing a sonic boom on the ground. Breaking the sound barrier produces a lot of noise. It is possible to reduce the noise by using boomless cruise technology, technically called as Mach Cutoff. This method is based on Whitham theory and See Bass and George sonic-boom minimization theory, and it relates to the nacelle integration of the engine [30]. Engine nacelles conventionally located under the trailing edge of the wing. According to [28], engine nacelles could be mounted on the aft fuselage behind the wing trailing edge so that the interference lift disturbances are closer to the desired expansion region on the conceptual aircraft's F-function. This nacelle-mounting option was used in the design of the Langley SBJ concept, which is a supersonic business jet concept designed for low sonic boom [29]. The keys to achieving a low-boom design would include the successful integration of engine nacelles.

Figure 3.7: Off-Design Cycle Parameters Trade Studies for the HECTOR – *Cruise BPR vs SFC*

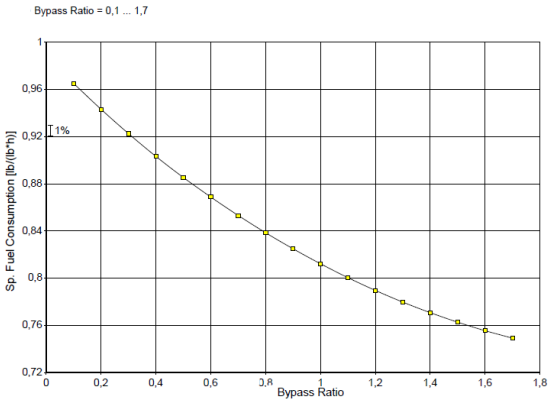

Having the variable bypass technology and fully-variable nozzle in the HECTOR engine, combining higher thrust with lower TSFC was achieved at off-design conditions. Figure 3.7 presents the relationship between cruise bypass ratio and SFC at subsonic cruise conditions to offer similar or less cost-per-mile to subsonic private jets. From the iterative cycle examination relating on-design parameters to off-design performances, it was conceivable to create the last cycle attributes for each off-design conditions. The key parameters of the HECTOR engine off-design missions are summarized in Table 3.2.

Table 3.2: Key Parameters of the HECTOR Off-Design Missions

Mach Number	**0**	**0.98**	**2.4**	**3.0**
Altitude (ft)	0	40,000	40,000	50,000
Thrust (lbf)	24,764.84	6,922.49	32,448.33	38,439.32
TSFC (lb/lbfhr)	0.5020	0.7491	1.1918	1.2547
TET (°R)	2723.15	2756.09	2895	3203.4
OPR	31.878	29.652	18.534	17.954
FPR	2.728	2.788	2,347	2.3
BPR	1.7	1.7	0,3152	0.3139

Table 3.3: Key Parameters of the HECTOR Engine All Design Missions

Mach Number	**0**	**0.98**	**1.15**	**2.1**	**2.4**
Altitude (ft)	0	40,000	40,000	40,000	50,000
Thrust (lbf)	24,764	6,922	7,194	28,567	32,439
TSFC (lb/lbfhr)	0.502	0.749	0.791	1.096	1.192
TET (°R)	2723	2756	2776	2840	2895
OPR	31.878	29.652	27.127	21.105	18.534
FPR	2.73	2.79	2.7	2.5	2.35
BPR	1.7	1.7	1.6	0.7	0.3

3.5 Performance Comparison with the Baseline Engine Model

Since the cycle parameters of the baseline engine given in the RFP are at the take-off conditions, to make a meaningful comparison, cycle parameters for supersonic cruise are obtained and stated at the Table 3.4 by using "Off-Design" tool of the GasTurb. By analyzing the Figure 3.4, the required thrust for the supersonic cruise is not satisfied by the baseline engine. Hence, it would not be suitable to compare the baseline engine with the HECTOR engine by also considering the immense difference between the required thrust values.

Table 3.4: Comparison the Engine Performance the HECTOR and the Baseline Engine

Flight Condition	**Cycle Parameter**	**Baseline Engine**	**HECTOR**	**Percent Difference**
Takeoff	Thrust (lbf)	21,698	24,764	+14.13%
	TSFC (lb/lbf.hr)	0.475	0.502	+5.79%
Subsonic Cruise (M = 0.98)	Thrust (lbf)	5,040	6,922	+37.34%
	TSFC (lb/lbf.hr)	0.782	0.749	-4.2%
Supersonic Cruise (M = 2.1)	Thrust (lbf)	3,568	28,567	+700%
	TSFC (lb/lbf.hr)	1.714	1.096	-36.01%

By depending on the literature and the improvements in the supersonic jet engines, producing 28,567 lbf thrust with a thrust specific fuel consumption of 1.096 is a significant achievement. This should be considered as a phenomenal performance gain and establish a major selection criteria for the HECTOR engine.

Yet, after checking the required thrust for the subsonic cruise, both the baseline engine and the HECTOR satisfy this requirement. If these engines in subsonic cruise were to be compared, by having 37.34% more thrust produced, a shorter flight time is achievable with the HECTOR engine than the stated interval in the RFP. Also, having less fuel consumption than the baseline engine has improved the TSFC by 4.2%. Both gaining more thrust and decreasing the thrust specific fuel consumption at the same time, the HECTOR completely dominates the subsonic cruise mission over the baseline engine.

3.6 Engine Weight Analysis

To investigate the engine weight, a wide scope of research is made about the techniques and ways. Comparative analysis of mathematical models, such as Torenbeek E. (Delft University of Technology), Clavier J. (Cranfield University), Kuz'michev (Samara National Research University) and WATE++ program (NASA) of turbofan engine weight estimation were analyzed [24]. Among the various applications and trials that have been worked upon, one noteworthy technique appears to give the most precise outcomes, which is WATE++ program that has been created by NASA in a joint effort with Boeing [16]. Since this whole program isn't openly accessible, an essential variant has been found from the referenced MIT report. In this less complex form, the factors that impact straightforwardly the engine weight are OPR, BPR and core mass flow. The engine weight can be estimated by using Equation 3.1,

$$W_{engine} = a \times (\frac{\dot{m}_{core}}{100})^b \times (\frac{OPR}{40})^c \tag{3.1}$$

For the engines with current technology (late 1990s through 2000s):

- $a = (-6.590 \times 10^{-1})BPR^2 + (2.928 \times 10^2)BPR + 1915$
- $b = (6.784 \times 10^{-5})BPR^2 - (6.488 \times 10^{-3})BPR + 1.061$
- $c = (-1.969 \times 10^{-3})BPR + 0.0711$

For the engines with advanced materials (including carbon composites, CMC, MMC, and TiAl):

- $a = (-6.204 \times 10^{-1})BPR^2 + (2.373 \times 10^2)BPR + 1702$
- $b = (5.845 \times 10^{-5})BPR^2 - (5.866 \times 10^{-3})BPR + 1.045$
- $c = (-1.918 \times 10^{-3})BPR + 0.0677$

This variant of the estimation is utilized for turbofan engines. Since the ideology of this equation and strategy is comparable, a comparison between the weight of the baseline engine model with the HECTOR is done by adding the estimation error according to the take off condition.

Table 3.5: Weight Estimation of the HECTOR engine and the baseline engine

Parameter	**Baseline**	**HECTOR**
$\dot{m}_{core}$ (lb/s)	177.41	180.11
OPR	21	32
BPR	1.7	1.7
$W_{estimation}$ (lbm)	4214	3812
W_{real} (lbm)	4515	4084

New engine design weight is calculated in Table 3.5 with 6.67% error margin. Also, almost 11% reduction in weight is obtained, that is approximately 430 lbm, compared to the baseline engine.

4. Mission Specification and Profile

As mentioned before, the weight of the HECTOR engine is significantly less than the baseline engine. Thus, the mission segment analysis has been done based on the new weight of the aircraft by subtracting the weight difference from the maximum take-off weight given in the RFP.

Table 4.1: Mission Segment Analysis of the Supersonic Business Jet Operating with the HECTOR

Segment	Starting Height (ft)	End Height (ft)	Duration (hr)	Range (km)
Warm-up and Taxi	0	0	0.15	/
Take-off	0	25,000	0.05	/
Subsonic Climb	25,000	30,000	0.015	/
Transonic Climb	30,000	40,000	0.015	/
Supersonic Cruise (M = 2.1)	40,000	40,000	/	6000
Supersonic Cruise (M = 2.4)	40,000	40,000	/	2500
Descend and Landing	40,000	0	0.15	/

For the estimation of the fuel weight, Equations 4.1 and 4.2 are used [44].

$$FuelWeight = F_n \times TSFC \times Duration \tag{4.1}$$

$$FuelWeight = W_i(1 - W_f/W_i) \tag{4.2}$$

$$\frac{W_3}{W_2} = exp\left(Range \times \frac{TSFC}{V \times (L/D)}\right) \tag{4.3}$$

Table 4.2: Mission Segment Fuel Weight Analysis of the Supersonic Business Jet Operating with the HECTOR

Segment	Estimated Weight After Segment (lbm)	Estimated Fuel Usage (lbm)	Fuel Percent Usage	TSFC	F_n
Warm-up and Taxi	140,785.8	4,354.2	4.57%	/	/
Take-off	139,542.6	1,243.2	1.31%	0.5020	24,764.84
Subsonic Climb	139,387.2	155.4	0.16%	0.7491	6,922.49
Transonic Climb	139,218.0	169.2	0.17%	0.7820	7,211.32
Supersonic Cruise (M = 2.1)	66,156.38	75,355.8	79.22%	1.0964	28,567.02
Supersonic Cruise (M = 2.4)	52,567.87	13,588.3	14.28%	1.1918	32,448.3
Descend and Landing	52,314.87	253	0.29%	/	/
Total		95,119.1			

Considering the range given in the RFP, duration between the specified segments in the Tables 4.1 and 4.2 are estimated. Also, in this estimation, the criterion set in [42] were taken into consideration.

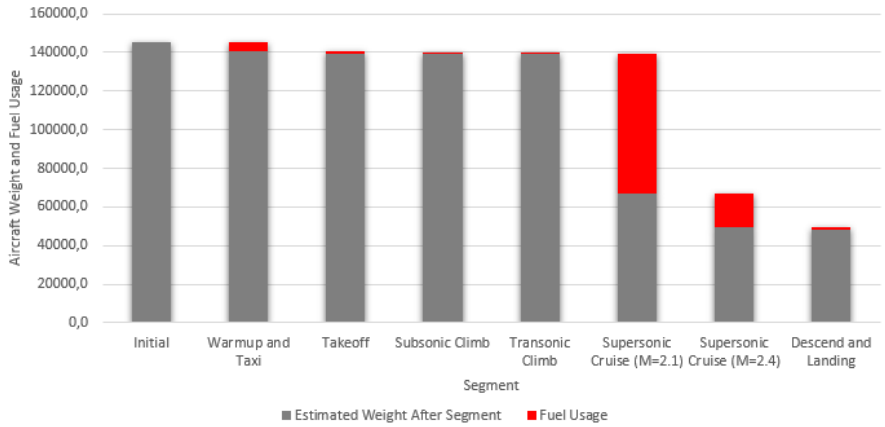

Figure 4.1: Aircraft Estimated Weight and Fuel Usage

In the RFP, it states that if 2.4 Mach is achievable, the total fuel weight usage should not exceed 97,400 lbm. By taking this information into account, supersonic cruise at Mach 2.4 is included as a mission segment.

After obtaining the total fuel weight needed to accomplish the required missions, the HECTOR engine, as shown in the Table 4.2, it has been observed that the fuel usage limitation set in the RFP is met. Furthermore, the fuel usage was even less than this set limit.

5. Engine Inlet Design

A supersonic inlet is expected to deliver the necessary mass flow rate to the fan while reducing the mach number to the inlet conditions of the fan. Since the flow will go through shock waves, it is important to keep the total pressure loss at minimum. Furthermore, it plays an essential role in reducing the fan noise. The design of the inlet starts by first selecting the type of the inlet [13].

5.1 Inlet Type

The three supersonic inlet types are given as [32],

1. Internal Compression,
2. Mixed Compression,
3. External Compression.

The internal compression is not considered to be of any use by most experts due to its poor performance at nonzero angle of attack values and its requirement of a large throat area for large Mach number [32]. Since the HECTOR engine is required to fly at mach numbers as large as 3, such a design is out of the question.

The mixed compression inlet on the other hand, yields a higher performance at high mach numbers. However, it is mostly used when the flight Mach number is larger than 2.5 [32]. Considering that the HECTOR engine is expected to fly mostly at Mach 2.1, such a design would minimally increase the efficiency while adding extra weight, cost and complexity to the system.

The external compression offers a good in between to the two types mentioned above. It can operate at large Mach numbers while being lighter, cheaper and simpler than mixed compression [32]. Thus, an external compression supersonic inlet is deemed to be the best for the HECTOR engine.

The number of ramps to be used highly depends on the flight Mach number. As the flight Mach number increases, to obtain reasonable pressure recovery factors, the number of ramps should also be increased. The design procedure is started using 2 ramps. After the performance of the inlet is assessed, it has been observed that increasing the number of ramps would yield only small performance increases while affecting the weight and the cost of the system significantly.

Hence, the inlet of the HECTOR is decided to be, 2 ramp external compression supersonic inlet.

5.2 Inlet Design Methodology

The design of the inlet of the HECTOR engine focuses on obtaining an optimum pressure recovery factor (PRF) while ensuring it is light, cheap, and simple. In order to set a starting point, first the literature is searched for already existing supersonic inlets and their respective PRF values as shown in Figure 5.1.

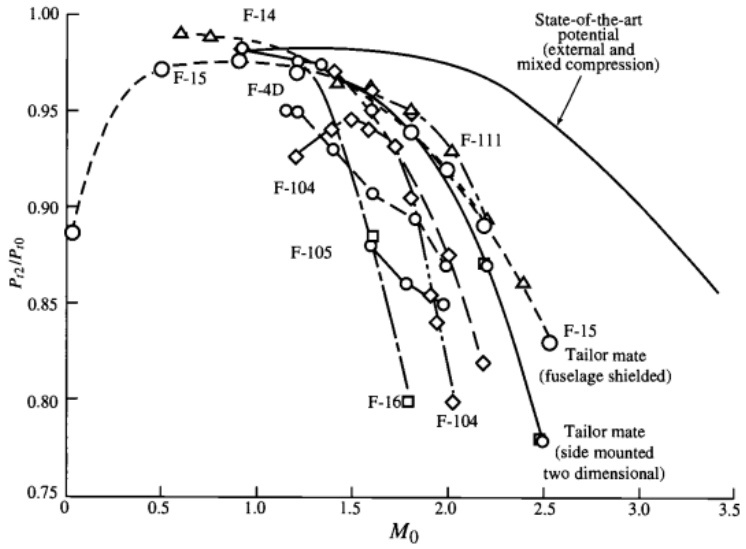

Figure 5.1: PRF of various supersonic aircraft [32].

As shown in Figure 5.1, the PRF at Mach number 2.1 is around 0.96 for state-of-the-art and is around 0.94 for aircraft capable of flying at such large Mach numbers. Similarly, using the

MIL-E-5008B standards the PRF can be calculated as shown in Equation 5.1 [13].

$$PRF = 1 - 0.075(M_\infty - 1)^{1.35} \tag{5.1}$$

Using equation 5.1, the PRF is calculated to be 0.915. After the design of the supersonic inlet is complete, a comparison with these values is necessary to ensure that the design procedure is carried out successfully.

The design of the supersonic inlet is done using the inviscid supersonic relations for the oblique and the normal shock respectively. For the oblique shocks that occur at the start of each ramp, following equations are used [19].

$$tan\Theta_a = 2cot\beta_a \frac{M_\infty^2 sin^2\beta_a - 1}{M_\infty^2(\gamma + cos2\beta_a) + 2} \tag{5.2}$$

$$M_{n\infty} = M_\infty sin\beta_a \tag{5.3}$$

$$M_{na}^2 = \frac{1 + \left(\frac{\gamma-1}{2}\right)M_{n\infty}^2}{\gamma M_{n\infty}^2 - \left(\frac{\gamma-1}{2}\right)} \tag{5.4}$$

$$M_a = \frac{M_{na}}{sin(\beta - \theta)} \tag{5.5}$$

The equations are then altered to calculate the aerodynamic properties after the second oblique shock as well. Then, the aerodynamic properties after the normal shock are calculated by simply using Equation 5.4.

3D plots are then created to better understand the effect of the ramp angles on the PRF. Finally, the same analysis is carried out at off-design conditions to evaluate the performance of the inlet.

In order to find the geometrical relations between the ramps and the cowl-lip, Figure 5.2 is taken as a reference.

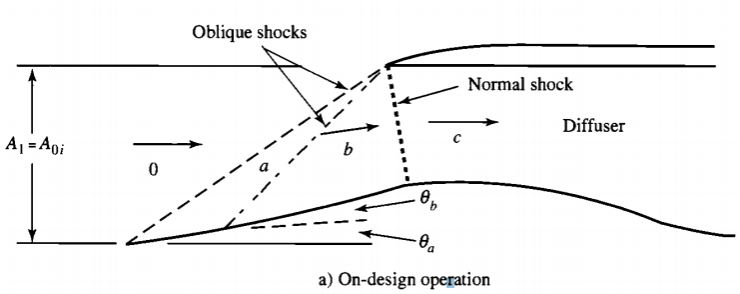

Figure 5.2: Sketch of the design at cruise conditions [32].

After the shock wave angles are calculated for both of the ramps and the length of the first ramp is defined, the point where the shock waves coincide will indicate the starting point of the cowl lip.

5.3 Inlet Sizing and Performance

As mentioned in Section 5.2, firstly 3D plots for the design condition are obtained to find the optimum ramp angles using a MATLAB code written by the HECTOR team(see Appendix A).

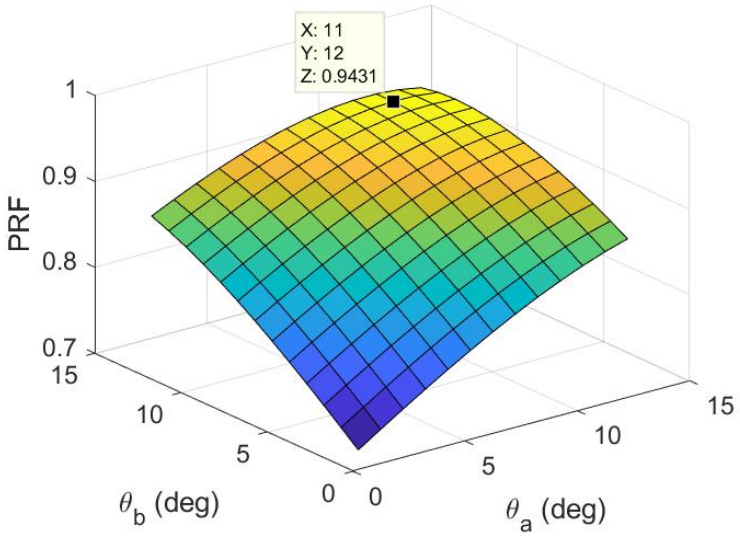

Figure 5.3: PRF values for different ramp angles at $M_\infty = 2.1$. The point shown indicates the optimum first and second ramp angles and the respective PRF.

As illustrated in Figure 5.3, there is an optimum angle for both ramps that results in the highest PRF. This point is taken as the design point of the inlet and the performance was reevaluated for flight Mach number of 3.

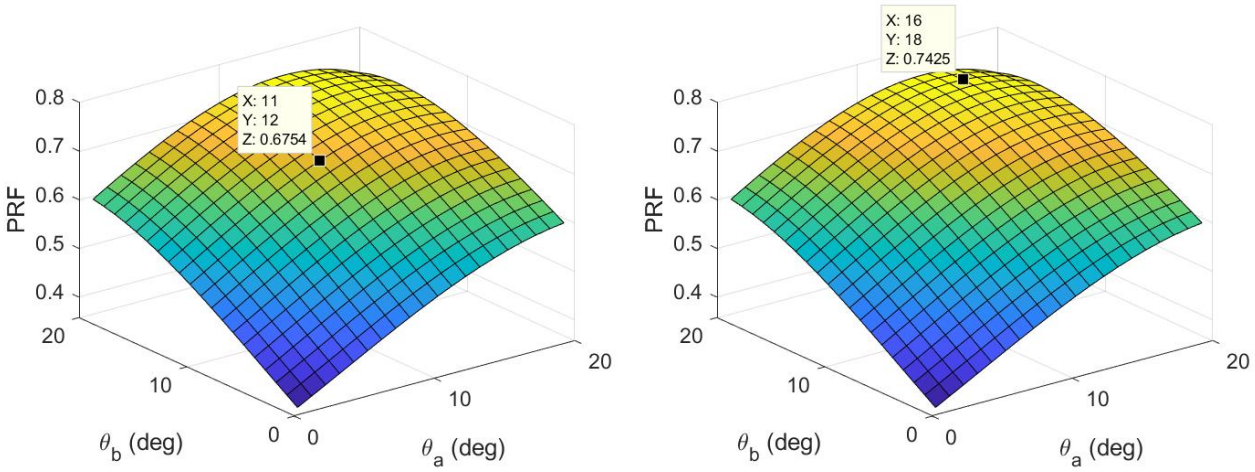

(a) Design point. **(b)** Optimum PRF

Figure 5.4: PRF values for different ramp angles at $M_\infty = 3$.

As shown in Figure 5.4, the PRF is significantly, 9%, less than the optimum PRF at Mach 3. Thus, a variable inlet design is essential to obtain a high PRF at off-design conditions. The performance of the inlet along with its aerodynamic parameters are given in the Table 5.1.

Table 5.1: HECTOR inlet aerodynamic and performance parameters.

M_∞	$p_{0\infty}$ (psi)	Θ_a (deg)	M_a	p_{0a} (psi)	Θ_b (deg)	M_b	p_{0b} (psi)	M_c	p_{0c} (psi)	PRF (%)
2.1	2.73	11	1.695	2.67	12	1.262	2.61	0.806	2.58	94.31
3	2.73	16	2.204	2.39	18	1.500	2.18	0.701	2.03	74.25

When checked, the PRF calculated at the design condition is highly similar to the values obtained by using the three method mentioned in Section 5.2. The sizing of the inlet was carefully done to ensure that the fan inlet conditions are matched using the Area-Mach relation, Equation 10.3 [19]. Following figures show the inlet design sizing.

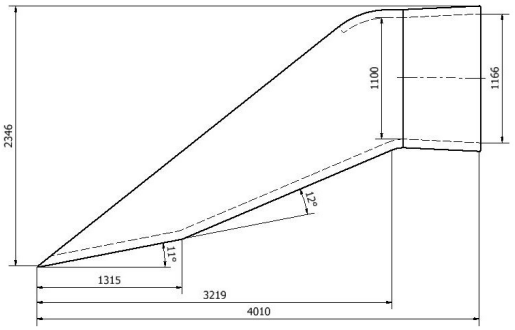

(a) Geometrical parameters of the inlet. Dimensions are in mm.

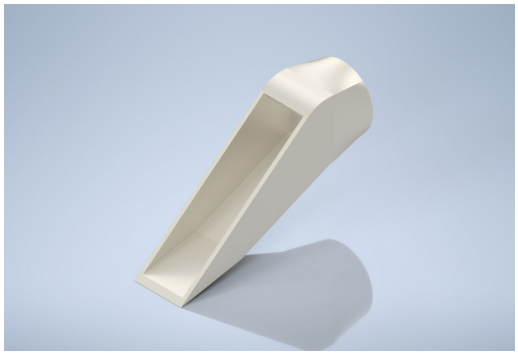

(b) 3D view of the inlet.

Figure 5.5: Sizing of the inlet.

6. Compression System Design

In this chapter, detailed turbomachinery design has been done by using the GasTurb and AxSTREAM Turbomachinery tools. After obtaining the thermodynamics properties and geometrical constraints from GasTurb, as shown in the Tables 6.2 and 6.4, they are used as boundary conditions for AxSTREAM Turbomachinery analysis. By defining total temperature, pressure and mass flow rate obtained from GasTurb 1-D analysis, 1-D and 2-D analyses are achieved in AxSTREAM software.

The compression system of the HECTOR engine is based on a two-spool concept with a transonic fan and low-pressure compressor which is run by the low-speed spool and a high-pressure compressor operating on the high-speed spool. At the first stage of the design of the transonic fan and high pressure compressor, the tip relative Mach number should be decided since it is affected by shaft rotational speed [13].

Table 6.1: Range and Typical Values of Each Design Parameters for Compression System [13]

Parameter	Range of Values	Typical Values
Flow Coefficient, ϕ	$0.3 \leq \phi \leq 0.9$	0.6
Axial Mach Number, M_z	$0.3 \leq M_z \leq 0.6$	0.55
Degree of Reaction	$0.1 \leq$ °R ≤ 0.90	0.5 (for M <1)
D-Factor, D	D ≤ 0.6	0.45
Tip Tangential Mach Number, M_t	1.0-1.5	1.3
Reynolds Number Based on Chord	300,000 $\leq Re_c$	>500,000
Stage Average Aspect Ratio, AR	$1.0 \leq$ AR ≤ 4.0	<2.0
Stage Average Solidiy, σ	$1.0 \leq \sigma \leq 2.0$	1.4
Loading Coefficient, ψ	$0.2 \leq \psi \leq 0.5$	0.35
Polytropic Efficiency, e_c	$0.85 \leq e_c \leq 0.92$	0.9
Tip Relative Mach Number (1^{st} Rotor), $(M_{1r})_{tip}$	$(M_{1r})_{tip} \leq 1.7$	1.3-1.5
Hub Rotational Speed, wr_h	$wr_h \leq 380$ m/s	300 m/s
Tip Rotational Speed, wr_t	$450 \leq wr_t \leq 500$ m/s	500 m/s
De Haller Criterion, W_2/W_1	$W_2/W_1 \leq 0.72$	0.75
Compressor Pressure Ratio per Spool	π_c <20	up to 20
Aspect Ratio, Fan	$\sim$ 2-5	<1.5
Aspect Ratio, Compressor	$\sim$ 1-4	~ 2
DCA Blade (Range)	$0.8 \leq$ M ≤ 1.2	Same
Axial Gap Between Blade Rows	$0.23c_z$ to $0.25c_z$	0.25 c_z
NACA-65 Series (Range)	M ≤ 0.8	Same
Taper Ratio	$\sim$ 0.8- 1.0	0.8

To achieve an outstanding compression system design, some key parameters which play an important role in the design process should be considered. In compression system design, averaged flow and stage loading coefficients, De-Haller number, blade solidity and diffusion factor establish a design criteria for compressor. To meet the best compressor design, these parameters are iterated until they have a compromise with the specified ranges in the Table 6.1. Also, by using 1-D and 2-D analyses, 3-D blade design including temperature, pressure, and mach number distribution for each stage can be achieved.

The HECTOR engine consists of 2-stage fan and 7-stage high pressure compressor. Although the number of compressor stages is stated in the RFP as 6 for booster and 7 for high pressure compressor, 13 in total, the total compressor stage for the HECTOR engine is decided to be 7. Analyzing the modern turbofan engines, such as Pratt&Whitney F119, and since decreasing both weight and length are currently the most important struggles in aeroengine design, having 7 stages for the high compressor of the HECTOR engine is considered to be the best choice.

6.1 Fan (LPC) Design

In the Table 6.2, thermodynamic properties and geometrical constraints are obtained from GasTurb to be used in AxSTREAM Turbomachinery calculations are shown.

Table 6.2: Properties of Low Pressure Compressor

Thermodynamic Properties and Geometrical Dimensions of LPC			
Total Pressure, $P_{t_{inlet}}$ (psia)	24.89	Polytropic Efficiency e_c	0.9
Total Temperature, $T_{t_{inlet}}$ (°R)	733.49	Adiabatic Efficiency η_c	0.89
Total Pressure, $P_{t_{outlet}}$ (psia)	61.87	Total Pressure Ratio π_c	2.485
Total Temperature, $T_{t_{outlet}}$ (°R)	973.43	Number of Stages	2
Mass Flow Rate $\dot{m}$	692.72	1^{st} Stage Blade Height (in)	16.53
Shaft Rotational Speed (rpm)	8000	Tip Diameter (in)	48.1

By considering the polytropic efficiency to be a function of work and flow coefficients, AxSTREAM generates possible design options. The design with the highest efficiency value among these is then selected. This option is based on meeting the key design parameters, such as De-Haller number and diffusion coefficient. Since the LPC Inlet Tip Diameter is decided to be 48.1 inches from GasTurb, it is given as the maximum fan diameter input while designing the LPC in the AxSTREAM and the result of the design is shown in the Figure 6.1.

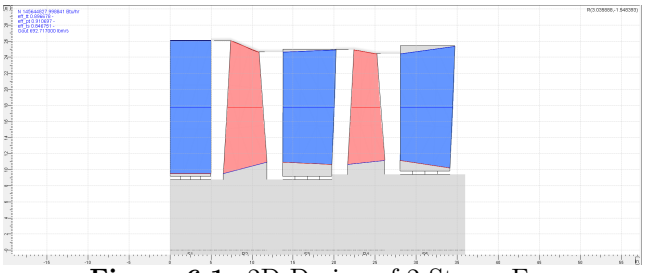

Figure 6.1: 2D Design of 2-Stages Fan

Detailed design parameters obtained from AxSTREAM for each stage in low-pressure compressor are given in the Table 6.3. When each parameter is compared with the typical values, it is seen that the results are consistent with the values stated in the Table 6.1.

Table 6.3: Detail Design Parameters of Low Pressure Compressor

Variables	Stage 1		Stage 2	
	Rotor	Stator	Rotor	Stator
Flow Coefficient	0.58		0.55	
Stage Loading	0.51		0.48	
De Haller Number	0.71	0.72	0.70	0.72
Degree of Reaction	0.69	0.34	0.71	0.29
Aspect Ratio	2.72	2.18	2.32	1.94
Solidity	3.34	2.17	2.70	2.73
Number of Blades	30	34	36	41
Stagger Angle	30.82	24.09	37.13	22.05
Inlet Metal Angle	50.91	37.86	44.37	41.52
Outlet Metal Angle	66.45	93.93	61.36	94.35
Blade Chord (in)	6.17	6.00	5.25	5.13
Leading Edge Radius (in)	16.81	12.21	9.96	9.47
Trailing Edge Radius (in)	13.07	13.07	12.21	9.96
Mach Number	0.71	0.49	0.62	0.43
Mean Radius	17.21	17.21	17.21	17.21
Hub to Tip Ratio	0.45	0.44	0.47	0.55
Stage Pressure Ratio	1.64		1.32	

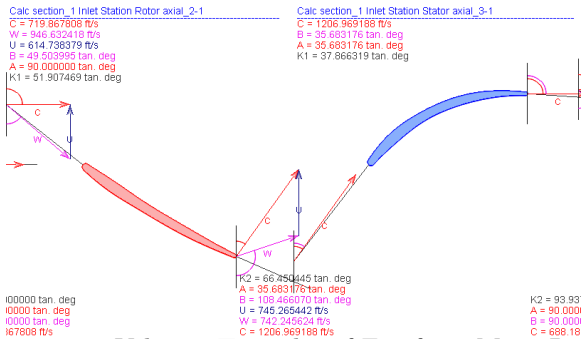

Figure 6.2: Velocity Triangles of Fan from Mean Radius

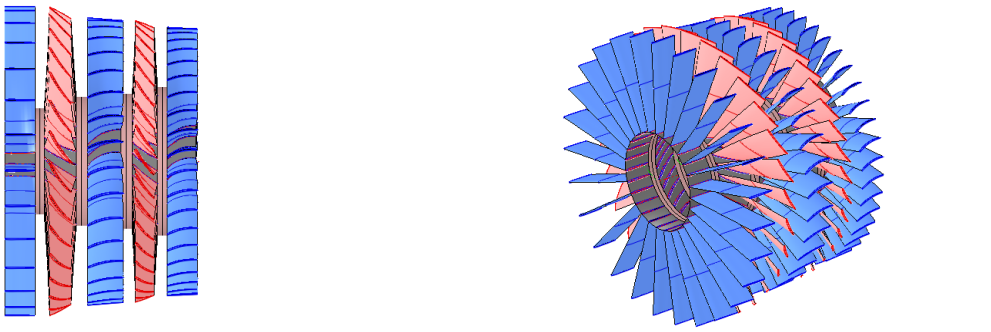

(a) 2-Stage Fan Side View **(b)** 2-Stage Fan

Figure 6.3: 3D Design of Fan

The velocity triangles of the first stage of the low-pressure compressor is shown in the Figure 6.2. For each stages, velocity triangles and pressure, temperature and mach distributions are added to the Appendix D.

6.2 HP Compressor Design

The following results, which are tabulated in the Table 6.4, are obtained as performance analysis and optimization for the HECTOR engine that will be used to determine the lower and upper limits of these parameters required for a detailed design in AxSTREAM. After specifying the upper and lower limits for these parameters, some optimizations for the HECTOR engine are created for preliminary design in AxSTREAM.

Table 6.4: Properties of High Pressure Compressor

Thermodynamic Properties and Geometrical Dimensions of HPC			
Total Pressure, $P_{t_{inlet}}$ (psia)	61.25	Polytropic Efficiency e_c	0.90
Total Temperature, T_{tinlet} (°R)	973.42	Adiabatic Efficiency η_c	0.89
Total Pressure, $P_{t_{outlet}}$ (psia)	525.39	Total Pressure Ratio π_c	8.578
Total Temperature, $T_{t_{outlet}}$ (°R)	1829.49	Number of Stages	7
Mass Flow Rate $\dot{m}$	538.62	1^{st} Stage Blade Height (in)	7.19
Shaft Rotational Speed (rpm)	12000	Tip Diameter (in)	35.97

The preliminary design of the rotor and stator are completed by using the values given in Table 6.4 and is shown in Figure 6.4.

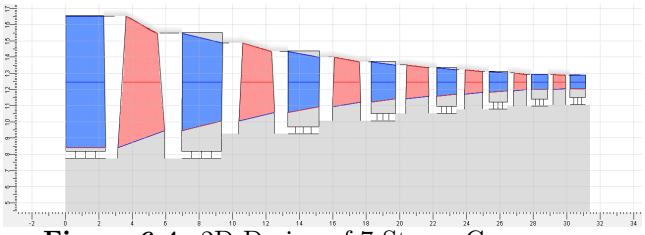

Figure 6.4: 2D Design of 7-Stages Compressor

After the analysis in the AxSTREAM is completed, detailed design parameters are obtained for each stage. When comparison has been done between the typical values stated in the Table 6.3 and detailed design parameters in the Table 6.5, they are quite consistent.

Table 6.5: Detail Design Parameters of High Pressure Compressor

Variables	Stage 1		Stage 2		Stage 3		Stage 4	
	Rotor	Stator	Rotor	Stator	Rotor	Stator	Rotor	Stator
De Haller Number	0.7632	0.8642	0.7665	0.7665	0.7665	0.7665	0.7665	0.7665
Flow Coefficient	0.569		0.6		0.6		0.6	
Aspect Ratio	2	1.743	1.964	1.860	1.818	1.705	1.657	1.534
Solidity	1.5	1.8	2.419	1.950	1.327	1.335	1.082	0.807
Averaged Loading Coefficient	0.331		0.331		0.331		0.331	
Number of Blades	15	28	27	29	33	35	39	40
Stagger Angle	54.99	15.10	38.55	38.55	38.55	38.55	38.55	38.55
Inlet Metal Angle	49.876	29.961	45.405	31.838	42.696	33.463	43.434	34.849
Outlet Metal Angle	55.767	68.843	58.857	67.869	65.798	68.207	70.971	69.034
Degree of Reaction	0.5		0.5		0.5		0.5	
Blade Chord (in)	6.27	3.28	3.51	3.19	2.83	2.64	2.41	2.31
Leading Edge Radius (in)	0.07	0.061	0.054	0.048	0.042	0.034	0.032	0.029
Trailing Edge Radius (in)	0.035	0.031	0.027	0.023	0.021	0.019	0.016	0.015
Relative Mach Number	1.214	0.659	0.899	0.873	0.849	0.827	0.806	0.788
Mean Radius (in)	12.47	12.47	12.47	12.47	12.47	12.47	12.47	12.47
Hub to Tip Ratio	0.508	0.611	0.676	0.738	0.782	0.819	0.846	0.867
Stage Pressure Ratio	1.492		1.449		1.395		1.315	

The velocity triangles of the first stage of the high-pressure compressor is shown in the Figure 6.5. For each stage, velocity triangles and pressure, temperature and mach distributions are added to the Appendix D.

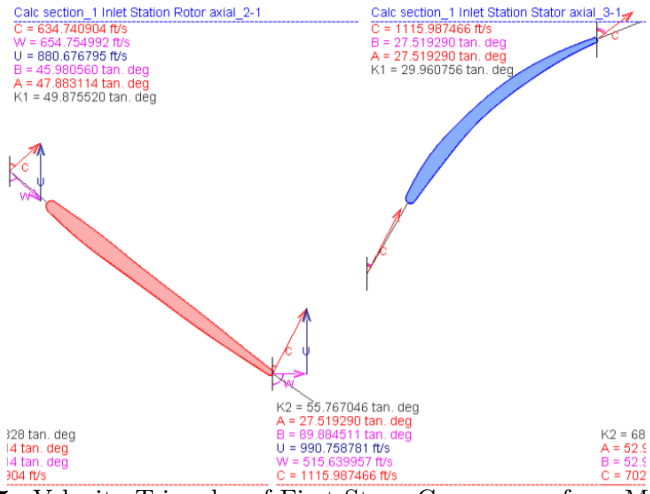

Figure 6.5: Velocity Triangles of First Stage Compressor from Mean Radius

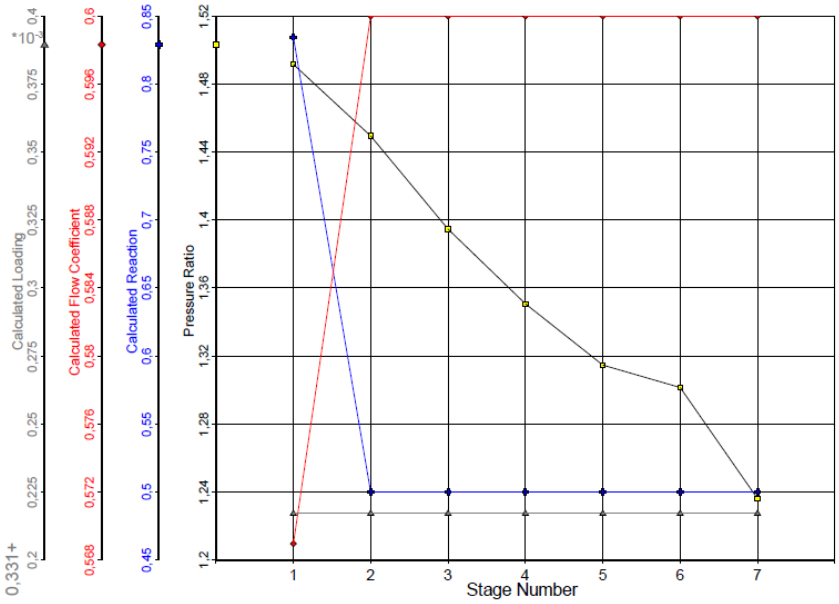

Figure 6.6: Main Design Parameters of the High-Pressure Compressor

The Figure 6.6 shows the changes of four important design parameters, which are pressure ratio calculated through high-pressure compressor, calculated reaction, flow coefficient and loading among the stages of HPC. Besides, in the Figure 6.7, the colormap showing the variation of the flow coefficient with stage loading represents the regions where De-Haller number and D-factor are affected. The HECTOR engine is in the region which De-Haller number is 0.75, D-Factor is 0.45. If the ranges stated in the Table 6.1 are checked, the HECTOR engine operates in a desired region considering these two important parameters for the compression system design.

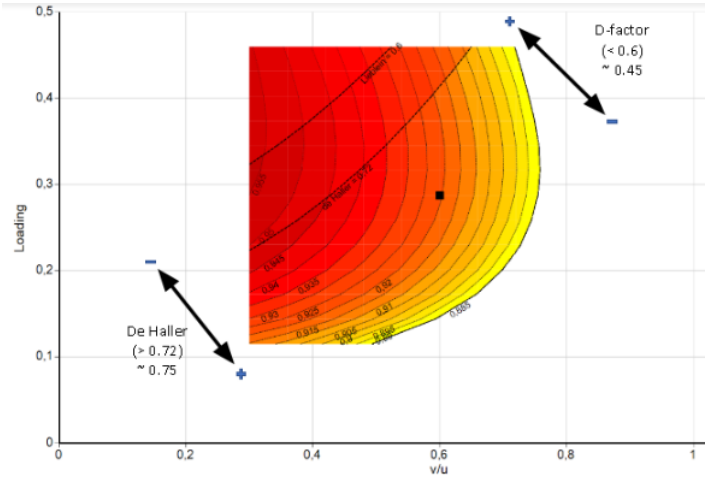

Figure 6.7: Operating Point of the HPC

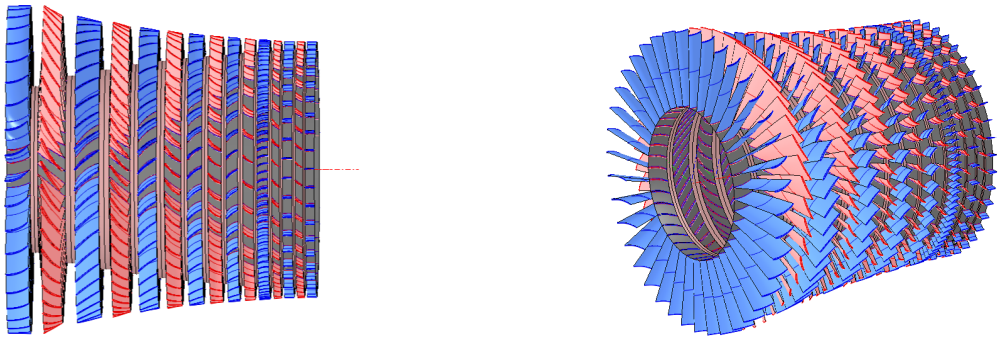

(a) 7-Stage Compressor Side View **(b)** 7-Stage Compressor

Figure 6.8: 3D Design of Compressor

7. Combustion System Design

This chapter presents combustion chamber of the engine where air and fuel mixture is burned. To obtain a high combustion efficiency, good mixing has vital importance. It needs to be considered that having highly efficient combustion chamber is possible by fast atomization of liquid fuel into quite small droplets [27]. To have adequate droplets, the appropriate type of swirler should be selected by considering the requirements.

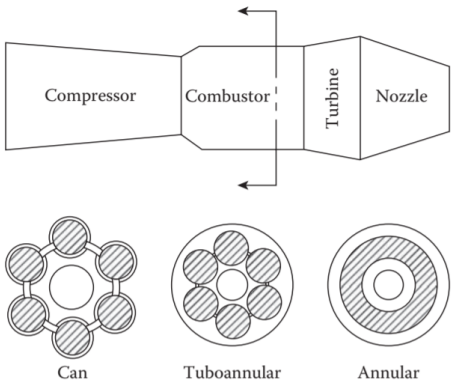

Figure 7.1: Types of combustion chambers [27]

As seen in Figure 7.1, there are three types of combustion chambers which are can, tuboannular and annular combustors. Annular combustion type is mostly used one due to its clean aerodynamic design with the other advantages like having the lowest pressure loss (approximately 5% of the combustor inlet total pressure) [27], providing more uniform combustion, less surface area and shorter size compared to other types. By considering the advantages listed above, an annular type combustion chamber is selected for the HECTOR engine.

7.1 Design Point Specifications

Table 7.1: Combustion Chamber Design Parameter Assumptions [13, 27, 32, 33]

Design Parameters	Range
Reference velocity (ft/s)	16.40 - 50
Pattern factor (PF)	0.2 – 0.3
Stoichiometric FAR (fuel-to-air ratio)	0.0685
Snout discharge coefficient	1
Equivalence ratio in the primary zone	1.2 – 1.6
Equivalence ratio in the secondary zone	0.4 – 0.8
The ratio of primary zone length to flame tube height	1
The ratio of secondary zone length to flame tube height	1.2
Atomizer ALR (Air liquid ratio)	>8
Total pressure loss in diffuser	%1
Required area ratio of pre-diffuser (AR)	1.5 – 4
Length to inlet height ratio (L/H1)	4 – 20
Reference velocity (ft/s)	15-60

7.2 Pre-diffuser Configuration

Since compressor axial flow velocity is as high as 204.59 ft/s (M = 0.1), before combustion takes place, this velocity should be reduced ideally through a short distance which is done by using a pre-diffuser between the compressor exit and the burner entrance. The table 7.2 shows the different types of pre-diffusers.

Table 7.2: Relative Merits of Various Diffuser Types [27]

Diffuser Type	Merits	Drawbacks
Aerodynamic or faired	Low pressure loss	• Relatively long • Performance susceptible to thermal distortion and manufacturing tolerances • Performance and stability sensitive to variations in inlet velocity profile
Dump higher than for faired type	• Relatively short • Insensitive to variations in inlet flow conditions	Pressure loss about 50%
Vortex-controlled	• High performance • Short length • Low pressure loss	• Requires minimum of 4% air bleed • Design procedures not fully established
Hybrid too low for turbine established	• High performance • Short length • Low pressure loss • Low bleed air requirement	Bleed air pressure
Hybrid with pre-diffuser	• High performance • Low pressure loss • Low bleed air requirement • High bleed air pressure	Needs extra length

After reviewing the Table 7.2, it is decided to select a hybrid configuration for the HECTOR engine. Since it provides combination of a vortex-controlled diffuser and conventional wide-angled post-diffuser located at the exit, compared with the conventional diffusers of the same length, the hybrid diffuser can achieve a static pressure recovery of at least 25% [27]. Thus, by using a hybrid diffuser, superior combustion performance can be achieved.

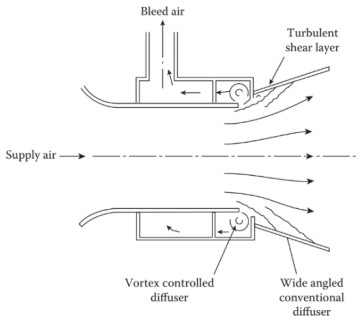

Figure 7.2: Hybrid Diffuser[27]

7.3 Fuel Atomizing Flow

Since liquid atomization and evaporation play an important role in the performance of a gas turbine, fuel should be atomized into small droplets to increase evaporation rate. By using Pre-filmed Airblast Atomizer in the design of the HECTOR engine, minimum drop sizes are obtained to provide maximum physical contact between air and the liquid. Besides, it is also important to subject high-velocity air at the both atomizing lips, as seen in the Figure 7.2, since this situation yields the optimum atomization condition. In addition to the advantages of the airblast atomizer, combustion occurs in the absence of soot formation which results in cool liner walls and minimum exhaust smoke. Thus, component parts are protected from overheating since airblast atomizers have ability to create Central Recirculation Vortex (CRV).

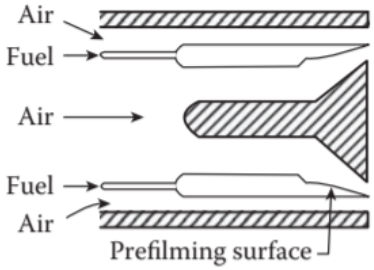

Figure 7.3: Pre-filming airblast atomizer[27]

The main disadvantage of this configuration is having poor atomization at the low air velocity passing through the atomizer. This problem is solved by combining pressure-swirl atomizer at low fuel flows with airblast atomization at relatively high flow rates [27]. Hence, this technology is selected to be used in the design of the HECTOR engine by considering the requirements, which are to operate efficiently both in subsonic and supersonic cruise conditions.

In the pre-filming type air blast atomizer design considerations of the HECTOR engine, Table 7.3 is prepared by following the methods derived from [32].

Table 7.3: Pre-filming type air blast atomizer design parameters

Injection System	Supersonic Cruise
Number of Fuel Injectors	18
Swirler Hub to Tip Ratio	0.7 – 0.9
Total Swirler Area (in^2)	487.38
Swirler Blade Angle	45
Swirl Number	0.86

7.4 Pre-diffuser Calculation

According to [32], to obtain high flat-wall diffuser efficiency, $2\theta = 9^\circ$ should be satisfied. Furthermore, length to inlet height ratio and the area ratio should be between 4 and 20, and 1.5 and 4, respectively. By combining pre-diffuser calculation methods stated in [32] and AxSTREAM results, L/H_1 ratio has determined as 12.3. If it is checked with the Figure 7.4a the region in which the HECTOR engine operates is safe in terms of stall condition.

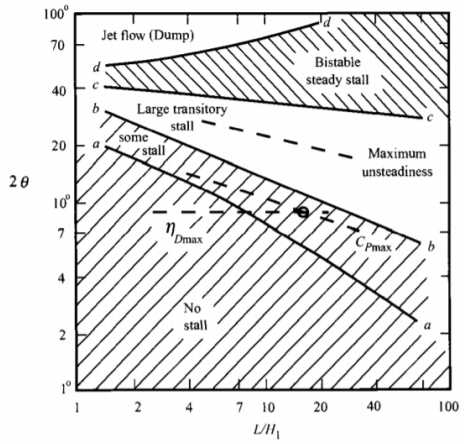

(a) Operating regimes of a flat-wall diffuser

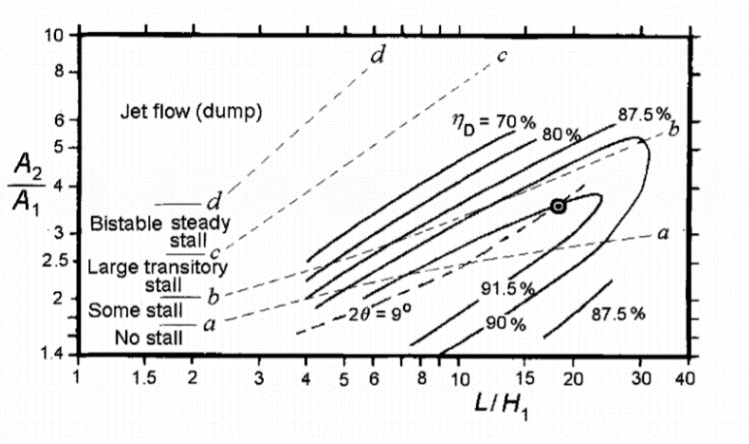

(b) Diffuser effectiveness on performance map of flat-wall diffuser

Figure 7.4: Historical trends for deciding pre-diffuser performance

After ensuring that the operation is not in the stall region, it is necessary to find pre-diffuser efficiency to calculate pressure drop across the diffuser part of the combustion chamber. By considering L/H_1 and A_2/A_1 ratios, from the Figure7.4b it is noted that the HECTOR engine operates with pre-diffuser efficiency of 91.5% at the no stall region with $2\theta = 9^o$.

$$\pi_D = 1 - \frac{(1 - \frac{1}{AR^2})(1 - \eta_D)}{1 + \frac{2}{\gamma M_1^2}} = 0.99 \cong 1\% \tag{7.1}$$

After calculating pressure drop across the pre-diffuser, 1% loss is obtained. Hence, the assumption which is made at the Table 7.1 is valid.

7.5 Combustor Air Partitioning and Equivalence Ratios

Equivalence ratio, air flow rate and flow fraction values of each zone and many other on-design parameters are found by following the methods stated in [32], and they are tabulated in the Table 7.4.

Table 7.4: Combustion chamber on-design conditions

Design Parameter	**Value**
Total air mass flow rate (lb/s)	514.5
Total fuel mass flow rate (lb/s)	13.19
Mach number at combustor inlet	0.1
Heating value of fuel (BTU/lb)	18553
Total temperature at combustor inlet (R)	1829.49
Total temperature at combustor outlet (R)	2840
Total pressure at combustor inlet (psia)	525.39
Total pressure at combustor outlet (psia)	499.12
Compressor blade pitch radius (in)	17.25
Swirler hole number	18
Primary zone equivalence ratio	0.724
Primary zone air flow rate (lb/s)	265.95
Primary zone flow fraction	0.516
Secondary zone equivalence ratio	0.507
Secondary zone air flow rate	379.79
Secondary zone flow fraction	0.221
Dilution zone flow fraction	0.123
Pattern Factor	0.257
Stoichiometric FAR ratio	0.06850
Reference velocity (ft/s)	50
Diffuser pressure loss	1%
Atomizer ALR (Air liquid ratio)	10
Required area ratio of pre-diffuser (AR)	3.02
Length to inlet height ratio (L/H1)	12.3

Fuel-to-air ratio, 0.025, with 308.625 lb/s mass flow of the air excluding bleed air is separated as 25% (38.57 lb/s) for primary zone, 36.67% (56.58 lb/s) for secondary zone and 38.33% (59.15 lb/s) for the dilution zone by considering dome flow partitions stated in [32].

7.6 NOx Emission

NOx emission is another key aspect in the design of the combustion chamber. To design a low emission combustion chamber, it is necessary to provide sufficient time and temperatures while reactions occur. The four key factors to be considered while designing a combustion chamber are, reducing equivalence ratio of the primary zone to achieve lean-burn combustion, improving injectors due to fuel atomization efficiency, reducing the high temperature residence time of the combustion chamber gas and improving the uniformity of the fuel- air mixture [47, 17].

RQL (Rich burn, quick Quench, Lean burn), LPP (Lean, Pre-mixed, Pre-vaporized) and LDI (Lean Direct Injection) are the commonly used combustion chambers in aeroengines. The technical comparison of these types are given in Table 7.5.

Table 7.5: Comparison of Combustion Chambers[43]

Low emission method	LPP	RQL	LDI
NOX emission	Extremely low	Very low	Very low
Combustion efficiency	Extremely high	High	High
Combustion stability	Flash back, combustion unstable, spontaneous combustion	No flash back	Low
Smoke	Extremely low	High	Low
Configuration	Short length, complex dome	Long length	Short length, complex dome
Development prospect	Common	Good	Best

By considering both the Table 7.5 and the requirements given in the RFP, it is decided to choose LDI configuration due to its low NOx emission and soot formation together with having high efficiency and short length. Compared to other two combustion chambers, LDI can reduce NOx emission more than the RQL combustor and LDI has less tendency to suffer from unstable combustion and flashbacks than LPP combustor.

7.7 Liner Material Selection and Advanced Cooling Technique

Due to its common usage in aeroengine industry, nickel-based super alloys have been standardized for combustion chamber liner material selection. Since higher overall engine performance is desired for decades, the HECTOR engine will utilize Hastelloy X nickel-chromium-iron-molybdenum alloy, which has superior high-temperature strength up to 2610 R° with an exceptional oxidation resistance and excellent fabricability characteristic. Hence, having these advantages makes this material a step further than others in the aerospace industry [49].

Figure 7.5: Convection/Film Cooling Method [17]

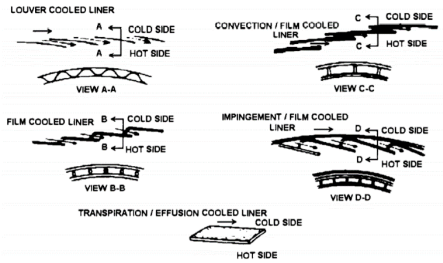

Figure 7.6: Liner Cooling Techniques [32]

Since the highest turbine inlet temperature given in the RFP is 2840 R°, protection for the liner part of the burner is required to compensate 200 R° temperature difference between the highest turbine inlet temperature and Hastelloy X's maximum service temperature to reduce the effects of hot streaking by an insulation of ultra-lightweight ceramic matrix composites such as CMC (SiC/SiC) tiles.

While CMC tiles provide movement of air flow among the holes in the combustor walls together with the convective film cooling liner behaves as an insulator by enhancing the convective heat

transfer characteristics between the pedestal tiles. These tiles not only augment the convective heat transfer, but also reduce cost since they are designed as removable pieces for maintenance. Although using ceramic materials as a cooling technique is considered as a developing technology, the HECTOR engine will use this promising technique for an efficient cooling.

7.8 Combustor Geometry

The methods used for the combustion chamber geometry of the HECTOR are determined by following the techniques stated in [32].

Y_{max} (in)	3.22	L_c (in)	27.56	Y_{max}/D_j	2.51
HE_{dome} (in)	8.05	A_{dome} (in^2)	731.81	A_{ref} (in^2)	1073.09
D_j (in)	1.88	$A_{passage}$ (in^2)	341.28	L_c/H_d	2.33

$$PF = 1 - e^{(\frac{-20}{\frac{L_c}{H_d}\frac{\Delta P_{liner}}{q_{ref}}})} \tag{7.2}$$

μ_{ref}	$\Delta\ P_{liner}/q_{ref}$	PF
0.039	30	0.257

7.9 Combustor Efficiency

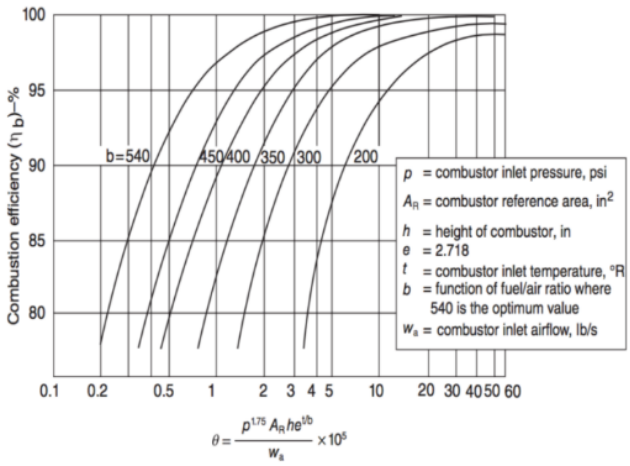

Figure 7.7: Combustion Efficiency & CLP Correlation[13]

For gas turbine engines, Lefebvre introduced the combustion loading parameter (CLP). This parameter has good correlation with the combustor efficiency and is given by Equation 7.3. 'b' is the reaction parameter which depends on the primary zone equivalence ratio, ϕ_{pz}.

$$CLP = \theta = \frac{P_{t3}^{1.75} A_{ref} H e^{\frac{T_{t3}}{b}}}{\dot{m}_3} \tag{7.3}$$

$$b = 382[\sqrt{2} \pm ln\frac{\phi_{pz}}{1.03}],\ \ (+)\ \ for\ \ \phi_{pz} < 1.03,\ \ \ (-)\ \ for\ \ \phi_{pz} > 1.03 \tag{7.4}$$

Table 7.6: Combustion Efficiency and CLP Correlation [13]

Design Parameter	Supersonic Cruise
Primary zone equivalence ratio	0.724
CLP	175.64×10^5
b	404
Combustion Efficiency	99.5%

7.10 Combustor Ignition Source

A surface discharge type igniter is selected for the HECTOR engine due to its common usage and high reliability for gas turbines. Ignitor should be located in the primary zone where air-fuel mixture passes over the electrodes. Yet, it is needed to locate the ignitor far enough from the hottest part of the primary zone, due to high temperatures caused by the recirculation bubble, electrodes might wear away. Also, ignitor should be close enough to stoichiometric region so that the ignition takes place, properly. Besides, considering flame propagation to neighboring primary zones, each primary zone does not have to have their own ignitor. Thus, and appropriate number and location should be decided by trial and error method [32]. By reviewing the literature, it has been decided for the HECTOR engine to have 2 spark ignitors.

7.11 Combustion Chamber Performance Parameters

The performance parameters of the combustion chamber are given in Table 7.7.

Table 7.7: Combustion Chamber Performance Parameters

Design Parameter	Value	Parameter	Value
Residence time (ms)	4	Air-liquid Ratio	10
Loading Factor ($kg/bar^{1.8}m^3s$)	0.07	Air-fuel Ratio	40.3
Combustion Intensity (MW/m^3bar)	55.76	Global equivalence ratio	0.365

7.12 Combustion Chamber Drawing of the HECTOR Engine

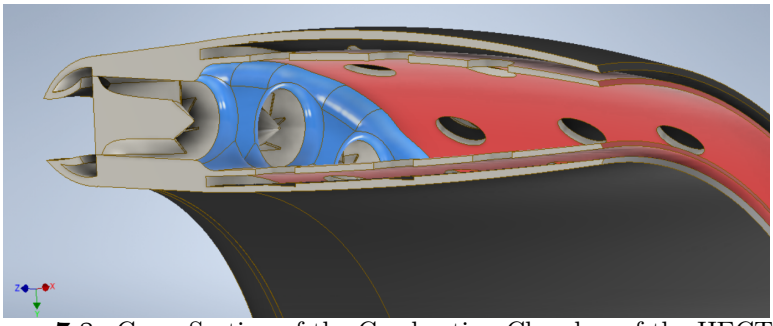

Figure 7.8: Cross-Section of the Combustion Chamber of the HECTOR

Figure 7.9: Combustion Chamber 3-D Drawing

8. Turbine Design

This chapter includes detailed information regarding the design of the turbine system of the HECTOR engine. Preliminary design parameters, typical ranges for design criteria, the performance characteristics and analysis results are stated in this chapter. The HECTOR engine operates with a high-pressure turbine (HPT) and low-pressure turbine (LPT). In a 2-spool design, power is transferred to the HPT by the high-pressure compressor, and the fan transmits power to the LPT. Thus, while designing the turbine where the energy required to rotate the compressor is taken from the core flow, component efficiencies and transmitted power by the shaft should be taken into account.

Table 8.1: Turbine Performance Parameters

Parameters for HPT	***Value***
Maximum AN^2	4 x 10^{10} - 5 x 10^{10} $in^2.\ rpm^2$
Axial Mach Number, M_z	1.4-2.0
Exit Mach Number	0.4-0.5
Exit Swirl Angle	0-40 deg
Parameters for LPT	***Value***
Inlet Total Temperature	<2070°R
Hub/tip ratio at inlet	0.35-0.5
Maximum stage loading at hub	2.4
Exit Mach Number	0.4-0.5
Exit Swirl Angle	0-40 deg

In the development of turbine technology, increasing HPT inlet temperature, cooling airflow and stage loading coefficient of LPT should be taken into account. At the design stage of the turbine, these parameters highly affect overall pressure and by-pass ratios. Also, by considering these parameters together with the efficiency, to obtain a reduction in TSFC is possible. In the HECTOR engine, design methodology applied for the compressor design in AxSTREAM is also applied for the turbine design. In this process, range for the parameters, which are stated in the Table 8.1, required for the detailed preliminary design in AxSTREAM are determined using GasTurb. Among potential design points created in AxSTREAM after indicating desired range for each parameter, the point which meets the design criteria and has maximum efficiency for the turbine is selected for detailed design. After that, by using selected optimum design point, 3D design of rotor, stator and blade for each stage are created.

Zweifel Coefficient, aspect ratios as blade height to chord, solidity, pitch and chord values for each stage of turbomachinery are the most important design criteria of the turbine design.

The HECTOR engine consists of 1-stage high-pressure and 3-stage low-pressure turbines. The design parameters are stated in the upcoming sections by considering each stages.

8.1 High-Pressure Turbine Design

In the Table 8.2, thermodynamic properties and geometrical constraints that are obtained from GasTurb to be used in AxSTREAM Turbomachinery calculations are shown. By examining total efficiency values as a function of flow and work coefficients, AxSTREAM generates possible design options. The design that has the best efficiency value among these specified designs is selected. This option is based on meeting the key design parameters such as Zweifel Coefficient, aspect ratios as blade height to chord, solidity, pitch and chord values.

Table 8.2: Properties of High Pressure Turbine

Thermodynamic Properties and Geometrical Dimensions of HPT			
Total Pressure, $P_{t_{inlet}}$ (psia)	499.12	Polytropic Efficiency e_c	0.90
Total Temperature, T_{tinlet} (°R)	2840	Adiabatic Efficiency η_c	0.89
Total Pressure, $P_{t_{outlet}}$ (psia)	110.92	Total Pressure Ratio π_c	4.50
Total Temperature, $T_{t_{outlet}}$ (°R)	2060.24	Number of Stages	1
Mass Flow Rate $\dot{m}$	523.07	1^{st} Stage Blade Height (in)	4.01
Shaft Rotational Speed (rpm)	12000	Tip Diameter (in)	40.1

Table 8.3: Detailed Design Parameters of High Pressure Turbine

Variables	**Stage 1**	
	Stator	Rotor
Flow Coefficient	0.52	
Stage Loading	1.93	
Degree of Reaction	0.52	
Zweifel Coefficient	0.75	0.63
Aspect Ratio	1.24	2.18
Solidity	1.50	1.82
Number of Blades	40	85
Stagger Angle	50.63	34.12
Inlet Metal Angle	90	51.27
Outlet Metal Angle	20.19	.15.87
Mean Radius	15.56	15.56
Mean Diameter to Blade Height	7.75	0.44
Rotor Inlet Temperature	/	2840
AN^2	3.73×10^7	7.66×10^7
Exit Mach Number	1.04	0.64
Stage Pressure Ratio	4.50	

Detailed design parameters obtained from AxSTREAM are given in the Table 8.2. When each parameter is compared with the typical values, it is seen that the results are consistent with the values stated in the Table 8.1. For each stage, velocity triangles and pressure, temperature and Mach distributions are added to the Appendix D)

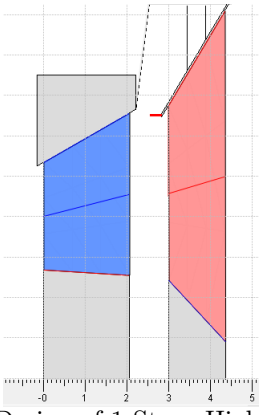

Figure 8.1: 2D Design of 1-Stage High Pressure Turbine

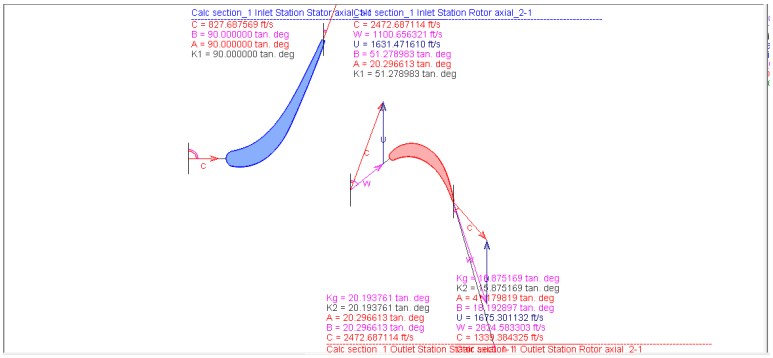

Figure 8.2: Velocity Triangles for High Pressure Turbine from Mean Radius

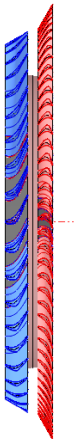

(a) 1-Stage HPT Side View

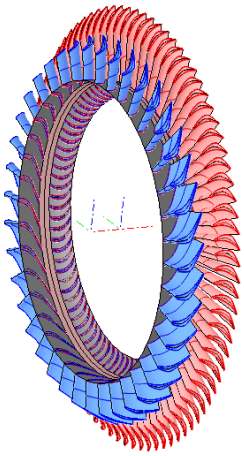

(b) 1-Stage HPT

Figure 8.3: 3D Design of High Pressure Turbine

8.2 Low-Pressure Turbine Design

Following results, which are tabulated in the Table 8.4, are obtained as performance analysis and optimization for the HECTOR engine that will be used to determine the lower and upper limits of these parameters required for detailed design in AxSTREAM. After specifying upper and lower limits for these parameters, some optimizations for the HECTOR are created for preliminary design in AxSTREAM.

Table 8.4: Properties of Low Pressure Turbine

Thermodynamic Properties and Geometrical Dimensions of LPT			
Total Pressure, $P_{t_{inlet}}$ (psia)	109.81	Polytropic Efficiency e_c	0.90
Total Temperature, T_{tinlet} (°R)	2043.6	Adiabatic Efficiency η_c	0.89
Total Pressure, $P_{t_{outlet}}$ (psia)	55.15	Total Pressure Ratio π_c	1.99
Total Temperature, $T_{t_{outlet}}$ (°R)	1755.35	Number of Stages	3
Mass Flow Rate $\dot{m}$	542.83	1^{st} Stage Blade Height (in)	8.83
Shaft Rotational Speed (rpm)	8000	Tip Diameter (in)	42.2

The preliminary design of the rotor and stator created by using the values given in Table 8.4 as shown in Figure 8.5. After the analysis in the AxSTREAM, detailed design parameters are obtained for each stage. When comparison has been done between the typical values stated in the Table 8.1 and detailed design parameters in the Table 8.5, they are quite consistent. The velocity triangles of the first stage of the low-pressure turbine is shown in the Figure 8.5. For each stages, velocity triangles and pressure,temperature and mach distributions are added to the Appendix D)

Table 8.5: Detail Design of Low Pressure Turbine

Variables	**Stage 1**		**Stage 2**		**Stage 3**	
	Stator	Rotor	Stator	Rotor	Stator	Rotor
Flow Coefficient	0.85		0.97		1.07	
Stage Loading	0.83		1.17		1.09	
Degree of Reaction	0.85		0.74		0.76	
Zweifel Coefficient	0.54	0.63	1.88	0.67	1.52	0.65
Aspect Ratio	2.72	6.73	3.70	9.15	4.86	11.80
Solidity	2.06	2.76	2.37	3.67	3.26	8.79
Number of Blades	37	72	37	71	36	66
Stagger Angle	0	66.49	0	61.95	0	62.61
Inlet Metal Angle	70.0	139.44	40.85	130.98	43.75	133.07
Outlet Metal Angle	90.0	23.29	80.99	25.78	90	25.84
Mean Radius	13.68	13.27	12.75	12.38	11.88	11.51
Mean Diameter to Blade Height	3.09	2.23	2.34	1.67	1.72	1.20
Rotor Inlet Temperature	/	2060.46	/	1946.68	/	1837.86
AN^2	3.13×10^7	4.09×10^7	3.60×10^7	4.75×10^7	4.25×10^7	5.72×10^7
Exit Mach Number	0.33	0.51	0.37	0.55	0.39	0.59
Stage Pressure Ratio	1.21		1.29		1.26	

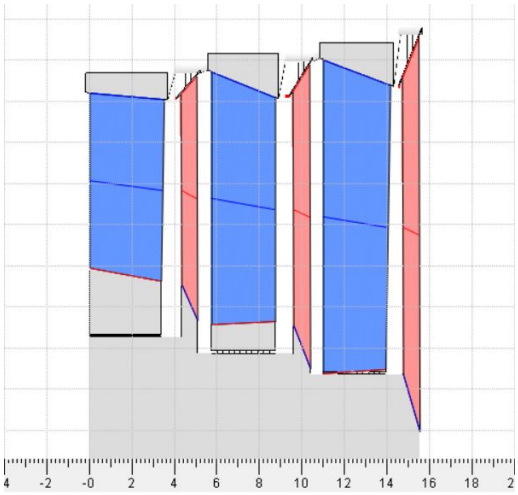

Figure 8.4: 2D Design of 3-Stage Low Pressure Turbine

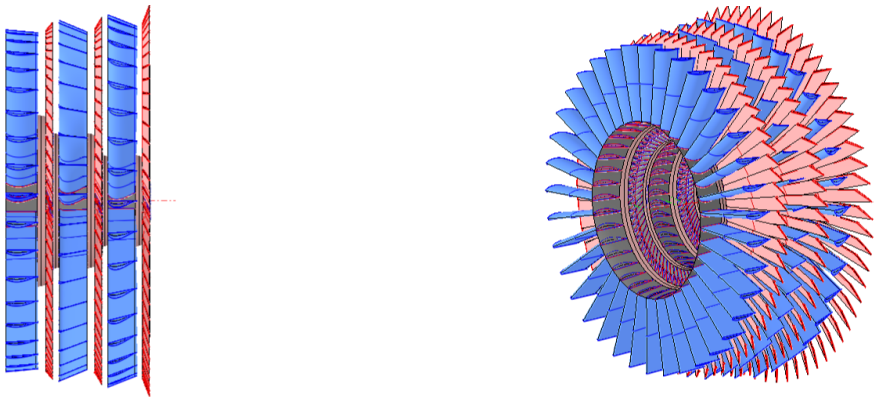

(a) 3-Stage LPT Side View **(b)** 3-Stage LPT

Figure 8.5: 3D Design of Low Pressure Turbine

8.3 Smith Chart

In the Smith Chart, efficiency of HPT and LPT are calculated as a function of flow coefficient and stage loading factor. By looking at this chart, it is possible to compare the efficiency value calculated in AxSTREAM with the efficiency value determined from the Smith Chart, as a result of turbine performance analysis. In AxSTREAM, average flow coefficient is approximately 0.52 and average loading factor is 1.93 for HPT, while these values are approximately 0.97 and 1.1 for LPT, respectively. As indicated by blue signs in the Figure 8.6, average efficiency values are between the efficiency curves of 0.90 and 0.91 for both HPT and LPT. If the Tables 8.4 and 8.2 are checked, results obtained from AxSTREAM and the Smith Chart have strong correlation in terms of efficiency values.

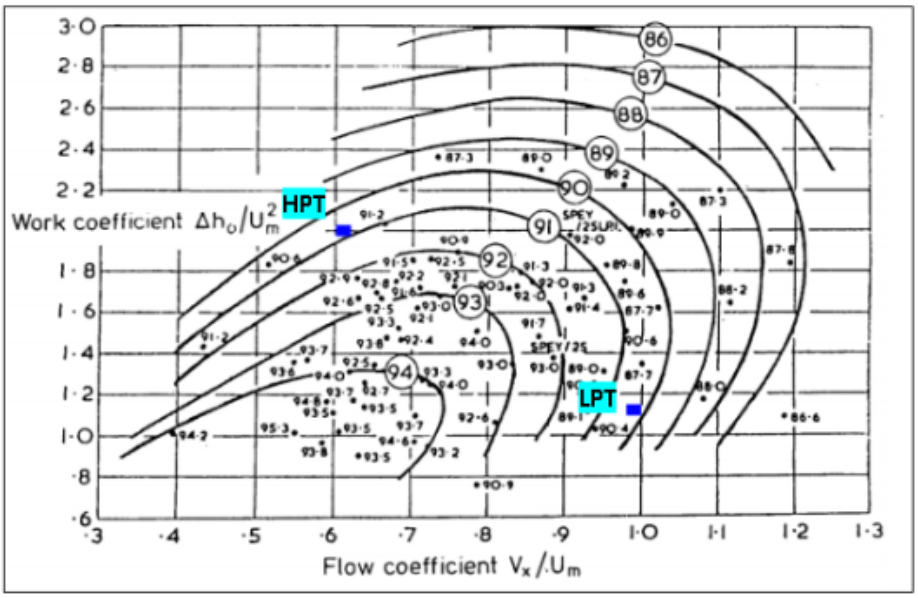

Figure 8.6: Smith Chart for Turbine of the HECTOR at supersonic cruise

8.4 Turbine Blade Cooling

Modern trends of gas turbine engines focus on increasing turbine inlet temperatures to reduce specific fuel consumption and improve the overall performance of the engine. However, operating at very high temperatures reduces the life of the turbine blades and blades, while the permissible temperature level of the cycle is limited by the melting point of the materials. Therefore, turbine blade cooling is required to reduce blade metal temperature to acceptable levels for materials that increase the engine's thermal capacity. The turbine inlet temperature (TET) has more than doubled in the past 60 years because of the contribution and development of turbine cooling systems.

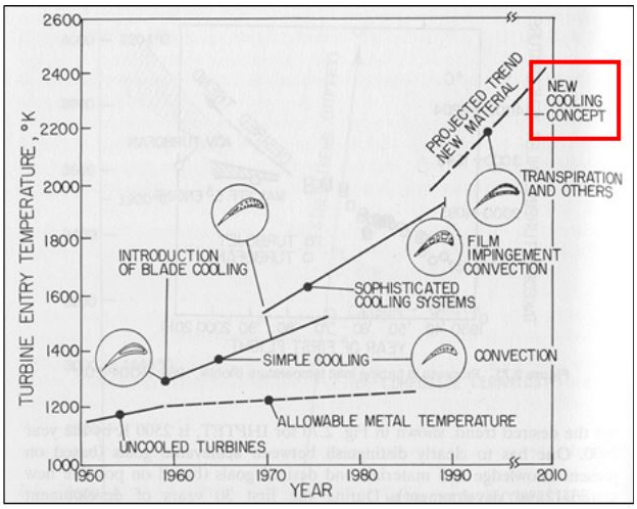

Figure 8.7: TET-Years [26]

Blade cooling is nothing but cooling air which is taken from high pressure compressor (HPC) outlet passes through the turbine blades. In order to avoid malfunction, this cooling process also requires the turbine blade life to be designed by avoiding local hot spots and to predict the metal temperature. There are different turbine cooling techniques can be classified as convective, impingement, film, full-coverage film and transpiration film cooling.

Convective cooling works mainly with air flow through the internal channels. In convective cooling, heat is transferred by conduction through the blade and then by convection into the air flowing through the blade. In addition, impingement cooling works with high flow rate air flow strokes and this type of cooling is used for heavy heat loads.Film cooling is main component of the overall cooling of turbine airfoils. As it can be observed in Figure 8.8, there are holes in the body of the airfoil for allowing the coolant to pass from the inner cavity to the outer surface throwing the refrigerant.

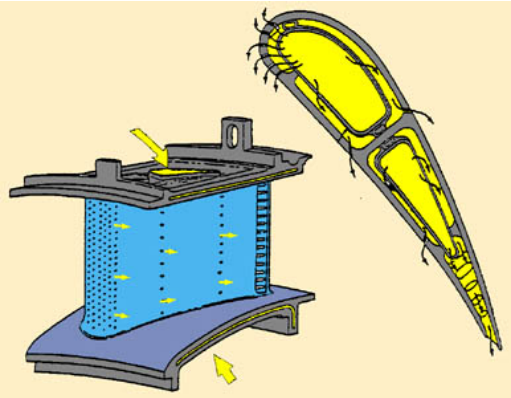

Figure 8.8: Film-Cooling

9. Mixer Design

Initially, flow streams are divided by the splitter and they join each other at the end of the splitter. In other words, using a forced flow lobed mixer, the core flow is mixed with the fan flow from the bypass duct for creating vortex flow to increase exchange of momentum and energy between the stream. Applying such a device to supersonic ejectors is useful for reducing take-off noise and increasing the thrust and heat exchangers. The parameters of the mixer design and sketch of the mixer of the Hector engine are shown in Figure 9.1b.

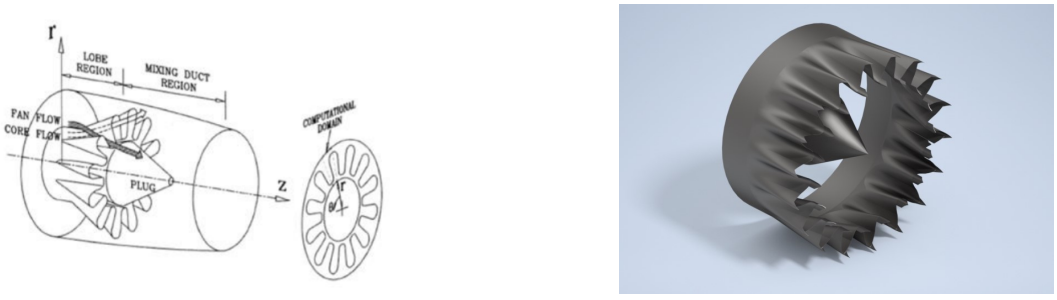

(a) Mixer Flow [50]

(b) Mixer 3-D Drawing

Figure 9.1: Mixer Design

10. Exhaust System Design

An efficient exhaust system is essential in a low-noise engine design. Furthermore, the nozzle is expected to ideally expand the exhaust gas while producing low drag [13]. Thus, a special attention is payed to the design and optimization of the nozzle.

10.1 Nozzle Inlet Conditions

The inlet conditions for the nozzle are determined by the analysis done in GasTurb and are given in Table 10.1.

Table 10.1: Nozzle inlet conditions.

M_{in}	T_{in} (^oR)	p_{in} (psi)	D_{in} (in)	$\dot{m}$ (lb/s)
0.46	1548	48.7	41.7	699

10.2 Nozzle Design Methodology

Before designing the nozzle, it is important to decide if it is necessary to use a converging diverging nozzle or a converging nozzle is enough. As suggested by [13], if the converging diverging nozzle yields at least 5% more thrust than a converging nozzle, a converging diverging nozzle should be designed. The ratio of the thrust produced by the converging diverging nozzle to the thrust produced by the converging nozzle can be written as shown in Equation 10.1 [13].

$$\frac{F_{g-CD}}{F_{g-Conv.}} = \sqrt{\frac{1 - NPR^{-\frac{\gamma-1}{\gamma}}}{\frac{\gamma-1}{\gamma+1}}} \frac{\gamma}{\gamma + \left(1 - \left(\frac{\gamma+1}{2}\right)^{\frac{\gamma}{\gamma-1}} . NPR^{-1}\right)} \tag{10.1}$$

Using Equation 10.1 with $NPR = 20.78$, for ideal expansion, shows that using a converging diverging nozzle yields 13.09% more thrust. Thus, a converging diverging nozzle is deemed to be suitable for the HECTOR engine.

Since the engine is required to operate in various altitude and Mach number values, to ensure that the flow is ideally expanded for all conditions, a fully variable design is essential.

The design of the nozzle was carried out using Method of Characteristics. The algorithm was implemented in MATLAB by the HECTOR team and a Graphical User Interface (GUI) was built afterwards to aid the design procedure (see Appendix B).

Since Method of Characteristics provides a good way to design the nozzle to have isentropic, or as close to it as possible, behavior, it will help to reduce the noise [13].

Although nozzle is designed using Method of Characteristics, the created algorithm includes some empirical equations to estimate the boundary layer development. Since the losses in the nozzle are predominantly caused by the accelerated turbulent flow and its effect on the development of the boundary layer, such an addition is essential in estimating the nozzle performance correctly [5].

In order to put a starting point to the exit mach number of the nozzle, knowing that the mass flow rate is $\dot{m} = 699lb/s$, assuming that ideal expansion is achieved, and the mass flow rate of the fuel is negligible, the difference between the velocity of the exit and free stream air can be estimated using Equation 10.2.

$$F = \dot{m}\Delta V \tag{10.2}$$

Then, knowing the required thrust in cruise, $F = 28,670\ lbf$, the exit air can be estimated to be $1318\ ft/s$ faster than the freestream. This value will be used as a sanity check after the calculations are completed.

Furthermore, by using the Area-Mach relation given in Equation 10.3 [19], the exit area is calculated to be compared with the output of the method of characteristics to ensure that the calculations are carried out correctly.

$$\left(\frac{A}{A*}\right)^2 = \frac{1}{M^2}\left[\frac{2}{\gamma+1}\left(1+\frac{\gamma-1}{2}M^2\right)\right]^{(\gamma+1)/(\gamma-1)} \tag{10.3}$$

Finally, in order to find the adiabatic efficiency of the nozzle, Figure 10.1 is used.

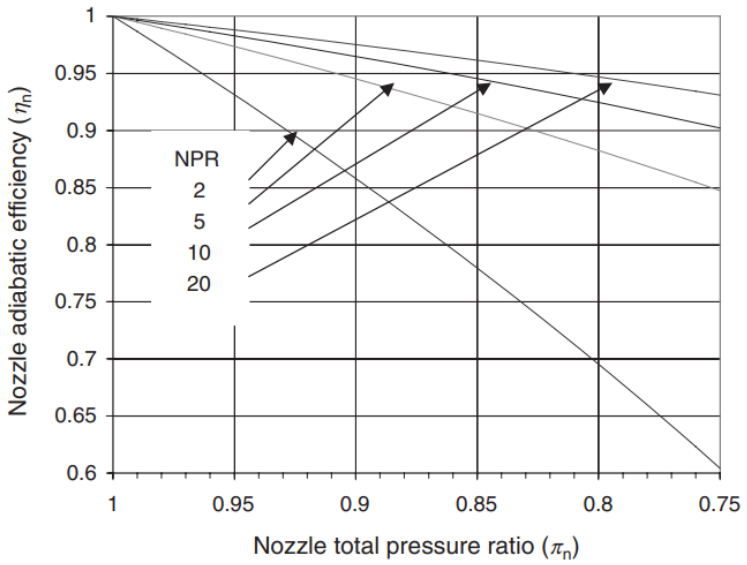

Figure 10.1: Nozzle adiabatic efficiency [13].

10.3 Nozzle Performance

Using the GUI created by the HECTOR team, the exit mach number of the nozzle is increased slowly to ideally expand the flow. After the ideal expansion is achieved, the mesh density is increased to increase the accuracy of the results. For illustration purposes, mesh density of 25 will be shown.

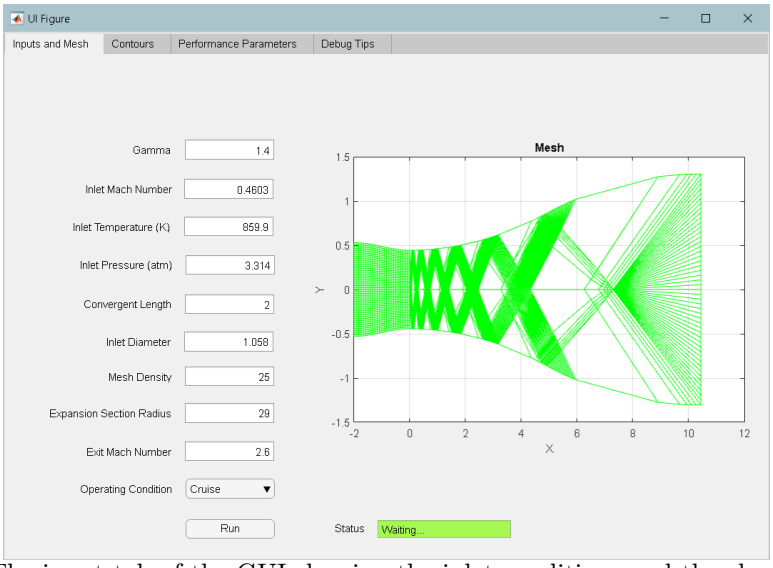

Figure 10.2: The input tab of the GUI showing the inlet conditions and the characteristic mesh.

As shown in Figure 10.2, the characteristic mesh is successfully created. The exit Mach number is set to 2.6 while the expansion section radius is set to the lowest possible value. These ensure that the flow is ideally expanded.

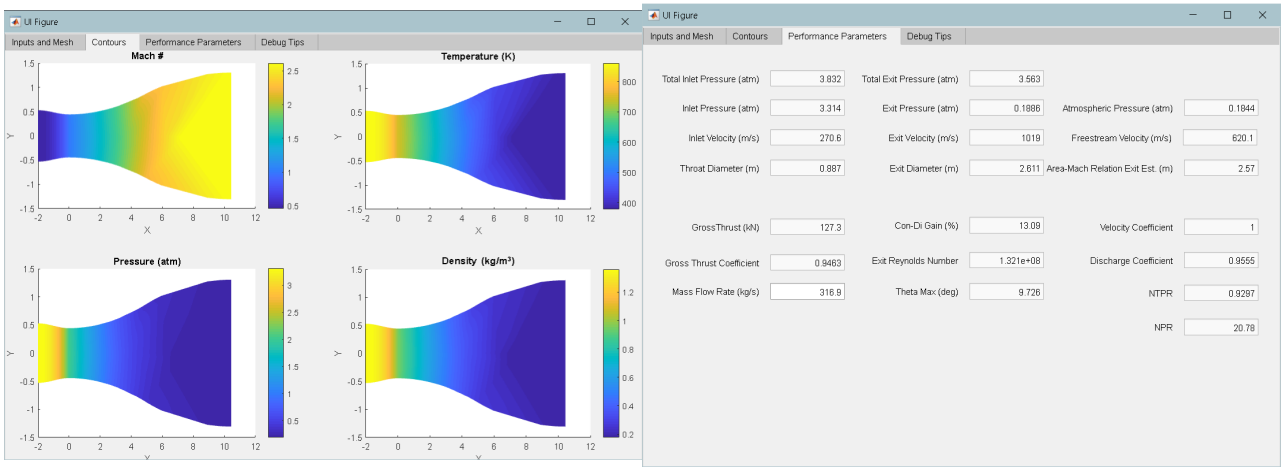

(a) Evolution of the aerodynamic properties. **(b)** Performance parameters.

Figure 10.3: Nozzle performance obtained using Method of Characteristics.

As mentioned before, various parameters are estimated to check the accuracy of the design. First, from Figure 10.3b it can be observed that the exit velocity is rough $400m/s$ higher than the free stream velocity. The exit pressure is equal to the atmospheric pressure, within two percent accuracy. The required thrust at cruise is also provided.

While designing the nozzle it has been noted that if the expansion section radius is too low, some of the characteristics lines will leave the nozzle without reflecting from the wall. This implies that there exists a maximum for the deflection angle. For the cruise conditions, this parameter, θ_{max}, is about 10 degrees. Due to this restriction on the maximum deflection angle, the nozzle is rather lengthy.

Comparing the exit diameter of the nozzle calculated using method of characteristics with the value calculated using Equation 10.3, it is noted that the values are within 2% accuracy. This implies that to ideally expand the nozzle, the exit diameter of the nozzle should be $A_{exit} = 3984 \sim 4046\ in^2$. Considering the maximum envelope diameter of the baseline engine, if ideal expansion is desired, then it is not possible to keep the same diameter for the HECTOR. To further check the accuracy of the results, following figure that shows how the gross thrust coefficient changes for different throat-to-exit area ratios and NPR values is used.

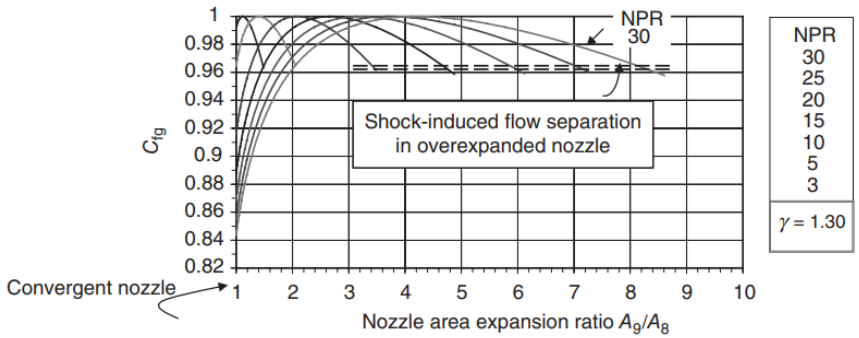

Figure 10.4: Gross thrust coefficient for different NPR and area ratios [13].

For the NPR of 20, it is noted that the highest gross thrust coefficient occurs when the throat–to-exit area ratio is roughly 4. Checking the performance parameters of the nozzle, a similar value is observed. Thus, it is concluded that the ideal expansion is not possible for the given envelope diameter. Due to the importance of ideally expanding the flow, this constraint is lifted to be $D_{max} = 71.2\ in$.

Then, to reduce the resulting length of the engine, the deflection angle restriction is lifted. It is expected that the characteristic lines not reflecting from the wall does not occur in a real nozzle, hence, the nozzle characteristics can be preserved while the angle is increased.

The performance parameters of the nozzle are given below.

Table 10.2: Performance of the HECTOR nozzle at cruise conditions.

Condition	C_D	π_n	NPR	η_n	C_{fg}
$M_\infty = 2.1$	0.9555	0.9297	20.78	0.98	0.9463

The sizing of the nozzle, including suppression channels, is shown below. The importance and effect of the suppression channels will be discussed later on.

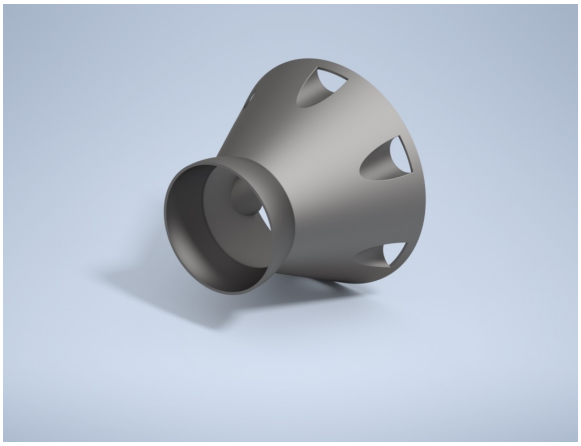

(a) 3D model.

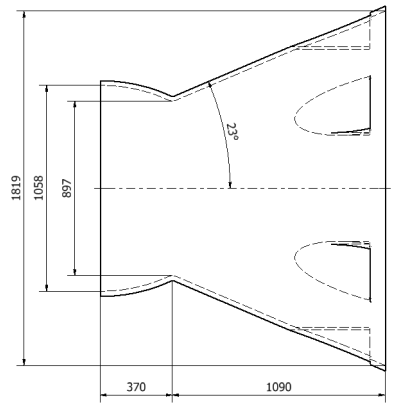

(b) Geometric parameters.

Figure 10.5: Nozzle sizing. Dimensions in mm.

10.4 Nozzle Area Scheduling

As a fully variable nozzle is proposed, it is important to define the area ratio of the exit and the throat for various operating points. As in subsonic regime, the nozzle becomes a converging nozzle, only the supersonic regime is investigated. Following figure shows the variation of the area ratio with the flight Mach number.

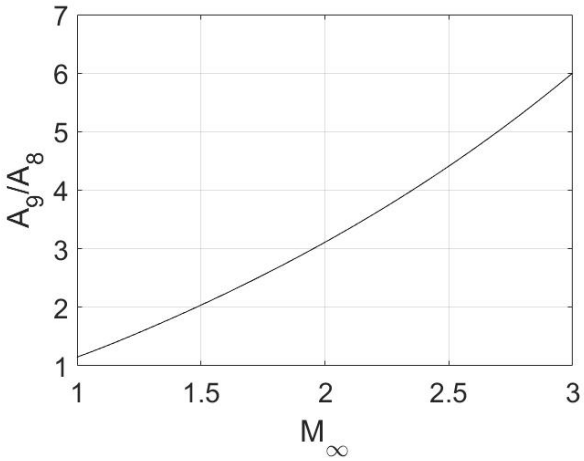

(a) Variation with the flight Mach number.

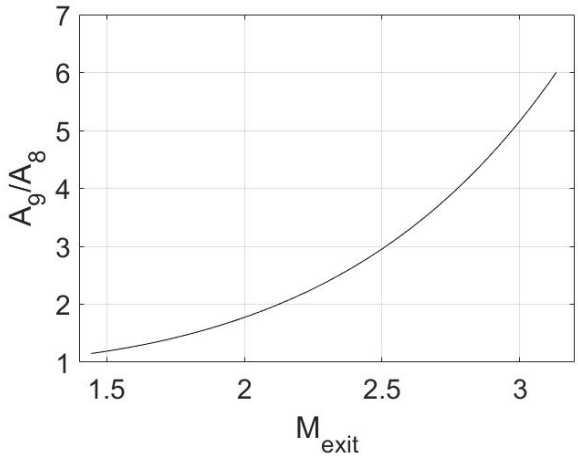

(b) Variation with the exit Mach number.

Figure 10.6: Variation of the throat-to-exit area ratio of the nozzle.

11. Overall Structural Design

11.1 Material Selection

Material selection is one of the most vital procedures required to increase the engine performance. Determination of materials is also important for the engine life-cycle. Hence, for every component of the engine, estimated lifetime should be known. To design the engine successfully, thermodynamic, aerodynamic and structural requirements are provided. The performance improvement of an engine is limited with development of material science.

Material technology is developing year by year. In the development of material technology, performance and cost are major players. The essential process is to design an engine that is more efficient, have a higher performance and strength, and is safe.

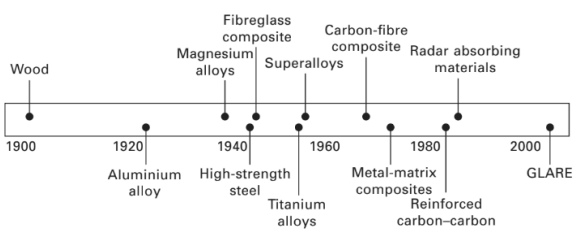

(a) Material Types Timeline

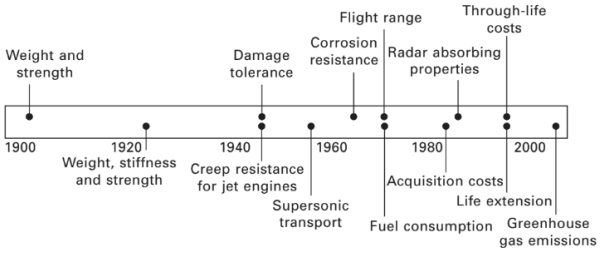

(b) Material/Materials Properties Timeline

For each component of the HECTOR engine, the selection of materials depend on the literature review, historical trends and experiences. Although used materials in the past and present are sourced, the material to be used in the future are investigated for each component of the engine. As shown in Figure [?], the Titanium, Aluminum, Carbon, Ceramic-Matrix and Metal-Matrix Composites are becoming much lighter than before [53].

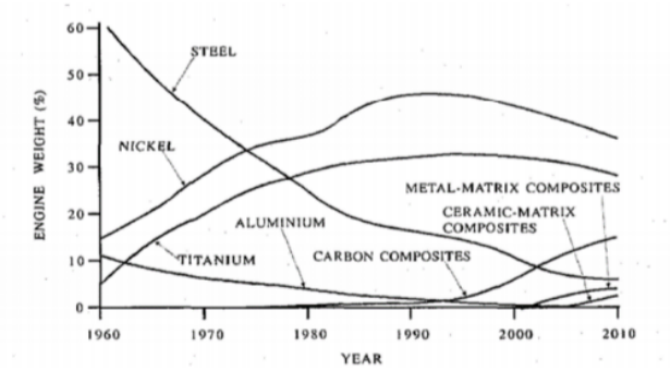

Figure 11.2: Common Materials used in engines [53].

As shown Figure 11.3, Ceramics, CMC, Carbon-Carbon Composites are the most reliable materials to resist high temperatures. Additionally, Inter-Metallic Compounds, Metal-Matrix Composites and Polymer Matrix Composites are also in development.

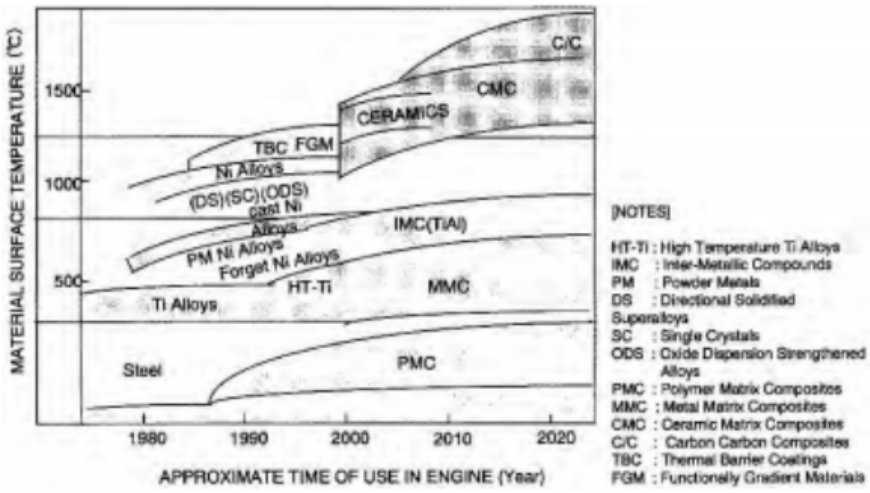

Figure 11.3: Common Materials in development of high temperature Turbine [53].

11.2 Common Material Properties

11.2.1 Polyimide Composites

Heat resistance and mechanical properties of the polyimide composites are beneficial for aero-engines as they have high temperature resistance. In between theseveral variants of polyimide composites, especially the organic hybrid polyimide composite resin resists up to 1300°R for extended periods of time.

Table 11.1: Material Properties of SiCf/Ti Composites

Material Property	**Value**
Max Service Temperature(R)	1256
Density(lb.in-3)	0.04805
Tensile Strength(ksi)	287
Young's Modulus(msi)	20

11.2.2 Metal-Matrix Composites

Metal-matrices have high temperature resistance, strength and ductility increasing its toughness. Although they are heavier than polymers and very complex to process, they can be used in areas such as the skin of supersonic aircraft and their engines.

11.2.3 Ceramic-Matrix Composites

Ceramics-Matrix Composites (CMCs) consist of alumina, silica, zirconia, and other elements refined from fine earth and sand or of synthetic materials, such as silicon nitride or silicon carbide. They have desirable properties such as superior heat resistance, low abrasive and corrosive properties. The Table 11.2 shows the CMC Properties [14].

Table 11.2: Material Properties of SiC Ceramic Matrix Composite [14]

Material Property	Value
Max Service Temperature(R)	3160
Density(lb.in-3)	0.0903
Tensile Strength(ksi)	46.56
Young's Modulus(msi)	41.3

11.2.4 TiAl Intermetallic Compounds

In the material selection, the aim is to find a material with a low density and that is able to withstand high stresses and temperatures. Upon literature review regarding TiAl intermetallic alloys, it has been noted that they have good mechanical properties and oxidation resistance at high temperatures, also high strength and resistance to crack propagation. Also, they have high resistance against fatigue due to their higher fracture toughness, good creep resistance at high temperatures, 2100°R. Therefore, TiAl intermetallic alloys are especially used in turbine blades thanks to their mechanical behavior at high temperatures, oxidation resistance, fracture toughness, and creep life [51].

Because Titanium Aluminide (TiAl) based alloys offer a good balance of properties due to their low density,$\sim 243 - 262 lb/ft^3$, good high temperature creep strength and oxidation resistance, and high melting temperature and particularly in the temperature range of 600–800 °C, TiAl systems provide a unique weight saving opportunity in the hot sections of jet engines, specifically when replacing the Ni-base alloy Low Pressure Turbine (LPT) blades with TiAl-based alloys [4]. Therefore, it can be considered for the turbine blades of the HECTOR engine. In Table 11.3, material properties of Ti-45Al-8Nb PST Single Crystals are given.

Table 11.3: Material properties of Ti-45Al-8Nb PST single crystals [8].

Material Property	Value
Max Service Temperature(R)	2100
Density($lb.in^3$)	0.1409
Tensile Strength(ksi)	92.39
Young's Modulus(msi)	20.305

11.2.5 Nickel-Based Superalloys

The nickel-based superalloys can be used for long intervals under middle or high temperatures in turbine components or bearings thanks to its high performance under these conditions. Moreover, nickel based alloys are used most extensively in the combustor, where elevated temperatures are maintained during the operation. Also, they have high creep-growth resistance, strength, and toughness under high temperatures [40].

11.3 Component Material Selection

11.3.1 Inlet Materials

In the aeroengines, inlet is the first module. Mass flow rate through the engines, which affects the produced thrust and the fuel consumption, depends on the efficiency of the inlet. Such

efficiency is achieved with proper geometry design and accurate production. Inlet must provide the exact amount of air necessary for different flight conditions. Thus, the material selection for the inlet is highly important. The inlet materials need to withstand high temperatures during supersonic cruise. The inlet must transfer the flow to the succeeding engine modules with little distortion for smooth running of the engine and efficient propulsion with a minimum disturbance to the external flow around the aircraft not to produce excess drag. Noise levels are an extremely important design consideration for the inlets. Therefore, using the right material is essential for noise absorption and suppression and to meet the international acoustics limitations [1].

Since fiber–reinforced plastic (FRP) has high strength and low density compared to steel, FRP materials are used in structures that experience high speeds, temperatures, and humidity levels [37].

Carbon fiber reinforced polymer (CFRP) is a strong material that contains carbon fibers. CFRP materials has many great advantages in aircraft and aeroengine design, such as reduced weight, fuel consumption, increased payload and range of flight. Moreover, CFRP materials have benefits increase toughness and durability and to decrease the maintenance cost and provide an increase in passengers comfort and safety, all of which have vital importance in aircraft and aeroengine design [1].

As a result, CFRP is chosen as the inlet material for the HECTOR engine and its mechanical properties are given in Table 11.4.

Table 11.4: Selected Material for inlet (CFPR) Metalic Properties

Selected Material Properties	**CFRP**
Maximum Service Temperature (R)	747
Density (lb/in^3)	0.058
Cost ($/lb)	27.2
Tensile Strength (psi)	0.17 x 10^6
Young Modulus (psi)	10.15 x 10^6
Elastic Modulus (psi)	19.14 x 10^6

11.3.2 Fan (LPC) Materials

Research on the candidate materials for the fan blades, their manufacturing process and structural analysis along with the ways to improve them began in the mid 70's and continues today. The goal in choosing the fan materials is to reduce weight, increase efficiency and decrease cost. This has driven the engine designers to choose materials that are based on carbon and Kevlar. Usually, composite materials, such as carbon-fiber, are used to achieve these goals due to their availability, manufacturability, stiffness, high strength and low weight. The reduced weight can reach up to 350lbs when used in fan casings and can be observed in modern engines like GEnx. This reduction results in a gain of 2 extra passengers.

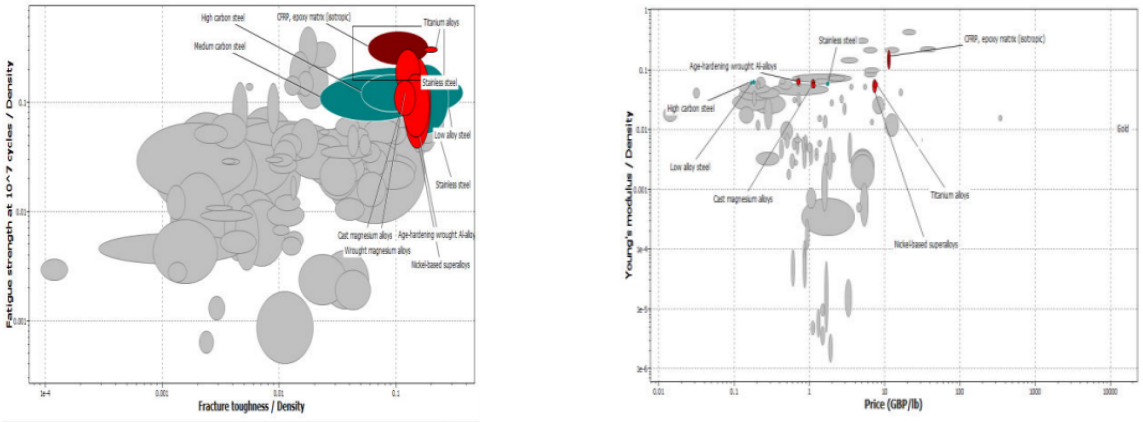

(a) σ_e/ρ variation with K_{1c}/ρ. **(b)** E/ρ variation with price.

Figure 11.4: Materiel comparison [41].

Figure 11.4 shows that the cast magnesium alloys, carbon steel, nickel based super alloys, titanium alloys are suitable for frontal fan blades. However, due to their low safety of margin, Carbon steel, and nickel based super alloys can not be considered. Hence, titanium alloys are the most suitable for the frontal fan blades [41].

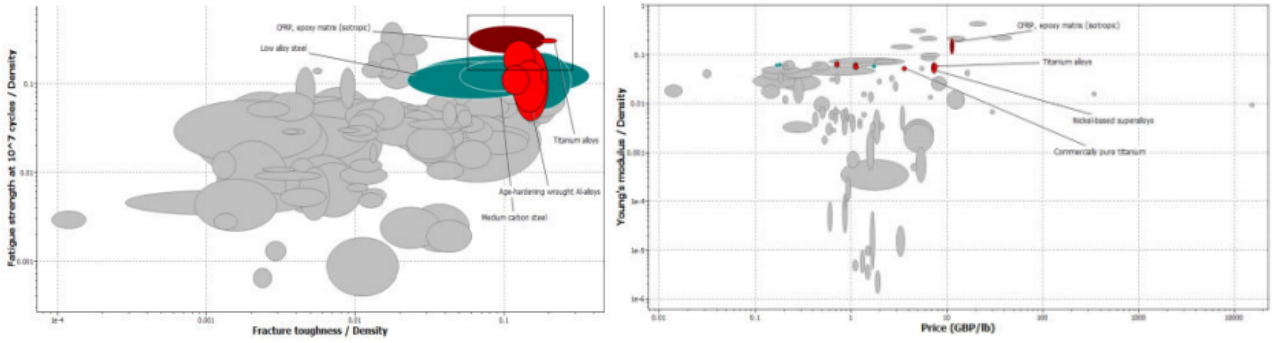

(a) σ_e/ρ variation with K_{1c}/ρ. **(b)** E/ρ variation with price.

Figure 11.5: Meterial comparison [41].

The Figure 11.5 shows that, CFRP (Carbon Fiber Reinforced Polymer) materials are the most ideal materials for frontal fan blade. .

A comparison between Ti-6Al-4V and CFRP is given in the Table 11.5 [41]. From this table it is noted that the CFRP is much more enhanced when compared to the Ti-6Al-4V. Thus, the CFRP has been selected to be used in frontal fan blades.

Table 11.5: Comparison between Ti-6Al-4V with CFRP[41]

Material Properties	Ṫi-6Al-4V	CFRP
Yield Strength(Pa)	1.09×10^8	5.5×10^8
Tensile Strength(Pa)	1.16×10^8	15.2×10^8
Compressive Strength (Pa)	1.74×10^8	6.3×10^8
Fatigue Strength at 10^7 cycles (Pa)	8.54×10^8	21.4×10^8
Melting Point (Celsius)	1.25×10^3	3.82×10^3
Density (kg/m^3)	1.476×10^3	9.36×10^3

By characterizing the materials according to their damage tolerance, ductility, high cycle fatigue (HCF) strength, and yield strength, suitable materials can be found for the fan blade. Reduced weight in a fan blade inherently means that lighter supporting structures become feasible including disks, bearings, and bearing supports, which in turn can affect aircraft structures such as pylons, wings, and the fuselage. GE, PW and RR typically use titanium-based materials in the fan blades. Recently, GE has started using composite materials and PW uses hybrid-metallic construction [41].

Titanium, composites and metal-matrix composites, hybrid-metallic materials are used in fan blades. When the composites are used as the fan blade material, it can reduce the overall engine weight up to 1000 lbs. Since reducing weight has a significant effect on the aircraft, GE-GEnx engine is uses composite materials for the fan blades. Also, metal matrix composites are too expensive for wider applications in fan blades. However, titanium is better in resisting damage, and withstanding lightness when compared to others and has improved strength. On the other hand, hybrid-metallic structures became popular in the fabrication of fan blades and are developed by PW to provide both weight and structural benefits. Unlike composite materials, hybrid-metallic materials are easier to fabricate into fan blades of any size or dimensions and reduce the cost [41].

Furthermore, titanium is versatile in the fabrication of the fan blades thanks to its metallic properties, availability, ease in fabrication, and low life cycle cost. Fan blades which are made of titanium materials show have shown high performances. Titanium has perfect yield and tensile strength and also has low density. These all result in highest strength to weight ratio in today's technology. Even though steel is as strong as titanium, the fact that titanium has 56% lower density than steel, makes it much more desirable [41].

Finally, the temperatures at the fan inlet, and the outlet, and pressure across the fan are considered along with the cost. When the weight is of concern, Nickel-based alloys are heavier than CMC materials. When the cost is focused, CMCs and SiC are much more expensive [6, 34]. The material selection for the fan blades is decided to be Titanium, specifically Ti-6Al-4V, for the HECTOR engine due to its low density, excellent yield and tensile strength and good protection against FOD (foreign object damage).Table 11.6 shows the properties of the chosen material.

Table 11.6: (Ti-6AL-4V) Chosen Material Properties [6, 34]

Material Properties	Ṫi-6Al-4V
Maximum Service Temperature (R)	1170
Density (lb/in^3)	0.16
Young Modulus (psi)	16.53 x 10^6
Yield Stress (psi)	0.16 x 10^6
Cost ($/lb)	9.1-11.3

11.3.3 HP Compressor Materials

Compressor is the part of the engine where the taken air is compressed, hence temperature increases in the compressor. In the HECTOR engine, according to output of the GasTurb, the total temperature for the inlet is 973 °R, and for the outlet it is 1829 °R. Total pressure at the inlet is 61 psi and 525 psi at the outlet. As the compressor experiences higher temperature values, the selected material for the compressor must be able to withstand these higher temperatures and should have resistance against crack propagation, fatigue and oxidation.

Titanium alloys can be used in the HP compressor disc and blades since it has high strength at high temperatures and has resistance against fatigue, crack propagation and oxidation. The chosen material for the compressor discs might not be suitable for the compressor blades, hence, they can be selected to be of different materials. Ceramic matrix materials and silicon carbide materials can be used thanks to their high strength. However they are more expensive than other high strength materials.

In Figures 11.6, 11.7 and 11.8 evolution of high-temperature capability of titanium alloys from conventional titanium alloys, comparison of mechanical properties of high-temperature titanium alloys and range of yield strength and fracture toughness in conventional titanium alloys, intermetallics, and composites at room temperature and at 1572 R are shown [12].

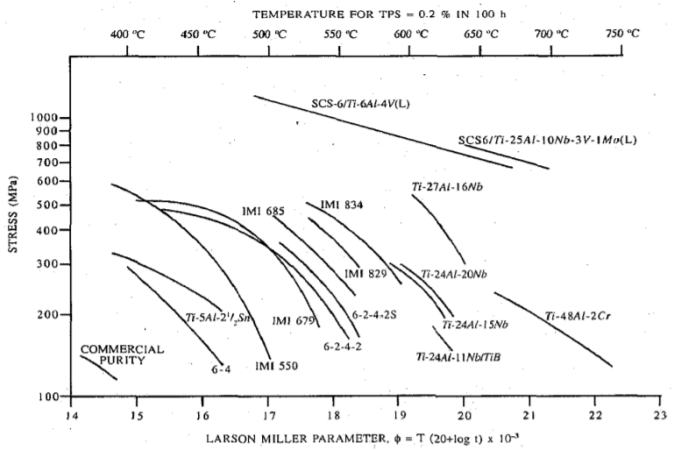

Figure 11.6: Evolution of high-temperature capability of titanium alloys from conventional titanium alloys [12]

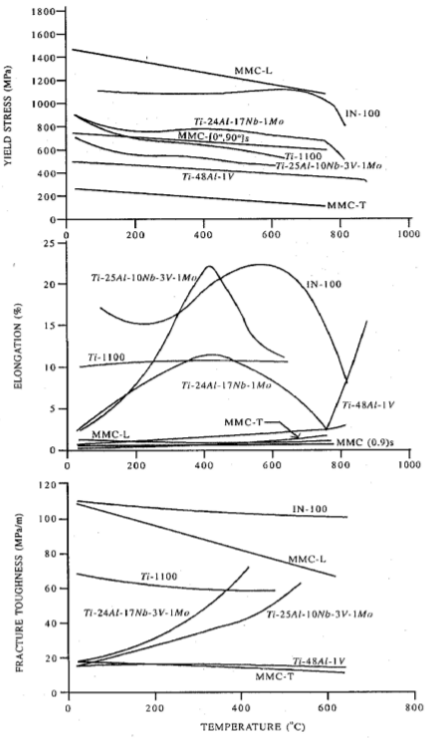

Figure 11.7: Comparison of mechanical properties of high-temperature titanium alloy [12]

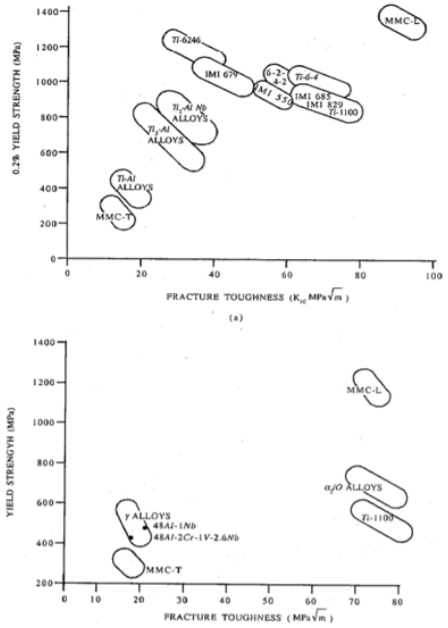

Figure 11.8: Range of yield strength and fracture toughness in conventional titanium alloys, inter metallics, and composites: (a) at room temperature and (b) at 600 °C [12]

As stated in [9], Ti-834 alloy is used for the compressor disc at high level of compression in Rolls Royce engines. Since the maximum service temperature of Ti-834 is 1550 °R, it can be suitable for compressor disc although it can not be used for the compressor blades. Compressor blades need to have a higher maximum service temperature. Ti-45Al-8Nb is chosen as the material of the blades due to its maximum service temperature of 2340°R [12, 11].

In Figures 11.9a and 11.9b, Ti-834 and Ti-45Al-8Nb microstructures are compared.

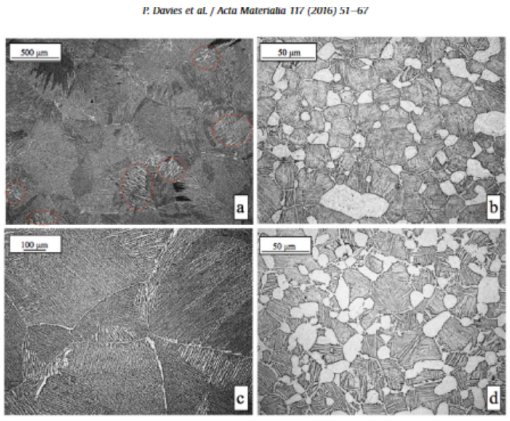

(a) Ti-834 Microstructure [9]

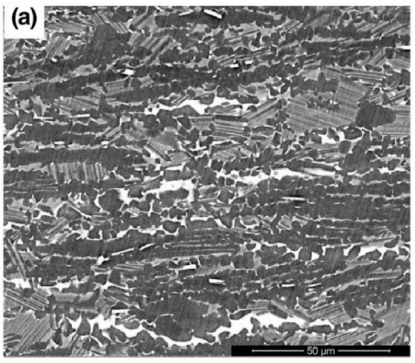

(b) Ti-45Al-8Nb Microstructure [11]

As a result, as shown in Tables 11.7 and 11.8, titanium is decided to be a suitable material for the HP compressor. Namely, Ti-834 is chosen as the material of the compressor disc and Ti-45Al-8Nb is chosen as the material for the compressor blades of the HECTOR engine.

Table 11.7: HP Compressor Disc Material Properties [11]

HP Compressor Disc Material Properties	**Ti-834**
Maximum Service Temperature (R)	1550
Density (lb/in^3)	0.164
Young Modulus (psi)	14.5 x 10^6

Table 11.8: HP Compressor Blade Material Properties [12]

HP Compressor Blade Material Properties	**Ti-45Al-8Nb**
Maximum Service Temperature (R)	2340
Density (lb/in^3)	0.151
Yield Strength (psi)	0.017 x 10^6

11.3.4 Combustion Chamber Materials

Combustion chamber temperature reaches to high levels in the engine. For the HECTOR engine, temperatures at the inlet and the outlet are 1829 °R and 2840 °R respectively. Furthermore, pressures reach 525 psi at the inlet and 499 psi at the outlet. Therefore, material selection has vital importance in combustion chamber walls as they need to resist this high temperatures.

For many years, Inconel (nickel-chromium-iron), nickel based and cobalt-based superalloys are used in combustion chambers by Pratt & Whitney engines. Thanks to its higher temperature and oxidation resistance along with low density, CMC (Ceramic Matrix composites) has started to be widely used in combustion chambers as well. Ceramic Matrix Composites are commonly used in some engines like Trent and LEAP due to its increased engine durability in credible tests [46].

Due to its high temperature resistance, creep and oxidation resistances, SiC Matrix materials are used by NASA for ultra-high temperature applications, such as combustion chamber, and also C/SiC is used because of its higher temperature resistance, lower weight and cost [10].

Silicon Carbide coated with Yttrium-stabilized Zirconium (YSZ) is suitable for the combustion chamber as YSZ can resist high temperatures, up to 2060-2070°R. On the other hand, it is much more expensive than SiC materials. However, it can still be suitable for the combustion chamber as it can reduce the maintenance cost [21].

Consequently, as shown below in Table 11.9, the selected material is C/SiC CMC (hafnium layered) for the combustion chamber of the HECTOR engine. SiC materials have a long lifespan as SiC materials have the highest service temperatures. Therefore, although the initial cost is higher for SiC materials, maintenance cost is less. In addition, Hastelloy X is also deemed to be suitable for the combustion chamber of the HECTOR engine.

Table 11.9: (C/SiC CMC) Chosen Material Properties[39, 31]

Selected Material Properties	**C/SiC CMC**
Maximum Service Temperature (R)	4451.2
Density (lb/in^3)	0.0722
Tensile Strength (psi)	0.79 x 10^6
Cost ($/lb)	104.3

11.3.5 Turbine Materials

The turbine is responsible from generating the power for the other components which are the fan and compressor to provide rotation. Combustion air produced turbine blade rotation and transmit the power to the shaft rotation which goes through four section introduced so far. Therefore, it rotates in a wide operating temperature range. Turbine section is presented to the harshest condition in terms of temperature and pressure, as shown in the Figure D.9. This is why, selection of turbine section materials have to satisfy certain requirements such as high creep strength, high temperature fatigue strength, and high temperature corrosion resistance. Because of their high creep strength, the materials presented at the high pressure and temperature of the turbine are selected as Ni-based superalloys, while the materials in low pressure and temperature sections are chosen as stainless steels, Co-based and Ni-based superalloys.

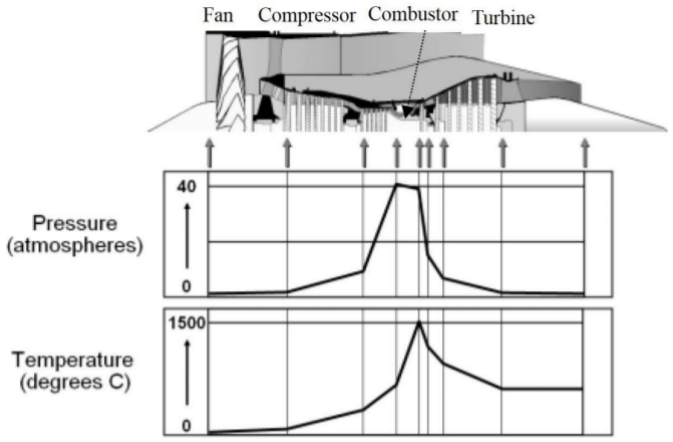

Figure 11.10: Temperature and pressure at which each part of the engine is exposed

Powder metallurgy is an extensive method in manufacturing super alloys, it is especially used for Nickel-based super alloys to produce high strength alloys to be used in turbine discs [36]. As a result, Nickel-based super alloy was decided to be used in turbine disc of the HECTOR engine. In addition, the turbine blade temperature exceeds 2650°R and can reach up to 3200°R in the latest engines. Thus, Zirconia, (ZrO^2), can be used as a thermal barrier coating over Ni-Co-Cr-Al-Y Alloys with high temperature and corrosion resistance to improve the HECTOR engine turbine blade performance. Figure 11.11 shows the design for the turbine blade cooling passages and rough design of thermal barrier coating with Zirconia (ZrO^2), Ni-Co-Cr-Al-Y Alloys and Ni-based super alloy.

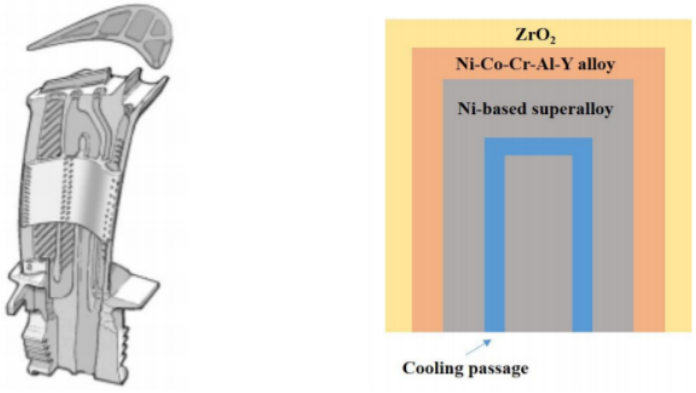

Figure 11.11: Design for turbine blade cooling passages (Left) and Rough design of thermal barrier coating (Right)

For the GEnx-1B, TiAl alloys are chosen for the low pressure turbine stages to reduce weight, and for the high pressure turbine stages are made of Ni-based superalloys such as Rene' N5 manufactured by GE. Although the 4^{th} and 5^{th} generation of superalloys have good properties on temperature and creep strengths, oxidation resistances are low. However, 6^{th} generation superalloys have creep strength at high temperatures and better oxidation resistance. Therefore, for the comparison to select suitable material for the HECTOR, some of different generation materials such as CMSX-10, TMS-138, TMS-196 and TMS 238 are selected. In this comparison,

selection is focused on oxidation, creep resistance, thermal and mechanical strength at high temperatures and pressures. In the following figures, for the CMSX-10, TMS-138, TMS-196 and TMS 238, stress vs LPM graph, cyclic oxidation tests on mass change according to one-hour cycles, metal loss in hot corrosion test, creep rapture life with oxidation resistance are shown [22].

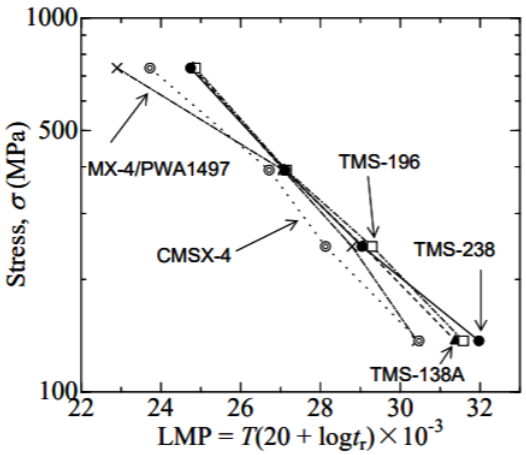

(a) Stress vs LPM Graph[22]

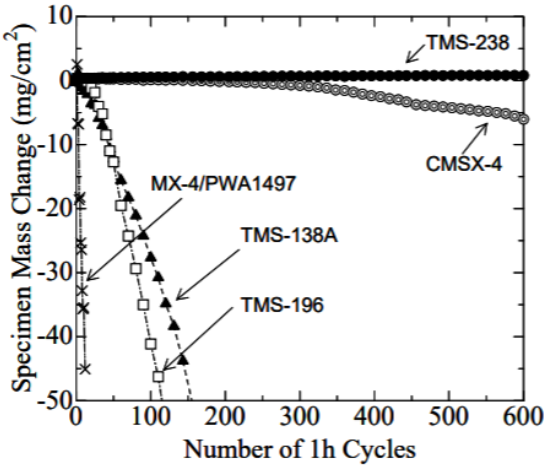

(b) cyclic oxidation tests on mass change according to one-hour cycles[22]

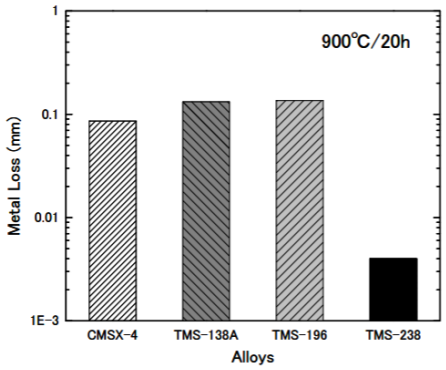

(a) metal loss in hot corrosion test[22]

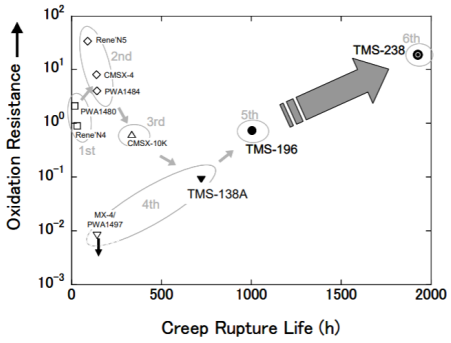

(b) creep rapture life with oxidation resistance[22]

To conclude, after examining the temperature variations, HPT reaches to temperature from 2840°R to 2060°R and LPT reaches from 2060°R to 2043°R, and the pressure across the turbine, HPT reaches from 499 psia to 110 psi, due to its mechanical and environmental properties, better oxidation resistance and hot-corrosion resistance T-238, which is a 5th generation single crystal super alloy, was chosen as the high pressure turbine material for the HECTOR engine.

11.3.6 Mixer Materials

Mixer section is important to increase the thrust produced by engine and to decrease the component noise which is known as the jet noise. Therefore, to reduce the overall engine noise level, absorbent materials are used for the mixer. Absorbent materials are selected to dissipate

the higher frequency noise associated with the flowing fan air.[3]. Moreover, the materials are choosing for the nozzle materials which are Inconel, stainless steel alloys, titanium, Hastelloy X, N155 and CFRPs are also suitable for the mixer materials. For the HECTOR engine, N155 is selected as a mixer material.

11.3.7 Nozzle Materials

One of the most commonly used material is Inconel which is nickel-chromium alloy while designing the nozzle component. This material has resistance to the extreme temperatures, whether exhaust gases are hot or cold. Also, it has excellent capabilities on oxidation and corrosion resistance. Another one is stainless steel alloys which are made of carbon, nickel , chromium, and others. It is highly resistant to the extreme temperatures. Also, it is possible to be improved by adding more nickel and chromium to increase its corrosion resistance. Besides, titanium has high tensile strength to density ratio, companies such as AirBus and Boeing commonly use this material in their newer designs. In addition to these, CFRP (carbon fiber reinforced polymer) and Hastelloy X can be used for the nozzle [36].

As shown below in Table 11.10, GE engines use FSX 414, a GE-patented cobalt base alloy for nozzle designs. When cobalt base alloys are compared to the nickel based alloys, they have superior strength at very high temperatures. Also, cobalt base alloys are compared to X40 and X45, they have a two-three fold oxidation resistance. For the other material selections of nozzle, GTD222 which is the development of GE a nickel based superalloy is higher creep strength compared to FSX414. When resources are done, N155 which is used for later stage nozzles of GE engines is an iron-based superalloy and has good weld ability [36].

Table 11.10: Nozzle Materials[36]

Grade	Chemical composition	Remarks
X40	Co-25Cr10Ni8W1Fe0.5C0.01B	Cobalt-base superalloy
X45	Co-25Cr10Ni8W1Fe0.25C0.01B	Cobalt-base superalloy
FSX414	Co-28Cr10Ni7W1Fe0.25C0.01B	Cobalt-base superalloy
N155	Cr20Ni20Co2.5W3Mo0.20C	Iron-base superalloy
GTD-222	Ni-22.5Cr19Co2.0W2.3Mo1.2Ti0.8Al0.10V 0.008C1.0B	Nickel-base superalloy

This is why, the HECTOR team decided to use N155(Iron-base superalloy) as a nozzle material.

11.3.8 Shaft Materials

Shaft is a rotating member which provides transmission power. Many shafts are made from low-carbon, cold-drawn or hot rolled steel. The selected shaft material has an important effect on the critical speed of the shaft, so its effect on the overall system should not be ignored. Therefore, shaft materials should be chosen before starting the shaft calculations. The shaft should resist high temperatures and be as light as possible so that the rotation is not restricted by the excessive weight is prevented. Also, using high strength materials can dominate over deflection. In Rolls Royce engines, carbon fiber composites are chosen as the material for the shaft due to their high sustainability to stress caused by high speeds [38]. Therefore, heat-treated steel materials such as CMV (Chrome-Molybdenum-Vanadium) is decided for the HECTOR engine.

11.3.9 Bearing Materials

Bearing materials used in the HECTOR engine need to withstand high temperatures. Under high temperature conditions and considering certain mechanical properties such as creep-growth resistance, strength and toughness [40], as explained in the part of Nickel-based super alloys, bearing material is decided as is for the HECTOR engine.

11.4 Engine Vibration Calculation

Due to the weight of the bare machine, internal and external housings will form a complex vibration system with the three rotors and will be included in the range of vibration characteristics. The method used for sub-structuring transfer matrix is therefore to assess and divide the HECTOR into four substructures: low and high pressure compressor, a core machine cabinet, and a bypass case. The sub-structure transfer matrix method is thus applied. The transfer matrix method is divided into ten axial sections for each individual sub-structure (left to right in the airflow direction). Each part of the section is characterized by the four state parameters X, Θ (positive anti-clockwise direction), M (positive rotation axis is positive) and Q (shaft recovery torque is positive), they are characterized on the cross-section displacements, corners, moments and shears 11.1

$$P = \begin{bmatrix} X & \theta & M & Q \end{bmatrix}^T \tag{11.1}$$

By passing on the status parameters of the left section through the shaft section, the parameters of the right section of the shaft shall be calculated. This process of calculation is carried out in a matrix. The geometric and mass characteristics can be used to divide each axis segment into four types. The mass station is integrated with the roulette station, the elastic support station, and the elastic hinge station. In practice, their matrix is combined with the massless sections of the shaft, which are grouped as shown in equation 11.2

$$\begin{bmatrix} T_{11} & T_{12} & T_{13} & T_{14} \\ T_{21} & T_{22} & T_{23} & T_{24} \\ T_{31} & T_{32} & T_{33} & T_{34} \\ T_{41} & T_{42} & T_{43} & T_{44} \end{bmatrix} = \begin{bmatrix} 1 + [\frac{l^3}{6EI}](m\Omega^2 - k) & l(1 + [\frac{l}{2EI}](J\Omega^2) & \frac{l^2}{2EI} + \frac{1}{C_h} & \frac{l^3}{6EI}(1 - v) \\ \frac{l^2}{2EI}(m\Omega^2 - k) & 1 + \frac{l}{EI}(J\Omega^2 + C_v)\frac{l}{EI} + \frac{l}{C_h} & \frac{l^2}{2EI} & \\ l + \frac{l^3(1-v)N}{6EI}(m\Omega^2 - k) & Nl + (1 + \frac{l^2N}{2EI})(J\Omega^2 + C_b) & \frac{Nl}{C\ h} + 1 + \frac{l^2N}{2EI} & l + \frac{l^3(1-v)N}{6EI} \\ m\Omega^2 & 0 & 0 & 1 \end{bmatrix} \tag{11.2}$$

Parameter for 11.2 l **- shaft length,** v **- shear effect coefficient,** m **concentrated weight,** Ω**-precession angle frequency,** k **-elastic support lateral stiffness,** E **- elastic modulus,** I**- section moment of inertia,** J **equivalent moment of inertia,** C_b **angle stiffness of elastic support,** h **- bending stiffness coefficient of hinge,** N **- axis force. When the wheel rotates, the gyro moment is generated shown in below 11.3.**

$$J = (\frac{J_p\omega}{J_d\Omega} - 1)(J_d\Omega) \tag{11.3}$$

The important thing for above equation that when disk thickness H is significantly less than the diameter D (H/D $\lesssim$ 1/4), our 11.3 simply become;

$$J = (\frac{2\omega}{\Omega} - 1)(J_d\Omega) \tag{11.4}$$

Since the elastic support has no angular stiffness, the shear effect and axial force are not taken in comprehensive transfer matrix. In addition to this, we can take $v = 0$, $N = 0$, $C_b = 0$, $1/C_{h0} \to 0$ due to no elastic hinge in the structure. Therefore, the comprehensive shaft transfer matrix become: 11.5

$$T = \begin{bmatrix} 1 + [\frac{l^3}{6EI}](m\Omega^2 - k) & l(1 + [\frac{l}{2EI}](J\Omega^2) & \frac{l^2}{2EI} & [\frac{l^3}{6EI}] \\ \frac{l^2}{2EI}(m\Omega^2 - k) & 1 + \frac{l}{EI}J\Omega^2\frac{l}{EI} & \frac{l^2}{2EI} & \\ l & J\Omega & 1 & l \\ m\Omega^2 & 0 & 0 & 1 \end{bmatrix} \tag{11.5}$$

Doing some mathematical manipulations and assumptions like mass-less free end of length=0, critical speeds and natural frequencies of complex systems can be obtained.

During the selection process of the materials, the moment of inertia I, the length l, elastic modulus E, the mass m, and the polar moment of inertia J of each shaft part and their value of stiffness k are considered. While dealing with the HECTOR engine, these parameters are taken into account where they are supported.

12. Shaft Design

It is important to determine and evaluate the critical locations on the shaft structurally. If the torque along the shaft is assumed to be constant, then the shear stress due to torsion reaches maximum at the outer surfaces [7].

The power transmitted by the Shaft and the rotational speed of the high power and the low power shaft are determined by the analysis done in AxSTREAM and are given below.

Table 12.1: Shaft operating conditions.

Shaft	**Rotational Speed (RPM)**	**Power Transmission (MW)**
LP	8,000 RPM	42.684
HP	12,000 RPM	75.828

First, the basic layout of the components to be driven by the HP and LP shafts is created as shown below.

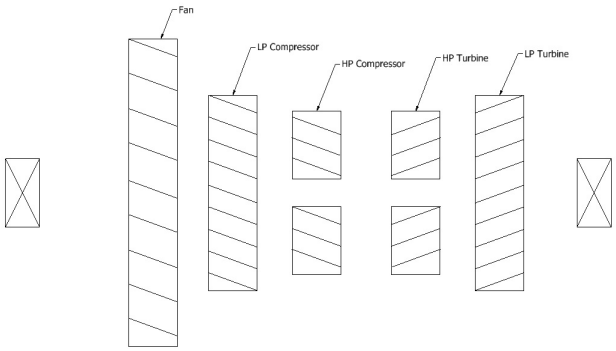

Figure 12.1: The layout of the components.

The factor of safety for the shaft is taken to be, $n = 2$. Then, the torsion on the shaft can be calculated using the information given in the Table 12.1. The bending moment caused by the components is deemed negligible compared to the torsion. The bending moment is in the range of a few newton meters whereas the torsion is in the range of tens of kilo-newton meters. Then, the von Mises stresses are calculated using the following simplified equations [7].

$$\sigma_a^{'} = \sqrt{3}(K_{fs,torsion}\tau_{a,torsion}) \tag{12.1}$$

$$\sigma_m^{'} = \sqrt{3}(K_{fs,torsion}\tau_{m,torsion}) \tag{12.2}$$

Then for torsion, the polar moment of inertia for the LP and HP shaft can be written as follows.

$$J_{LP} = \frac{\pi D_{LP}^4}{32} \tag{12.3}$$

$$J_{HP} = \frac{\pi}{32}(D_{HP}^4 - d_{HP}^4) \tag{12.4}$$

Then the mid range and alternating shear stresses can be written as shown below.

$$\tau_a = K_{fs}\frac{T_a c}{J} \tag{12.5}$$

$$\tau_m = K_{fs}\frac{T_m c}{J} \tag{12.6}$$

For a rotating shaft, the alternating torque is assumed to be insignificant. Thus, only the mid range shear stress plays a role in the calculation of the von Mises stresses. Then, the stress for the LP and HP shaft can be written.

$$(\sigma_m^{'})_{LP} = \sqrt{3}K_{fs}T_m\frac{16}{\pi D_{LP}^3} \tag{12.7}$$

$$(\sigma_m^{'})_{HP} = \sqrt{3}K_{fs}T_m\frac{16D_{HP}}{\pi(D_{HP}^4 - d_{HP}^4)} \tag{12.8}$$

ASME Elliptic Line equation can be written in the simplified form, for no alternating stresses.

$$\frac{n\sigma_{m,max}}{S_y} = 1 \tag{12.9}$$

Using the properties of AISI 1050, the maximum allowed midrange stress is calculated to be 290 MPa. Then, assuming a stress-correction factor of 1.6, the diameter of the LP shaft can be calculated using equation 12.7. Afterwards, assuming that the inner diameter of the HP shaft is almost equal to the outer diameter of the LP shaft, the diameter of the HP shaft is also calculated. The fitting between the HP and the LP shaft is left to be discussed along with the lubrication system.

Table 12.2: Shaft geometry.

Shaft	**Inner Diameter (m)**	**Outer Diameter (m)**
LP	-	0.14
HP	~ 0.14	0.17

13. Engine Noise Attenuation

In a low bypass engine, the exhaust jet is the main source of the noise. As the exhaust jet mixes with the free stream air, created shear between the jet and the atmosphere causes high frequency noise near the exit and low frequency noise downstream. As the high frequency noise is quickly absorbed by the atmosphere, the low frequency noise can be transferred to high frequencies reducing the engine noise [45].

13.1 Nozzle Noise Suppression

By including suppression channels, the mixing rate of the exhaust air to the atmosphere is increased [15]. Hence, the effective velocity difference between the free stream and the exhaust jet is less. As shown in Figure 10.5a, these channels are included in the design. The shape and the size of these channels are arbitrary as it requires extensive CFD analysis to design such channels and quantify their effects.

Furthermore, the internal mixer design as shown in Figure 9.1b increases the mixing rate between the core and the bypass air to allow further reduction the noise.

13.2 Noise Absorption

To reduce the noise of the overall engine, noise absorbing materials can be used. By lining the engine with honeycomb structured materials, the noise is reduced significantly. However, this method increases the weight and skin friction [15]. Since reducing noise is deemed more important then a slight increase in the fuel consumption, it is concluded that the engine design will include such lining materials.

14. Identification and Selection of Engine Subsystems

14.1 Anti-Icing System

The anti-icing system prevents ice formation in the engine and the leading edge of the inlet. These ices can lead to great damage to the engine and parts of the engine. It could be reducing the intake airflow when the inlet parts of the engine freeze, because the ice layer will reduce the intake area of the engine. Because of this happens engine performance reduces. Also, if the ice layer broken due to vibration of the engine, the broken pieces may be sucked into the interior engine that cause the interior parts of the engine such as blades, compressor or all parts to be damaged. Therefore, to prevent the ice formation and built up, Hector will use superhydrophobic coating, electrical system and hot air bleed system. The superhydrophobic coating able to reduce surface free energy and the work of adhesion of substrates by using non-expensive method. The electrical system would help to prevent ice buildup on the outer skin of the cowls on the inlet with heating pads. The hot air bleed system is pumped the hot bleed air which is taken from HPC stages and it distributes the hot air through the parts of the engine that prevents the formation of ice. Then, air exits through small holes in the wing edge. The implementation of the anti-icing system is shown in the Figure 14.1.

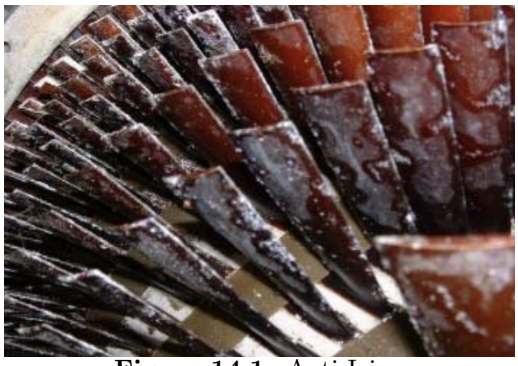

Figure 14.1: Anti-Icing

14.2 Secondary Power System

A secondary power system for an aircraft improve the power quality in the fixed frequency system by utilizing a variable frequency electrical distribution system that provides power to one or more loads that can tolerate distortion components. The secondary power system consists of Auxiliary Power System and Emergency Power System that works together and the controller as an integrated system. The Auxiliary/Emergency Power System is still using from Korean Aerospace Industries with T-50 and T-X. The Auxiliary Power System (APS) provides that the main engine has a self-start capability, power to drive the main aircraft accessories. Emergency Power System provides necessary emergency electric and hydraulic power for aircraft in case of losing the main aircraft accessories by emergency electric power to the EPS using shaft driven electric generator(BSG) and compressed air for the environmental control system(ECS).Schematic diagram of the Auxiliary Power System/Emergency Power System diagram in Figure 14.2

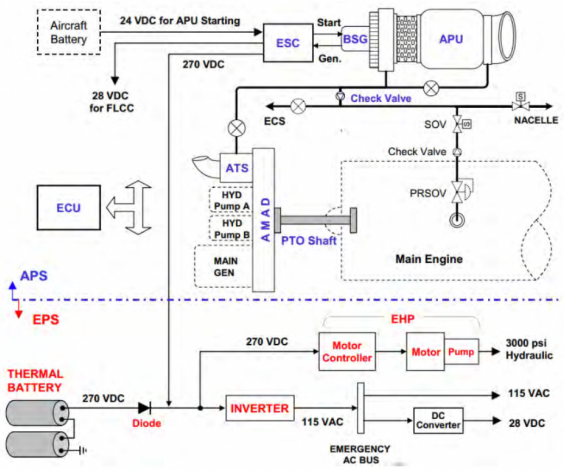

Figure 14.2: Secondary Power System

14.2.1 Auxiliary Power System

The Hector engine is started using an auxiliary power system (APS) which consist of auxiliary power system (APS), an electronic starter controller (ESC), an air turbine starter (ATS), an airframe mounted accessory drive (AMAD), an electronic control unit (ECU), a brushless generator (BSG), flow control valve and airframe mounted accessory drive as you can see in the Figure 14.2.The Auxiliary Power Unit (APU) is a small gas turbine engine which provides both pneumatic and shaft power. By supplying the compressed air from the APU to the ATS via airframe ducting, the APS converts the APU's pneumatic power to the shaft power and delivers the shaft air to the AMAD. Then, to start the main engine and AMAD-mounted accessories, AMAD transfers the shaft power to the power take-off shaft. Thus, main engine starts. In addition, by delivering engine shaft power to the AMAD using PTO shaft to provide primary flight control power for the aircraft. Moreover, Auxiliary Power System helps to decrease the fuel consumption and noise.

14.2.2 Emergency Power System

The Emergency Power System of Hector engine provides hydraulic and electrical emergency power simultaneously in case of shutdown. It works the shaft power of the APU is connected to the EPS when it is needed the DC electric power output of the batteries could be transferred into aircraft for providing hydraulic power.

14.3 Engine Control System

The Engine Control System of Hector engine is FADEC. FADEC control all aspects of aircraft engine performance and it consists of a digital computer, called an electronic engine controller (EEC) or engine control unit (ECU) which is brain of the system. Full Authority Digital Engine Control (FADEC) is the name of the system that manages the aircraft engine. From the first start manages the entire engine independently from start to shut down. Like many technological

developments, the FADEC system is first used in military aviation and then started to be used in civil aviation. It was used in PW4000 engine, firstly. When multiple input variables of the current flight condition are received, FADEC works. Some of the engine operating parameters such as fuel flow, stator vane position, bleed valve position is computed from EEC which analyzed receiving inputs up to 70 times per second. Moreover, FADEC control the engine starting and restarting. The main purpose of the FADEC is achieving optimum engine efficiency for a given flight condition.

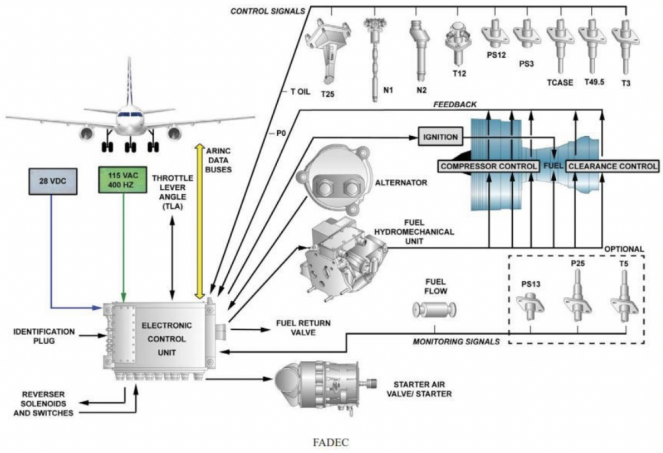

Figure 14.3: FADEC

14.4 Fuel System

The Hector engine use an electronically controlled fuel system with signals from FADEC. The fuel is pumped from the aircraft fuel tanks to a low-pressure system, then, it is transferred to a high-pressure system in order to pressurize the fuel and inject it into the combustor. Both low pressure and high-pressure systems have a filter to ensure high quality fuel. Also, to increase the life of the system and running engine efficiently, these filters play an important role.In case of an emergency, the fuel flow can be run manually and it can work without FADEC.

14.5 Lubrication Systems

Lubrication is critical in any application where moving parts are involved in the engine. The purpose of lubrication are primarily to improve energy efficiency by reducing friction and to improve component lifetime by reducing wear of the moving parts. An additional benefit of an efficient lubrication system is a reduction in engine operating temperature due to heat dissipation from the lubrication system. Commercial jet aircraft lubricants are primarily subjected to the standard SAE-5780.There are different type of specifications such as MIL-PRF-23699 specification which used by U.S. Air Force aircraft for pumpability at lower temperatures and MIL-PRF-23699 which used by Naval aviation for better high temperature properties. Many currently available products use both MIL-PRF-23699 and SAE-5780 specification because they are quite similar. In addition, although similar chemistries are used, changing in basestock composition MIL-PRF-23699 is available in three types, these types and their specifications are given in Table 14.1 Moreover, Additives are very important for all lubrication systems because they can give properties to the general lubricant that the base material does not have. In addition,

they can allow longer lubrication life by eliminating basestock separation modes. Some of the additives are boundary lubrication additives, antioxidants, anti-corrosion additives, anti-foaming additives, metal-deactivators, etc. [20]. Therefore, the HECTOR engine will be use these both specification and additives to increase energy efficiency and component life.

Table 14.1: Common Lubricant Specifications

Specification	Grade or Type	Viscosity (cS at 100°C)	Common Use
MIL-PRF-7808L	Grade 3	3	Best low temperature properties
MIL-PRF-7808L	Grade 4	4	Improved high temperature properties but higher pour point
MIL-PRF-23699	-	5	Good viscosity index, not suitable for very cold climates
MIL-PRF-23699	CI	5	Includes CI for use in maritime environments
MIL-PRF-23699	HTS	5	Best high temperature stability

14.5.1 Shaft Lubrication

The design and the notations of the shaft lubrication system are given below.

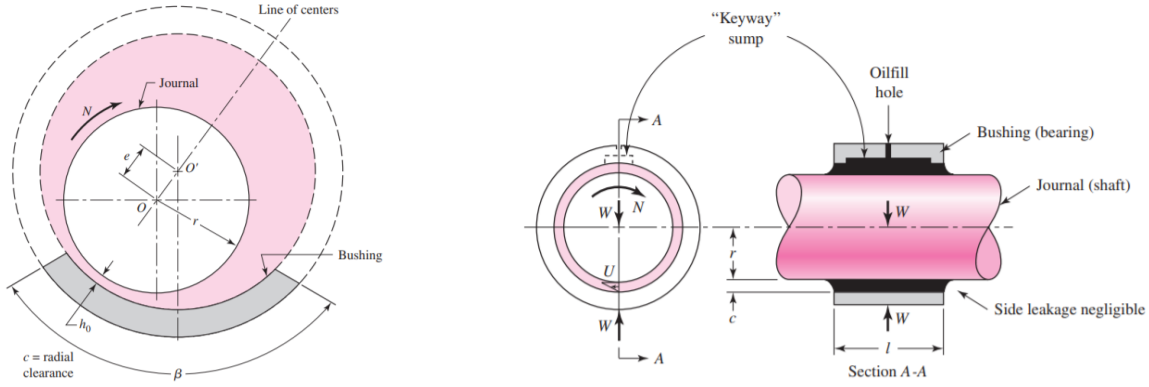

(a) Partial journal bearing.

(b) Petroff's lightly loaded journal bearing.

Figure 14.4: Nomenclature of the journal bearing [7].

Ensuring that thick-film lubrication is achieved is essential for stability. If thick film lubrication is achieved, an increase in temperature results in decrease in viscosity. As the viscosity decreases, the coefficient of friction also decreases in thick film lubrication. Hence, the temperature drops back down until the system is stable again.

On the other hand, if thick film lubrication is not achieved, the decrease in the viscosity results in an increase in the coefficient of friction, further increasing the temperature. This behavior is illustrated below [7].

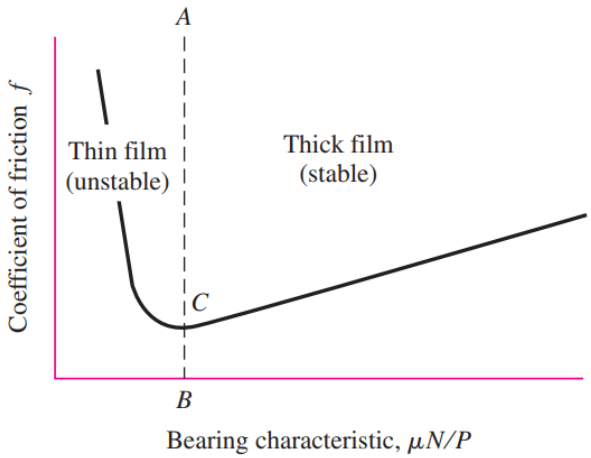

Figure 14.5: Variation of coefficient of friction with bearing characteristics [7].

The design parameters for the lubrication system are,

- The viscosity, μ
- The load per unit of projected bearing area, P
- The speed, N
- The bearing dimensions $r, c, \beta, and l$.

As all the design parameters except radial clearance are already determined, the lubrication system can be designed by optimizing the clearance value to obtain thick film lubrication. As both the journal and the bearing, or HP and LP shaft respectively, is rotating, effective rotational speed of the bearing should be calculated using the, journal angular speed, bearing angular speed, and the load vector angular speed respectively.

$$N = |N_j + N_b - 2N_f| \tag{14.1}$$

The load vector angular speed can be neglected for simplicity. To include the load vector angular speed, one needs to divide the components into sections each containing a single blade. The effective angular speed is then calculated using the values given in Table 12.1 to be $N = 3333.33 rev/s$.

The load on the bearing and the journal is determined using the AxSTREAM outputs and then divided by the projected area of the journal to obtain the bearing pressure $P = 28.028 kPa$.

Then, the only unknown in the Sommerfeld number is the radial clearance. In order to proceed, a fit type should be selected. The different types of fits in the basic hole system are given below [7].

Type of Fit	Description	Symbol
Clearance	*Loose running fit:* for wide commercial tolerances or allowances on external members	H11/c11
	Free running fit: not for use where accuracy is essential, but good for large temperature variations, high running speeds, or heavy journal pressures	H9/d9
	Close running fit: for running on accurate machines and for accurate location at moderate speeds and journal pressures	H8/f7
	Sliding fit: where parts are not intended to run freely, but must move and turn freely and locate accurately	H7/g6
	Locational clearance fit: provides snug fit for location of stationary parts, but can be freely assembled and disassembled	H7/h6
Transition	*Locational transition fit:* for accurate location, a compromise between clearance and interference	H7/k6
	Locational transition fit: for more accurate location where greater interference is permissible	H7/n6
Interference	*Locational interference fit:* for parts requiring rigidity and alignment with prime accuracy of location but without special bore pressure requirements	H7/p6
	Medium drive fit: for ordinary steel parts or shrink fits on light sections, the tightest fit usable with cast iron	H7/s6
	Force fit: suitable for parts that can be highly stressed or for shrink fits where the heavy pressing forces required are impractical	H7/u6

Figure 14.6: Fits using the basic hole system [7].

For the HECTOR, considering the temperature variation along the shaft, the journal pressures, and the rotational speeds, either free running fit or close running fit is considered suitable. To select one of the two, the performance of the lubrication must be analyzed and compared. The tolerance and the fit, using basic hole system, can be calculated using the following equations [7].

$$D_{max} = D + \Delta D \tag{14.2}$$

$$D_{min} = D \tag{14.3}$$

$$d_{max} = d + \delta_F \tag{14.4}$$

$$d_{min} = d + \delta_f - \Delta d \tag{14.5}$$

The tolerance grade is found from the tables provided in [7] to be,

- 0.040 mm for IT7,
- 0.063 mm for IT8,
- 0.100 mm for IT9.

Then similarly for the fundamental deviations for the shafts are found to be,

- -0.145 mm for d,
- -0.043 mm for f.

Since the basic hole system is used, fundamental deviation for the hole is set to be 0 by definition. Then for free running fit, for the shaft and the hole, the sizes are given.

- $D = 135.4^{+0.100}_{+0.000}$
- $d = 135.4^{-0.145}_{-0.245}$

Similarly, for the close running fit, the tolerances are given below.

- $D = 135.4^{+0.063}_{+0.000}$
- $d = 135.4^{-0.043}_{-0.083}$

Then, the clearance for both of the fit types are calculated along with the radius of the shaft for the worst case scenario.

- $c = 0.145mm$, $r = 135.255mm$ for free running fit,
- $c = 0.043mm$, $r = 135.357mm$ for close running fit.

First, we check the design constraint given in [7] as,

$$\frac{\mu N}{P} \geq 1.7x10^{-6}$$

Then, from Equation 14.5.1 it is noted that the absolute viscosity of the oil should be,

$$\mu \geq 14.32\mu reyn$$

By checking the viscosity measurements provided by [25] it is noted that the required viscosity is achievable if the average lubrication temperature is $T_{avg} \leq 273.15K$.

To further analyze the lubrication medium, the Sommerfeld number is calculated for the free running fit as follows.

$$S = \left(\frac{r}{c}\right)^2 \frac{\mu N}{P} = 0.345$$

Similarly, for the close running fit the Sommerfeld number is calculated to be, $S = 3.930$.

The performance parameters of the lubrication system is then read from the figures provided in [7] and are summarized below.

Table 14.2: Shaft lubrication performance parameters.

Fit Type	**Min. Film Thickness Variable,** $\frac{h_0}{c}$	**Eccentricity Ratio,** ϵ	**Position of Min. Film Thickness,** ϕ **(deg)**	**Coefficienct of Friction Variable,** $\frac{r}{c}f$	**Max. Film Pressure Ratio** $\frac{P}{P_{max}}$
Free Running Fit	0.91	0.08	68	5.8	0.84
Close Running Fit	1	0	70	78	0.85

By checking performance parameters provided in Table 14.2, it is noted that free running fit results in much lower coefficient of friction variable. After this parameter is divided by the radial clearance parameter, free running fit still results in less friction. Although free running fit has nonzero eccentricity, it is still negligible. Other performance parameters are observed to be similar for both. Thus, free running fit is deemed more suitable for the HECTOR. Extended list of performance parameters of the lubrication system is summarized below.

Table 14.3: Extended shaft lubrication performance parameters for free running fit.

Min. Film Thickness Variable, h_0 **(mm)**	**Eccentricity Ratio,** ϵ	**Position of Min. Film Thickness,** ϕ **(deg)**	**Coefficienct of Friction,** f	**Max. Film Pressure** P_{max} **(kPa)**	**Terminating Position of Film** θ_{P_0} **(deg)**	**Position of Max. Film Pressure** $\theta_{P_{max}}$ **(deg)**
0.132	0.08	68	$6.218x10^{-3}$	33.37	100	0

15. Performance Constraint Analysis

Performance constraint analysis shows that the combination of a minimum T_{SL}/W_{TO} as a function of W_{TO}/S needed for each segment to find the solution space for aircraft. Determination of the characteristics of an aircraft in all operations is critical. The constraining equations are developed from the following performance constraints: takeoff distance constraint, landing distance constraint, climb constraint and cruise constraint.

15.1 Drag Polar Estimation

For nearly all of the performance constraints, the drag polar for every flight configuration must be known to proceed. There are five main flight configurations which are the clean configuration (cruise), takeoff with landing gear up or down, and landing with landing gear up or down in total for the supersonic business jet. Using the previously calculated takeoff weight, the drag polar for each of the five main flight configurations of the supersonic business jet operating with the HECTOR can be determined using the techniques outlined in "Airplane Design, Part I: Preliminary Sizing of Airplanes" [44]. The drag polar coefficient for every flight configuration can be seen in the Table 15.1:

Table 15.1: Drag Polar Estimation for Supersonic Business Jet

Flight Configuration	Drag Polar
Low Speed, Clean	$C_D = 0.0219 + 0.1783C_L^2$
Takeoff, Gear Down	$C_D = 0.0669 + 0.1895C_L^2$
Landing, Gear Down	$C_D = 0.1219 + 0.2021C_L^2$
Takeoff, Gear Up	$C_D = 0.0419 + 0.1895C_L^2$
Landing, Gear Up	$C_D = 0.0969 + 0.2021C_L^2$

15.2 Takeoff Distance Constraint

One of the other most important performance constraints to need considering is the take-off distance. The takeoff field length used for the supersonic business jet was selected as 7,500 ft [35]. Thus, the following Equation 15.1 can be utilized to describe the takeoff performance constraint of the supersonic business jet [44]:

$$\left(\frac{T}{W}\right)_{TO} = \frac{4(4+\lambda)}{3(5+\lambda)} + \left[\frac{\frac{0.0447(W/S)_{TO}}{s_{TOG}\rho} + 0.72C_{Do}}{C_{L,max,TO}} + \mu_g\right] \tag{15.1}$$

In this equation, λ represents the bypass ratio of the engine at takeoff, $C_{Lmax,TO}$ (the range of $C_{Lmax,TO}$ for the supersonic business jet given in the [44] are taken into account) is the maximum lift coefficient at takeoff, μ_g is the ground friction coefficient (the value of asphalt as 0.03 taken from [44]) s_{TOG} is the ground run takeoff distance (takeoff field length of 7,500 ft), ρ is the density at sea level on a 27°F standard day, and C_{Do} is the parasite drag coefficient for the takeoff, gears down flight configuration [44].

15.3 Landing Distance Constraint

One of the other most important performance constraints to need considering is landing distance. The takeoff field length used for the supersonic business jet was selected as 7,500 ft [35]. The performance constraint of landing distance is a single value that the wing loading cannot exceed. Thus, the following Equation 15.2 can be utilized to describe the takeoff performance constraint of the supersonic business jet [44]:

$$\frac{W}{S} = \frac{\frac{1}{2}\rho V_{SL}^2 C_{Lmax,L}}{\frac{W_L}{W_{TO}}} \tag{15.2}$$

In this equation, ρ is the density at sea level on a 27°F standard day, V_{SL} is the stall speed during landing, $C_{Lmax,L}$ is the maximum lift coefficient during landing (the range of $C_{Lmax,TO}$ for the supersonic business jet given in the [44] are taken into account), and W_L/W_{TO} is the ratio of landing weight to takeoff weight (selected as 0.80 which is the average of the business jet and supersonic transport airplanes) [44].

15.4 Climb Constraint

One of the other most important performance constraints to need considering is climb constraint. Specifically, the supersonic business jet is sized for climb by FAR 25.121 (OEI), which is a balked landing climb with one engine inoperative [44]. For FAR 25.121 (OEI), the climb gradient (CGR) is constrained as 0.021 (configuration of gear down, approach flaps, take-off thrust on remaining

engines) [44]. With this information, the supersonic business jet climb constraint from FAR 25.121 (OEI) can be described using the Equation 15.3 as follows [44]:

$$\frac{T}{W} = \frac{N}{N-1}\left(\frac{1}{L/D} + CGR\right) \tag{15.3}$$

where N is the number of engines on the aircraft ($N = 2$), L/D is the lift-to-drag ratio in the approach position ($L/D = 9.2$, according to F-104 Starfighter's geometrical characteristics given in the RFP), and CGR is the climb gradient [44].

15.5 Supersonic Cruise Constraint

One of the other most important performance constraints to need considering is supersonic cruise. The supersonic cruise condition is at Mach 2.1 and 40,000 feet, where α, the thrust ratio is found as 1.15 and β, the weight ratio is calculated as 0.959 [32]. Also, for clean configuration K_1 has calculated as 0.1783, and K_2 is taken as 0 to obtain highest performance [32]. Thus, this supersonic cruise constraint can be formulated from a form of Equation 15.4, and is as follows:

$$\frac{T_{SL}}{W_{TO}} = \frac{\beta}{\alpha}\left\{K_1 \frac{\beta}{q}\left(\frac{W_{TO}}{S}\right) + K_2 + \frac{C_{DO} + C_{DR}}{\beta/q\,(W_{TO}/S)}\right\} \tag{15.4}$$

where α is the thrust ratio, β is the weight ratio, q is the dynamic pressure, K_1 is the viscous drag coefficient and C_{D0} is the parasite drag coefficient for the clean configuration according to the drag polar in the Table 15.1.

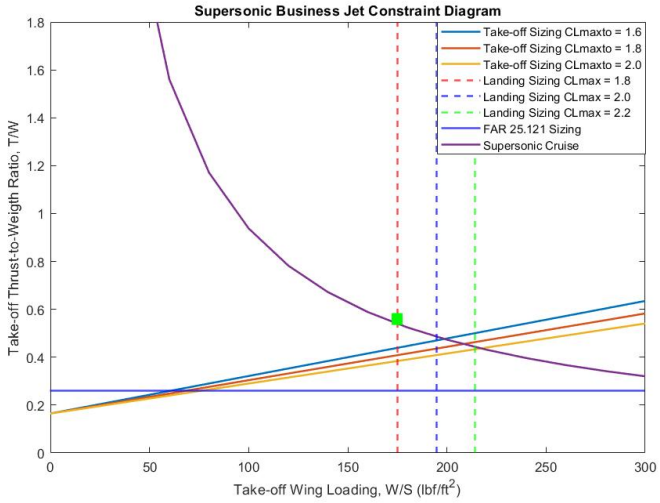

Figure 15.1: Aircraft Constraint Diagram for the Supersonic Business Jet

The green bullet point states that the operating design point in the solution space for the HECTOR engine.

16. Fuel Cost Analysis

Through the use of publicly available data from the Federal Aviation Administration's (FAA) Aerospace Forecasts [18], in the Figure 16.1a is generated to observe the trend in jet fuel prices from 2006 to 2034. The price of jet fuel from 2016 to 2034 are projections that account for economic such as inflation and GDP.

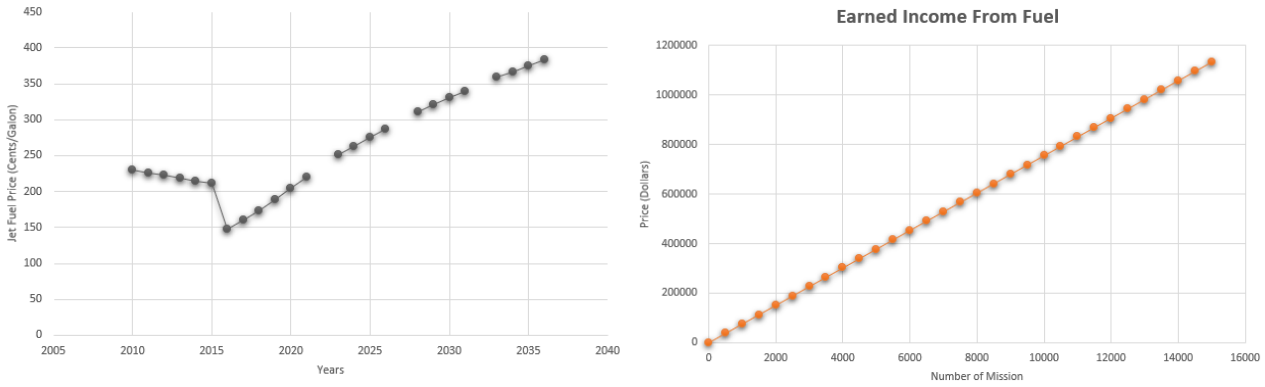

(a) Forecasted Trend of Jet Fuel Prices [18]

(b) Earned Income from Fuel

Figure 16.1: Fuel Cost Analysis

We note from the Figure 16.1a that jet fuel prices are going to cost approximately $3.42 per gallon in the entry- into-service year of 2025 for the supersonic business jet. Through a simple conversion from gallons to pounds (i.e. the density of jet fuel is 6.71 lb/gal), jet fuel is projected to cost $0.51 per pound in 2025. For each mission the HECTOR engine fulfilled, 11,391 gallon fuel is consumed which corresponds to 3,137 $ due to cost analysis. As per the RFP, the fuel consumption of the HECTOR engine is 2.34% less than the expected fuel usage. As seen in the Figure 16.1b, earned income from fuel is increasing persistently during the missions.

Bibliography

[1] F Ahmed. *El-Sayed and Mohamed S.* Emeara, 2016.

[2] GE Aviation. Ge successfully tests world's first rotating ceramic matrix composite material for next-gen combat engine. *General Electric Aviation*, 2015.

[3] Radhakrishna Ayyagari. Gas turbine mixer apparatus for suppressing engine core noise and engine fan noise, March 7 1978. US Patent 4,077,206.

[4] BP Bewlay, S Nag, A Suzuki, and MJ Weimer. Tial alloys in commercial aircraft engines. *Materials at High Temperatures*, 33(4-5):549–559, 2016.

[5] Donald R Boldman. *Heat transfer and boundary layer in conical nozzles.* National Aeronautics and Space Administration, 1972.

[6] H Breme, V Biehl, Nina Reger, and Ellen Gawalt. c metallic biomaterials: Titanium and titanium alloys. In *Handbook of Biomaterial Properties*, pages 167–189. Springer, 2016.

[7] Richard G Budynas and J Keith Nisbett. *Shigley's mechanical engineering design.* McGraw-Hill Education, 2020.

[8] Guang Chen, Yingbo Peng, Gong Zheng, Zhixiang Qi, Minzhi Wang, Huichen Yu, Chengli Dong, and Chain Tsuan Liu. Polysynthetic twinned tial single crystals for high-temperature applications. *Nature materials*, 15(8):876–881, 2016.

[9] P Davies, Robert Pederson, M Coleman, and S Birosca. The hierarchy of microstructure parameters affecting the tensile ductility in centrifugally cast and forged ti-834 alloy during high temperature exposure in air. *Acta Materialia*, 117:51–67, 2016.

[10] J DiCarlo, Nate Jacobson, Maricela Lizcano, and Ram Bhatt. Ultra high temperature (uht) sic fiber. In *NASA Aeronautics Mission Directorate FY11 Seedling Phase I Technical Seminar*, 2012.

[11] Zhihao Du, Kaifeng Zhang, Shaosong Jiang, Ruican Zhu, and Shuguang Li. High temperature mechanical behavior of ti-45al-8nb and its cavity evolution in deformation. *Journal of Materials Engineering and Performance*, 24(10):3746–3754, 2015.

[12] DSPJ Eylon, S Fujishiro, Pamela J Postans, and FH Froes. High-temperature titanium alloys—a review. *JOM*, 36(11):55–62, 1984.

[13] Saeed Farokhi. *Aircraft propulsion.* John Wiley & Sons, 2014.

[14] Monica Ferraris and Valentina Casalegno. Integration and joining of ceramic matrix composites. *Ceramic Matrix Composites: Materials, Modeling and Technology*, pages 549–567, 2014.

[15] Walter R Gordon. Jet noise suppressor nozzle. *The Journal of the Acoustical Society of America*, 73(1):396–396, 1983.

[16] EM Greitzer. Design methodologies for aerodynamics structures weight and thermodynamic cycles, final_report, vol. 2. *ed: MIT, March*, 2010.

[17] Frank Haselbach and Ric Parker. Hot end technology for advanced, low emission large civil aircraft engines. In *28th International Congress of the Aeronautical Sciences*, volume 2, page 3, 2012.

[18] Christy R Hileman, Cheryl A McNeil, and Paul Rogers. Fatal aviation accidents: Fiscal years 2009-2013. Technical report, Federal Aviation Administration, 2015.

[19] Anderson JD. Fundamentals of aerodynamics. *NY: McGraw-Hill*, 1991.

[20] David W. Johnson. Lubricants for turbine engines. *Recent Progress in Some Aircraft Technologies*, 2016.

[21] Yutaka Kagawa and Shuqi Guo. Ultrahigh temperature ceramic-based composites. *Ceramic Matrix Composites: Materials, Modeling and Technology*, pages 273–292, 2014.

[22] Kyoko Kawagishi, An-Chou Yeh, Tadaharu Yokokawa, Toshiharu Kobayashi, Yutaka Koizumi, and Hiroshi Harada. Development of an oxidation-resistant high-strength sixth-generation single-crystal superalloy tms-238. *Superalloys 2012*, pages 189–195, 2012.

[23] J Kurzke. The mission defines the cycle: Turbojet, turbofan and variable cycle engines for high speed propulsion; rto educational notes. Technical report, EN-AVT-185 Lecture, 2010.

[24] Venedikt Kuz'michev, Ilia Krupenich, Evgeny Filinov, and Yaroslav Ostapyuk. Comparative analysis of mathematical models for turbofan engine weight estimation. In *MATEC Web of Conferences*, volume 220, page 03012. EDP Sciences, 2018.

[25] Arno Laesecke, Clemens Junker, and Damian S Lauria. Viscosity measurements of three base oils and one fully formulated lubricant and new viscosity correlations for the calibration liquid squalane. *Journal of Research of the National Institute of Standards and Technology*, 124:1–41, 2019.

[26] Budugur Lakshminarayana. *Fluid dynamics and heat transfer of turbomachinery*. John Wiley & Sons, 1995.

[27] Arthur H Lefebvre and Dilip R Ballal. *Gas turbine combustion: alternative fuels and emissions*. CRC press, 2010.

[28] Robert J Mack. Nacelle integration to reduce the sonic boom of aircraft designed to cruise at supersonic speeds. Technical report, NASA Langley Research Center; Hampton, VA United States, 1999.

[29] Robert J Mack. A supersonic business-jet concept designed for low sonic boom. Technical report, NASA Langley Research Center; Hampton, VA United States, 2003.

[30] Robert J Mack and George T Haglund. A practical low-boom overpressure signature based on minimum sonic boom theory. *High-Speed Research: Sonic Boom, Volume 2*, 1992.

[31] R Mahmood and A Shirooyeh. *Mechanical Properties of Yttria-stabilized Zirconia Ceramics*. PhD thesis, University of Southern California, 2011.

[32] Jack D Mattingly, William H Heiser, and David T Pratt. *Aircraft engine design*. American Institute of Aeronautics and Astronautics, 2002.

[33] AM Mellor. *Design of modern turbine combustors*. Academic Pr, 1990.

[34] ASM Aerospace Specification Metals. Titanium ti-6al-4v (grade 5), asm material data sheet. *Florida, USA: ASM Aerospace Specification Metals Inc*, 2004.

[35] Nigel Moll. Civil supersonic. *Aviation International News*, 2017.

[36] Nageswara Rao Muktinutalapati. Materials for gas turbines–an overview. *Advances in gas turbine technology*, 23, 2011.

[37] Tomohiro Naruse, Toshio Hattori, Haruo Miura, and Kazuki Takahashi. Evaluation of thermal degradation of unidirectional cfrp rings. *Composite structures*, 52(3-4):533–538, 2001.

[38] Ruediger Oessenich, Andreas Freund, Mirko Filler, Ole Renner, and Alexander Pabst. Shaft of a gas-turbine engine, in particular a radial shaft or a shaft arranged at an angle to the machine axis, December 22 2015. US Patent 9,217,463.

[39] Jeanne F Petko, James Douglas Kiser, Mike Verilli, Terry McCue, and Hugh R Gray. Characterization of c/sic ceramic matrix composites (cmcs) with novel interface fiber coatings. Technical report, NASA Glenn Research Center, Cleveland, OH United States, 2002.

[40] Tresa M Pollock and Sammy Tin. Nickel-based superalloys for advanced turbine engines: chemistry, microstructure and properties. *Journal of propulsion and power*, 22(2):361–374, 2006.

[41] Srijith Bangaru Thirumalai Raj. Advanced material for front fan blade manufacturing. *variations*, 1:2, 2017.

[42] Daniel Raymer. *Aircraft design: a conceptual approach*. American Institute of Aeronautics and Astronautics, Inc., 2012.

[43] Fan Renyu and Zhang Man. Low emission commercial aircraft engine combustor development in china: From airworthiness requirements to combustor design. *Procedia Engineering*, 17:618–626, 2011.

[44] Jan Roskam. *Airplane Design: Preliminary configuration design and integration of the propulsion system*. DARcorporation, 1985.

[45] Claire Soares. *Gas turbines: a handbook of air, land and sea applications*. Elsevier, 2011.

[46] Andrew Sommers, Qin Wang, Xiaohong Han, Christophe T'Joen, Y Park, and Anthony Jacobi. Ceramics and ceramic matrix composites for heat exchangers in advanced thermal systems—a review. *Applied Thermal Engineering*, 30(11-12):1277–1291, 2010.

[47] Robert Tacina. Low no (x) potential of gas turbine engines. In *28th Aerospace Sciences Meeting*, page 550, 1990.

[48] Philip P Walsh and Paul Fletcher. *Gas turbine performance*. John Wiley & Sons, 2004.

[49] Fude Wang. Mechanical property study on rapid additive layer manufacture hastelloy® x alloy by selective laser melting technology. *The International Journal of Advanced Manufacturing Technology*, 58(5-8):545–551, 2012.

[50] Po-Wenn Wu, Yeng-Yung Tsui. Effects of lobe geometry on the mixing flow in multilobe mixers. *Numerical Heat Transfer: Part A: Applications*, 39(1):61–77, 2001.

[51] M Yamaguchi. High temperature intermetallics–with particular emphasis on tial. *Materials science and technology*, 8(4):299–307, 1992.

[52] Bing Yu, Rongcheng Miao, and Wenjun Shu. A rapid method for modeling a variable cycle engine. *JoVE (Journal of Visualized Experiments)*, 150:e59151, 2019.

[53] SJ Zinkle and LL Snead. Thermophysical and mechanical properties of sic/sic composites. Technical report, Oak Ridge National Lab., TN (United States), 1998.

Appendix A: Inlet Design Code (first page only)

```
%% This program is written by the METU - HECTOR team
%% AIAA Foundation Student Engine Design Competition 2019-2020
%% Undergraduate Team - Engine
%% Candidate Engines for a Supersonic Business Jet

clc
clear all
close all

%% Design Parameters
M_inf          = 2.1; %Freestream Mach Number
p0             = 18822.6873744; %Absolute air pressure at 40,000 ft (Pa)
gamma          = 1.4;
p_inf          = p0*((1 + (gamma - 1)/2*(M_inf^2))^ ...
                   (-gamma/(gamma - 1))); %Freestream pressure (Pa)
N              = 13;
theta_1(:,1,1) = linspace(1,N,N)/180*pi;  %Deflection angle of Ramp 1 (rad)
theta_2(1,:,1) = linspace(1,N,N)/180*pi; %Deflection angle of Ramp 2 (rad)
M_fan_inlet    = 0.619;
A_fan          = 1.06786238; %m^2

%% Freestream to Region 1 - Oblique Shock
for i = 1:N %theta_1
    beta_1(i,1,1) = fzero(@(beta) 2*cot(beta)*((M_inf^2)* ...
                    (sin(beta)^2)-1)/((M_inf^2)*(gamma+cos(2*beta))+2) ...
                    -tan(theta_1(i,1,1)),[theta_1(i,1,1),1]);
    M_ninf(i,1,1) = M_inf*sin(beta_1(i,1,1));
    M_n1(i,1,1)   = sqrt((1 + (gamma - 1)/2*(M_ninf(i,1,1)^2)) ...
                    /(gamma*(M_ninf(i,1,1)^2) - (gamma - 1)/2));
    M_1(i,1,1)    = M_n1(i,1,1)/sin(beta_1(i,1,1) - theta_1(i,1,1));
    p_1(i,1,1)    = p_inf*(1 + (2*gamma)/(gamma + 1)* ...
                    ((M_ninf(i,1,1)^2) - 1));
    p_01(i,1,1)   = p_1(i,1,1)*((1 + (gamma - 1)/2*(M_1(i,1,1)^2))^ ...
                    (gamma/(gamma - 1)));
end

%% Region 1 to Region 2 - Oblique Shock
for i = 1:N %theta_1
    for j = 1:N %theta_2
        beta_2(i,j,1) = fzero(@(beta) 2*cot(beta)*((M_1(i,1,1)^2) ...
                        *(sin(beta)^2)-1)/((M_1(i,1,1)^2)* ...
                        (gamma+cos(2*beta))+2)- ...
                        tan(theta_2(1,j,1)),[theta_2(1,j,1),1]);
        M_n1(i,j,1)   = M_1(i,1,1)*sin(beta_2(i,j,1));
        M_n2(i,j,1)   = sqrt((1 + (gamma - 1)/2*(M_n1(i,j,1)^2))/ ...
                        (gamma*(M_n1(i,j,1)^2) - (gamma - 1)/2));
        M_2(i,j,1)    = M_n2(i,j,1)/sin(beta_2(i,j,1) - theta_2(1,j,1));
        p_2(i,j,1)    = p_1(i,1,1)*(1 + (2*gamma)/(gamma + 1) ...
                        *((M_n1(i,j,1)^2) - 1));
        p_02(i,j,1)   = p_2(i,j,1)*((1 + (gamma - 1)/2*(M_2(i,j,1)^2)) ...
                        ^(gamma/(gamma - 1)));
    end
end

%% Region 2 to Region 3 - Normal Shock
for i = 1:N
    for j = 1:N
        M_3(i,j,1)  = sqrt((1 + (gamma - 1)/2*(M_2(i,j,1)^2)) ...
                      /(gamma*(M_2(i,j,1)^2) - (gamma - 1)/2));
        p_3(i,j,1)  = p_2(i,j,1)*(1 + (2*gamma)/(gamma + 1)* ...
```

Appendix B: Nozzle Design GUI (first page only)

```
%% This program is written by the METU - HECTOR team
%% AIAA Foundation Student Engine Design Competition 2019-2020
%% Undergraduate Team - Engine
%% Candidate Engines for a Supersonic Business Jet

classdef Nozzle_Design < matlab.apps.AppBase

    % Properties that correspond to app components
    properties (Access = public)
        UIFigure                        matlab.ui.Figure
        TabGroup                        matlab.ui.container.TabGroup
        Tab                             matlab.ui.container.Tab
        LabelNumericEditField           matlab.ui.control.Label
        M_inlet                         matlab.ui.control.NumericEditField
        LabelNumericEditField2          matlab.ui.control.Label
        T_inlet                         matlab.ui.control.NumericEditField
        Label                           matlab.ui.control.Label
        p_inlet                         matlab.ui.control.NumericEditField
        Label2                          matlab.ui.control.Label
        D_inlet                         matlab.ui.control.NumericEditField
        LabelNumericEditField5          matlab.ui.control.Label
        N_dens                          matlab.ui.control.NumericEditField
        LabelNumericEditField6          matlab.ui.control.Label
        R_exp                           matlab.ui.control.NumericEditField
        LabelNumericEditField7          matlab.ui.control.Label
        M_exit                          matlab.ui.control.NumericEditField
        LabelNumericEditField8          matlab.ui.control.Label
        L_inlet                         matlab.ui.control.NumericEditField
        LabelNumericEditField9          matlab.ui.control.Label
        Gamma                           matlab.ui.control.NumericEditField
        Mesh                            matlab.ui.control.UIAxes
        RunButton                       matlab.ui.control.Button
        StatusTextAreaLabel             matlab.ui.control.Label
        StatusTextArea                  matlab.ui.control.TextArea
        OperatingConditionLabel         matlab.ui.control.Label
        Altitude                        matlab.ui.control.DropDown
        Tab2                            matlab.ui.container.Tab
        M_cont                          matlab.ui.control.UIAxes
        T_cont                          matlab.ui.control.UIAxes
        p_cont                          matlab.ui.control.UIAxes
        d_cont                          matlab.ui.control.UIAxes
        PerformanceParametersTab        matlab.ui.container.Tab
        ThroatDiametermEditFieldLabel   matlab.ui.control.Label
        ThroatDiameter                  matlab.ui.control.NumericEditField
        ExitDiametermLabel              matlab.ui.control.Label
        ExitDiameter                    matlab.ui.control.NumericEditField
        ExitPressureatmLabel            matlab.ui.control.Label
        ExitPressure                    matlab.ui.control.NumericEditField
        TotalExitPressureatmLabel       matlab.ui.control.Label
        TotalPressure_Exit              matlab.ui.control.NumericEditField
        ExitVelocitymsLabel             matlab.ui.control.Label
        ExitVelocity                    matlab.ui.control.NumericEditField
        MassFlowRatekgsLabel            matlab.ui.control.Label
        m_dot                           matlab.ui.control.NumericEditField
        GrossThrustkNLabel              matlab.ui.control.Label
        SteadyThrust                    matlab.ui.control.NumericEditField
        AtmosphericPressureatmEditFieldLabel  matlab.ui.control.Label
        AtmosphericPressure             matlab.ui.control.NumericEditField
        NTPRLabel                       matlab.ui.control.Label
        NTPR                            matlab.ui.control.NumericEditField
        NPRLabel                        matlab.ui.control.Label
```

Appendix C: GasTurb Simulations

Appendix C1: Baseline Engine Validation

Station	W lb/s	T R	P psia	WRstd lb/s
amb		518,67	14,696	
2	479,001	518,67	14,696	479,000
13	301,594	650,06	29,392	168,819
21	177,408	623,79	26,453	108,087
22	177,408	623,79	26,453	108,087
24	177,408	853,05	74,068	45,142
25	177,408	853,05	72,586	46,063
3	172,086	1312,60	308,493	13,041
31	152,571	1312,60	308,493	
4	155,431	2492,00	293,068	17,084
41	164,301	2432,72	293,068	17,843
43	164,301	1997,56	117,720	
44	174,946	1958,22	117,720	
45	179,677	1937,77	114,225	44,682
49	179,677	1453,88	32,263	
5	180,268	1453,02	32,263	137,438
6	180,268	1453,02	31,940	
16	301,594	650,06	28,657	
64	481,862	962,79	29,778	
8	481,862	962,79	29,778	323,998
Bleed	0,000	1312,60	308,493	

Efficiencies:	isentr	polytr	RNI	P/P
Outer LPC	0,8622	0,8749	1,000	2,000
Inner LPC	0,9000	0,9079	1,000	1,800
IP Compressor	0,9197	0,9303	1,445	2,800
HP Compressor	0,9010	0,9180	2,730	4,250
Burner	0,9995			0,950
HP Turbine	0,9219	0,9136	3,271	2,490
LP Turbine	0,9268	0,9151	1,654	3,540
Mixer	0,6000			

HP Spool mech Eff 0,9800 Nom Spd 14372 rpm
LP Spool mech Eff 0,9900 Nom Spd 6482 rpm
P22/P21=1,0000 P25/P24=0,9800 P45/P44=0,9703

hum [%]	war0	FHV	Fuel
0,0	0,00000	18552,4	Generic

FN	= 21699,31	lb
TSFC	= 0,4745	lb/(lb*h)
WF	= 2,8601	lb/s
s NOX	= 0,5982	
Core Eff	= 0,4370	
Prop Eff	= 0,0000	
BPR	= 1,7000	
P2/P1	= 1,0000	
P3/P2	= 20,99	
P5/P2	= 2,1953	
P16/P13	= 0,9750	
P16/P6	= 0,89722	
P16/P2	= 1,95000	
P6/P5	= 0,99000	
P63/P6	= 1,00000	
P163/P16	= 1,00000	
XM63	= 0,56095	
XM163	= 0,37698	
XM64	= 0,46030	
A64	= 1352,51	in²
WBld/W2	= 0,00000	
A8	= 987,26	in²
CD8	= 0,96000	
XM8	= 1,00000	
PWX	= 100,0	hp
WBLD/W22	= 0,00000	
Wreci/W25=	0,00000	
Loading	= 100,00	%
e444 th	= 0,89002	
WBLD/W25	= 0,00000	
WCHN/W25	= 0,05000	
WCHR/W25	= 0,06000	
WCLN/W25	= 0,02667	
WCLR/W25	= 0,00333	
WLkBy/W25=	0,00000	

Figure C.1: Baseline Engine Validation

Mixed Flow Turbofan

Description		Point 1 Case 1	Point 2 Case 2	Point 3 Case 3	Point 4 Case 4
Number of Iteration Loops		1.1	16.1	35.1	53.1
Altitude	ft	40000	40000	40000	40000
Delta T from ISA	R	27	27	27	27
Relative Humidity [%]		0	0	0	0
Mach Number		0,98	1,15	2,1	2,4
Overboard Bleed	lb/s	0	0	0	0
Power Offtake	hp	100	100	100	100
Net Thrust	lb	5040,35	5253,23	3568,33	1360,59
Gross Thrust	lb	10247,7	12344,7	34517	50513,3
Sp. Fuel Consumption	lb/(lb*h)	0,781932	0,821879	1,71351	5,08201
Specific Thrust	ft/s	949,822	853,027	242,448	66,5223
Handling Bleed WB hdl/W22		0	0	0	0
Total Rel. Overb. Bld W bld		0	0	0	0
Fuel Flow	lb/s	1,09478	1,19931	1,69844	1,9207
Overall Pressure Ratio P3/P		22,4771	20,4749	8,18636	6,22249
HPT Pressure Ratio		2,47707	2,47806	2,43416	2,38497
LPT Pressure Ratio		3,61054	3,51852	2,60359	2,34403
Isentr. Inner LPC Efficienc		0,878715	0,910918	0,936268	0,900021
Polytr. Inner LPC Efficienc		0,88883	0,917886	0,938235	0,902006
Isentr. Outer LPC Efficienc		0,841818	0,872669	0,896954	0,862229
Polytr. Outer LPC Efficienc		0,857148	0,884283	0,90081	0,865537
Isentr. IPC Efficiency		0,882627	0,918012	0,98885	0,975947
Polytr. IPC Efficiency		0,898224	0,928638	0,989784	0,977694
Isentr. HPC Efficiency		0,899037	0,90239	0,905768	0,900618
Polytr. HPC Efficiency		0,916627	0,919129	0,919826	0,914088
Overall Compression Efficie		0,858717	0,885475	0,923894	0,91341
Isentropic HPT Efficiency		0,920484	0,920971	0,922302	0,922689
Polytropic HPT Efficiency		0,912098	0,912615	0,914206	0,914811
Thermodyn. HPT Efficiency		0,889541	0,889387	0,886558	0,884596
Isentropic LPT Efficiency		0,9167	0,918295	0,916444	0,914051
Polytropic LPT Efficiency		0,903283	0,905382	0,906652	0,905269
Overall Expansion Efficienc		0,915718	0,916984	0,918873	0,918618
Ambient Pressure Pamb	psia	2,72002	2,72002	2,72002	2,72002
Ram Pressure P1	psia	5,0324	6,18655	24,8999	39,8658
Inlet Temperature T2	R	497,226	527,485	783,426	894,278
Inlet Pressure P2	psia	5,0324	6,18655	24,8999	39,8658
Inlet static Pressure Ps2	psia	4,10299	5,12487	22,9006	37,1512

Figure C.2: Baseline Engine Off Design Missions

Appendix C2: HECTOR Engine GasTurb Results

Station	W lb/s	T R	P psia	WRstd lb/s
amb		389,97	2,720	
1	692,717	733,50	24,894	
2	692,717	733,50	24,894	486,300
13	154,104	1029,56	74,270	42,962
21	538,613	973,43	61,869	175,271
25	538,613	973,43	61,250	177,041
3	527,841	1829,49	525,390	27,729
31	514,375	1829,49	525,390	
4	523,076	2840,00	499,120	36,039
41	528,462	2830,27	499,120	36,347
43	528,462	2062,50	110,916	
44	533,848	2060,24	110,916	
45	542,825	2043,66	109,807	144,207
49	542,825	1757,78	55,148	
5	544,620	1755,35	55,148	266,993
6	544,620	1755,35	54,045	
16	154,104	1029,56	72,413	
64	698,724	1603,54	55,999	
8	698,724	1603,54	55,999	322,414
Bleed	2,693	1829,49	525,390	

Efficiencies:	isentr	polytr	RNI	P/P
Outer LPC	0,8841	0,9000	1,121	2,983
Inner LPC	0,8868	0,9000	1,121	2,485
HP Compressor	0,8698	0,9000	1,969	8,578
Burner	0,9995			0,950
HP Turbine	0,9152	0,9000	4,687	4,500
LP Turbine	0,9074	0,9000	1,496	1,991
Mixer	0,6000			

HP Spool mech Eff 0,9900 Nom Spd 12000 rpm
LP Spool mech Eff 0,9800 Nom Spd 8000 rpm

P2/P1= 1,0000 P25/P21=0,9900 P45/P44= 0,9900
Con-Di Nozzle:
A9*(Ps9-Pamb) 5229,912

FN	=	28567,02	lb
TSFC	=	1,0964	lb/(lb*h)
WF Burner	=	8,70016	lb/s
s NOX	=	3,2428	
BPR	=	0,2861	
Core Eff	=	0,6504	
Prop Eff	=	0,7581	
P3/P2	=	21,105	
P16/P6	=	1,33987	
A63	=	1229,58	in²
A163	=	134,27	in²
A64	=	1363,86	in²
XM63	=	0,42530	
XM163	=	0,79292	
XM64	=	0,46030	
P63/P6	=	1,00000	
P163/P16	=	1,00000	
A8	=	1003,25	in²
CD8	=	0,95000	
Ang8	=	25,00	°
P8/Pamb	=	20,58780	
WLkBy/W25	=	0,00000	
WCHN/W25	=	0,01000	
WCHR/W25	=	0,01000	
Loading	=	100,00	%
WCLN/W25	=	0,01667	
WCLR/W25	=	0,00333	
WBHD/W21	=	0,00000	
far7	=	0,01261	
WBLD/W25	=	0,00500	
PWX	=	100,0	hp
P16/P13	=	0,9750	
P6/P5	=	0,9800	
A9/A8	=	2,00000	
CFGid	=	0,98252	

Figure C.3: HECTOR Engine Design Point Output

	Units	St 2	St 21	St 25	St 3	St 4	St 44	St 45	St 5	St 6	St 13	St 16	St 64	St 8	St 9
Mass Flow	lb/s	692,717	538,613	538,613	527,841	523,076	533,848	542,825	544,62	544,62	154,104	154,104	698,724	698,724	698,724
Total Temperature	R	733,497	973,428	973,428	1829,49	2840	2060,24	2043,66	1755,35	1755,35	1029,56	1029,56	1603,54	1603,54	1603,54
Static Temperature	R	681,759	910,713	920,203	1826,44	2823,23	1955,49	1965,79	1707,15	1698,69	1015,46	1009,25	1547,75	1367,58	866,173
Total Pressure	psia	24,8945	61,8687	61,25	525,39	499,12	110,916	109,807	55,1476	54,0446	74,2697	72,413	55,9993	55,9993	55,9993
Static Pressure	psia	19,239	48,6124	49,9671	521,898	486,372	89,2658	93,4046	49,2848	47,3403	70,8535	67,3744	48,7063	30,0456	5,46368
Velocity	ft/s	791,239	883,17	813,61	204,591	501,498	1223,41	1055,04	817,53	886,364	418,698	502,514	868,555	1780,29	3100,32
Area	in²	1655,19	809,56	650,444	481,713	323,013	510,02	577,707	1231,1	1176,28	282,223	245,088	1363,86	953,091	1906,18
Mach Number		0,619	0,6	0,55	0,1	0,2	0,58127	0,5	0,414084	0,45	0,27	0,325	0,4603	1	2,1636
Density	lb/ft³	0,076166	0,144072	0,146559	0,771344	0,464864	0,125203	0,128247	0,077922	0,07522	0,167794	0,16018	0,084938	0,059298	0,017025
Spec Heat @ T	BTU/(lb*R)	0,242519	0,248153	0,248153	0,27341	0,303599	0,286308	0,285802	0,278361	0,278361	0,249755	0,249755	0,272475	0,272475	0,272475
Spec Heat @ Ts	BTU/(lb*R)	0,241791	0,246362	0,246633	0,273338	0,300163	0,28384	0,282983	0,276969	0,276725	0,249353	0,249175	0,270732	0,264947	0,248931
Enthalpy @ T	BTU/lb	47,4785	106,358	106,358	329,857	631,908	402,463	397,566	316,159	316,159	120,309	120,309	272,964	272,963	272,963
Enthalpy @ Ts	BTU/lb	34,9874	90,7708	93,1295	329,021	626,882	372,552	375,322	302,803	300,459	116,805	115,262	257,888	209,626	80,8778
Entropy Function @ T		1,09795	2,10947	2,10947	4,49744	6,45632	5,08047	5,04497	4,41927	4,41927	2,31245	2,31245	4,03772	4,03772	4,03772
Entropy Function @ Ts		0,840239	1,86833	1,90587	4,49077	6,43045	4,86326	4,88319	4,30687	4,28682	2,26254	2,24033	3,89819	3,4151	1,7105
Exergy	BTU/lb	82,6541	138,827	138,558	365,869	603,951	371,075	366,859	283,766	283,226	152,235	151,557	251,186	251,186	251,186
Gas Constant	BTU/(lb*R)	0,068607	0,068607	0,068607	0,068607	0,068606	0,068606	0,068606	0,068606	0,068606	0,068607	0,068607	0,068606	0,068606	0,068606
Fuel-Air-Ratio		0	0	0	0	0,016914	0,016567	0,016289	0,016234	0,016234	0	0	0,012808	0,012808	0,012808
Water-Air-Ratio		0	0	0	0	0	0	0	0	0	0	0	0	0	0
Inner Radius	in	7,21854	15,7736	16,7917	11,927	12,8238	12,5032	12,5032	7,50193	0	21,5867	19,57	0	0	0
Outer Radius	in	24,0618	21,0437	17,9862	17,2451	16,3483	17,8515	18,4451	21,1696	19,35	23,5758	21,4708	20,8358	17,8702	25,2723
Axial Position	in	12,0309	12,0309	46,103	88,8572	106,435	112,309	112,321	135,495	156,664	37,527	156,664	165,682	180,267	223,156

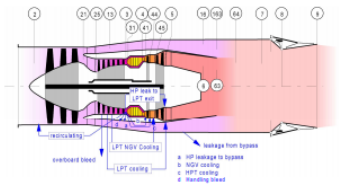

Figure C.4: HECTOR Engine GasTurb General Output

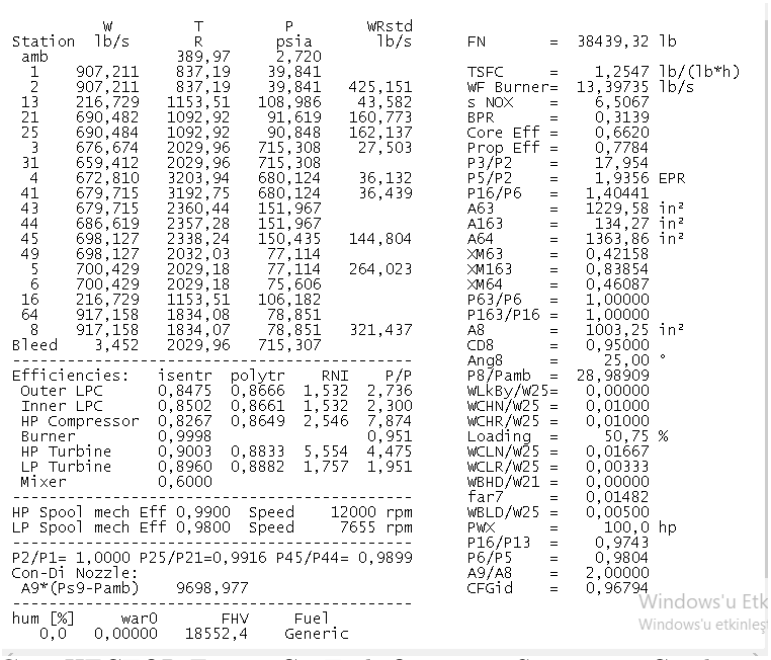

```
          W         T         P        WRstd
Station  lb/s       R        psia       lb/s
 amb                389,97    2,720
  1     907,211     837,19    39,841
  2     907,211     837,19    39,841   425,151
 13     216,729    1153,51   108,986    43,582
 21     690,482    1092,92    91,619   160,773
 25     690,484    1092,92    90,848   162,137
  3     676,674    2029,96   715,308    27,503
 31     659,412    2029,96   715,308
  4     672,810    3203,94   680,124    36,132
 41     679,715    3192,75   680,124    36,439
 43     679,715    2360,44   151,967
 44     686,619    2357,28   151,967
 45     698,127    2338,24   150,435   144,804
 49     698,127    2032,03    77,114
  5     700,429    2029,18    77,114   264,023
  6     700,429    2029,18    75,606
 16     216,729    1153,51   106,182
 64     917,158    1834,08    78,851
  8     917,158    1834,07    78,851   321,437
Bleed    3,452    2029,96   715,307
-----------------------------------------------
Efficiencies:   isentr  polytr    RNI    P/P
 Outer LPC      0,8475  0,8666  1,532  2,736
 Inner LPC      0,8502  0,8661  1,532  2,300
 HP Compressor  0,8267  0,8649  2,546  7,874
 Burner         0,9998                 0,951
 HP Turbine     0,9003  0,8833  5,554  4,475
 LP Turbine     0,8960  0,8882  1,757  1,951
 Mixer          0,6000
-----------------------------------------------
HP Spool mech Eff 0,9900  Speed    12000 rpm
LP Spool mech Eff 0,9800  Speed     7655 rpm
-----------------------------------------------
P2/P1= 1,0000 P25/P21=0,9916 P45/P44= 0,9899
Con-Di Nozzle:
 A9*(Ps9-Pamb)    9698,977
-----------------------------------------------
hum [%]     war0       FHV      Fuel
   0,0   0,00000   18552,4    Generic

FN       =  38439,32 lb

TSFC     =    1,2547 lb/(lb*h)
WF Burner=  13,39735 lb/s
s NOX    =    6,5067
BPR      =    0,3139
Core Eff =    0,6620
Prop Eff =    0,7784
P3/P2    =   17,954
P5/P2    =    1,9356 EPR
P16/P6   =   1,40441
A63      =   1229,58 in²
A163     =    134,27 in²
A64      =   1363,86 in²
XM63     =   0,42158
XM163    =   0,83854
XM64     =   0,46087
P63/P6   =   1,00000
P163/P16 =   1,00000
A8       =   1003,25 in²
CD8      =   0,95000
Ang8     =     25,00 °
P8/Pamb  =  28,98909
WLkBy/W25=   0,00000
WCHN/W25 =   0,01000
WCHR/W25 =   0,01000
Loading  =     50,75 %
WCLN/W25 =   0,01667
WCLR/W25 =   0,00333
WBHD/W21 =   0,00000
far7     =   0,01482
WBLD/W25 =   0,00500
PWX      =     100,0 hp
P16/P13  =    0,9743
P6/P5    =    0,9804
A9/A8    =   2,00000
CFGid    =   0,96794
```


Figure C.5: HECTOR Engine GasTurb Output at Supersonic Condition- Mach 3

Appendix D: Detailed Design Output of Turbomachinery by AXSTREAM and GasTurb

Appendix D1: LPC

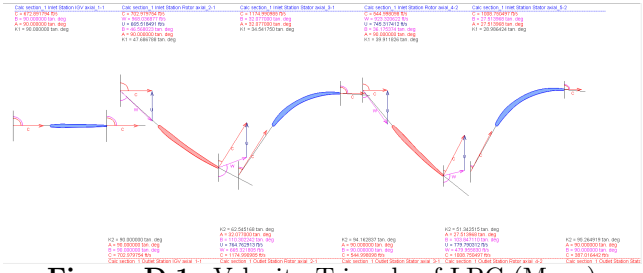

Figure D.1: Velocity Triangle of LPC (Mean)

Table D.1: Velocity Triangle Properties of LPC

	IGV Inlet	Rotor1 Inlet	Rotor1 Exit	Rotor2 Inlet	Rotor2 Exit
C (ft/s)	672.89	702.97	1174.99	544.99	1008.75
W (ft/s)	/	968.03	665.32	923.32	479.95
U (ft/s)	/	665.51	764.76	745.31	779.79
B (tandeg)	90.0	46.5	110.3	36.1	103.8
A (tandeg)	90.0	90.0	32.0	90.0	27.5
K (tandeg)	90.0	47.6	62.5	39.9	51.3

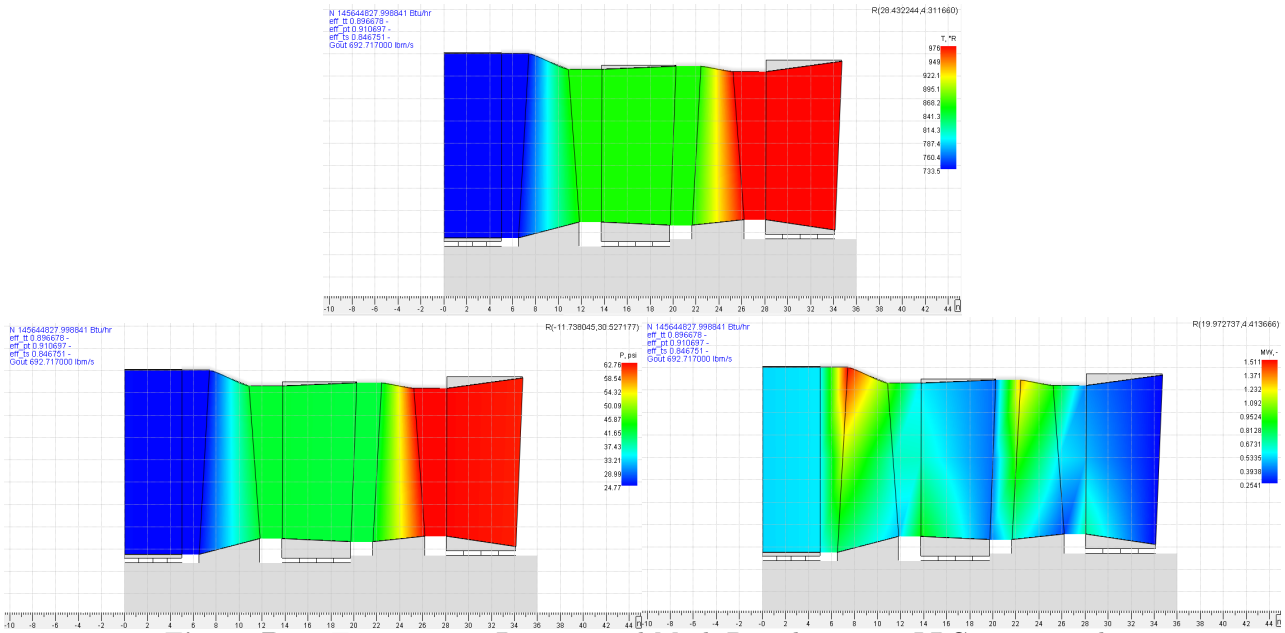

Figure D.2: Temperature, Pressure and Mach Distribution on LPC, respectively

Appendix D2: HPC

HPC Aero Design
Boundary Conditions

Cycle / Compressor Interface

		Cycle and Geometry Values
Pressure Ratio		8,57779
Number of Stages		7
Speed	RPM	12000
Length	in	41,5357
Inlet Area	in²	650,451
Inlet Pressure	psia	61,25
Inlet Temperature	R	973,428
Inlet Mass Flow	lb/s	538,619
Inlet Water-Air-Ratio		0
Exit Area	in²	481,717

Shape

		IGV	Stage 1	Stage 2	Stage 3	Stage 4	Stage 5	Stage 6	Stage 7
x Rotor Inlet	in		4,137	11,99	18,3	23,66	28,43	32,85	37,14
x Rotor Exit	in		7,734	14,73	20,52	25,55	30,11	34,44	38,74
x Stator Inlet	in	0	8,274	15,27	21,06	26,08	30,65	34,98	39,28
x Stator Exit	in	3,597	11,45	17,76	23,12	27,89	32,31	36,6	41
rm Rotor Inlet	in		14,83	14,82	14,8	14,78	14,75	14,73	14,7
rm Rotor Exit	in		14,83	14,81	14,79	14,77	14,74	14,72	14,69
rm Stator Inlet	in	14,83	14,83	14,81	14,79	14,76	14,74	14,71	14,68
rm Stator Exit	in	14,83	14,82	14,8	14,78	14,75	14,73	14,7	14,67

Figure D.3: HPC Aero Design- Boundary Conditions

HPC Aero Design
Output

Compressor Interface

		Mean Line Analysis Results	Cycle and Geometry Values
Pressure Ratio		8,5778	8,57779
Polytropic Efficiency		0,917162	0,9
Isentropic Efficiency		0,892039	0,869773
Exit Inner Radius	in	13,9779	13,9779
Exit Outer Radius	in	15,3372	15,3372

Stage Output

Stages		Stage 1	Stage 2	Stage 3	Stage 4	Stage 5	Stage 6	Stage 7
Pressure Ratio		1,492	1,449	1,395	1,351	1,315	1,301	1,236
Calculated Reaction		0,834	0,5	0,5	0,5	0,5	0,5	0,5
Calculated Flow Coefficient		0,569	0,6	0,6	0,6	0,6	0,6	0,6
Calculated Loading		0,331	0,331	0,331	0,331	0,331	0,331	0,331
Specific Work	hp/(lb/s)	45,154	45,093	44,968	44,821	44,666	44,507	38,911
Rel. Specific Work [%]		14,655	14,635	14,594	14,547	14,496	14,445	12,629
Polytropic Efficiency		0,8906	0,9290	0,9244	0,9175	0,9086	0,9469	0,9292
Isentropic Efficiency		0,8845	0,9253	0,9210	0,9142	0,9054	0,9451	0,9274
Rotor Tip Speed	ft/s	1883,52	1808,45	1746,42	1702,04	1669,12	1644,02	1622,41
Rotor Tip Mach Number		1,4135	1,35692	1,24947	1,16677	1,101	1,04679	0,988893

Figure D.4: HPC Aero Design- Stage Output

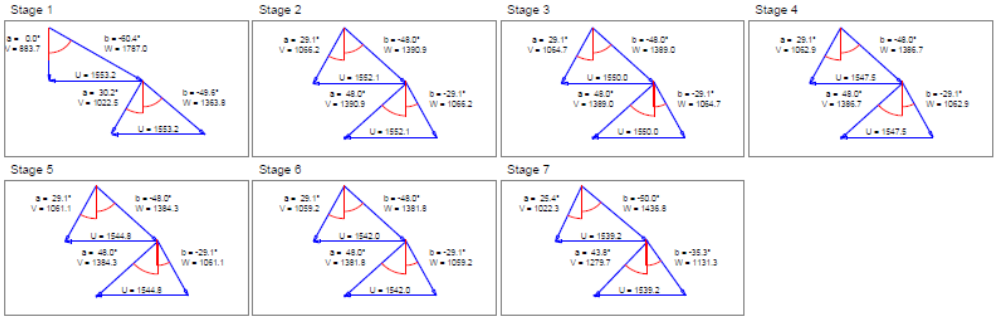

Figure D.5: Velocity Triangles of HPC (Mean)

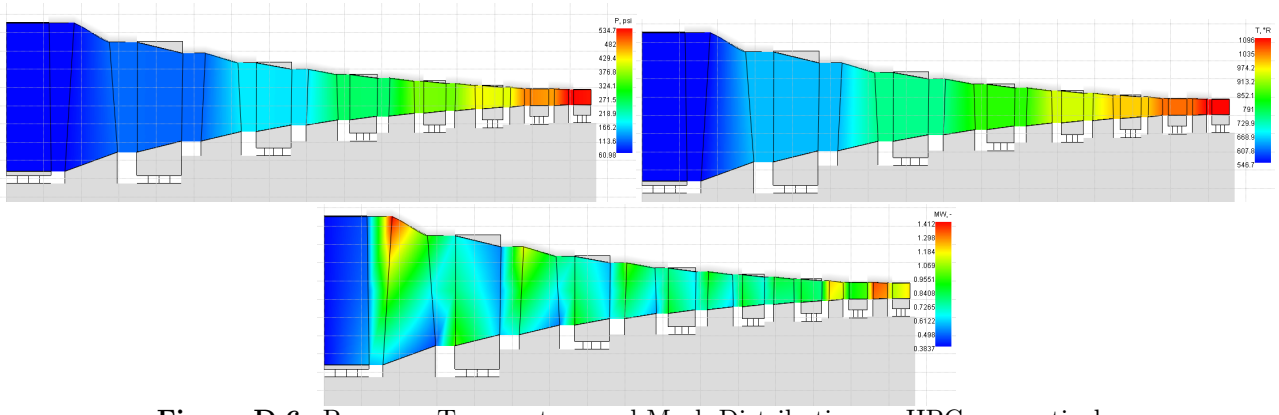

Figure D.6: Pressure, Temperature and Mach Distribution on HPC, respectively

Appendix D3: HPT

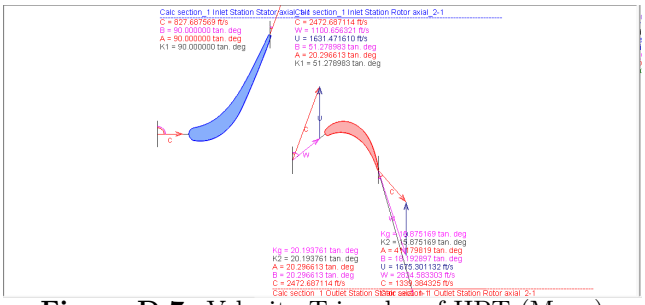

Figure D.7: Velocity Triangles of HPT (Mean)

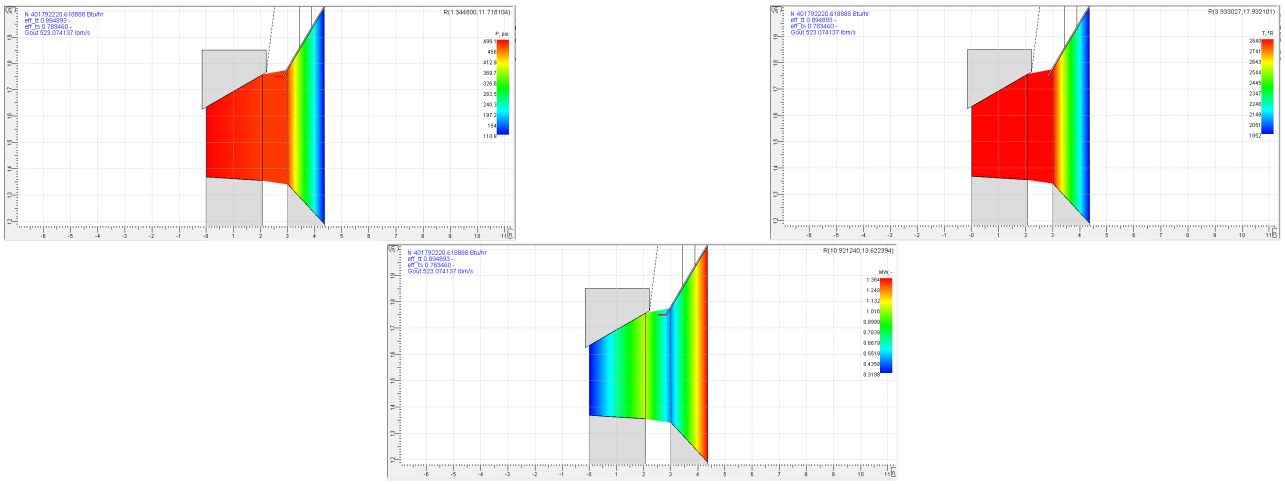

Figure D.8: Pressure, Temperature and Relative Mach Distribution on HPT, respectively

Appendix D4: LPT

Table D.2: Velocity Triangle Properties of LPT

	Rotor1 Inlet	Rotor1 Exit	Rotor2 Inlet	Rotor2 Exit	Rotor 3 Inlet	Rotor 3 Exit
C (ft/s)	738.03	1094.78	792.11	1098.51	800.99	1172.39
W (ft/s)	1134.06	1811.20	1035.55	1746.52	1095.75	1781.37
U (ft/s)	862.29	835.56	803.62	779.21	748.95	724.85
B (tandeg)	139.4	23.3	130.9	25.7	133.0	25.8
A (tandeg)	90.0	40.8	80.9	43.7	90.0	41.4
K (tandeg)	139.4	23.3	130.9	25.7	133.0	25.8

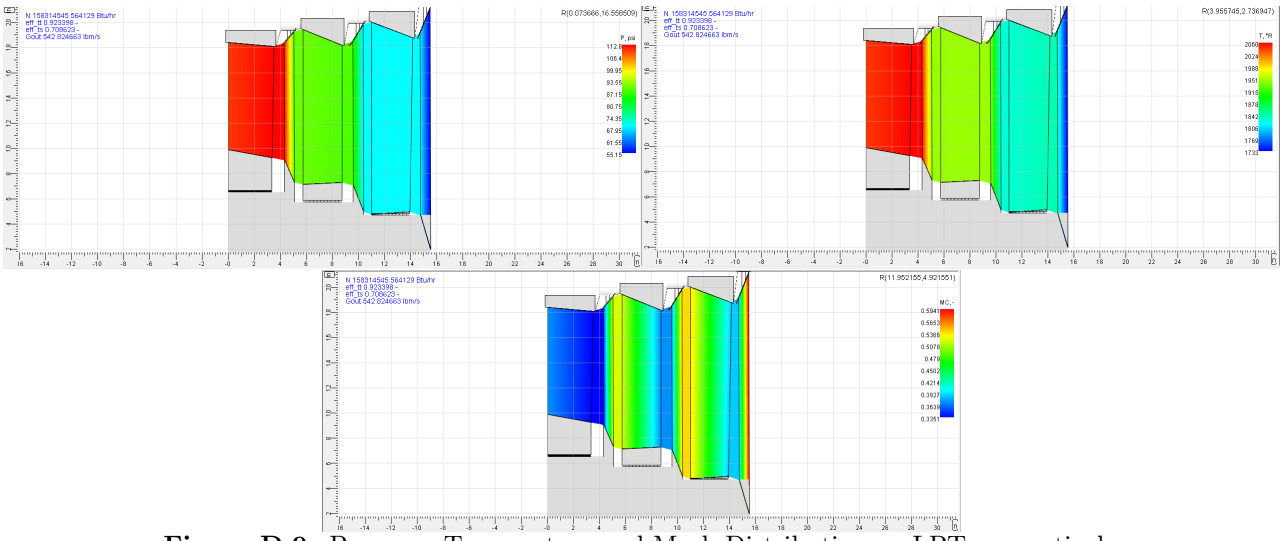

Figure D.9: Pressure, Temperature and Mach Distribution on LPT, respectively

Appendix E: Detailed 3D CAD Drawings by Autodesk Inventor Professional

Appendix E1: Intake Design

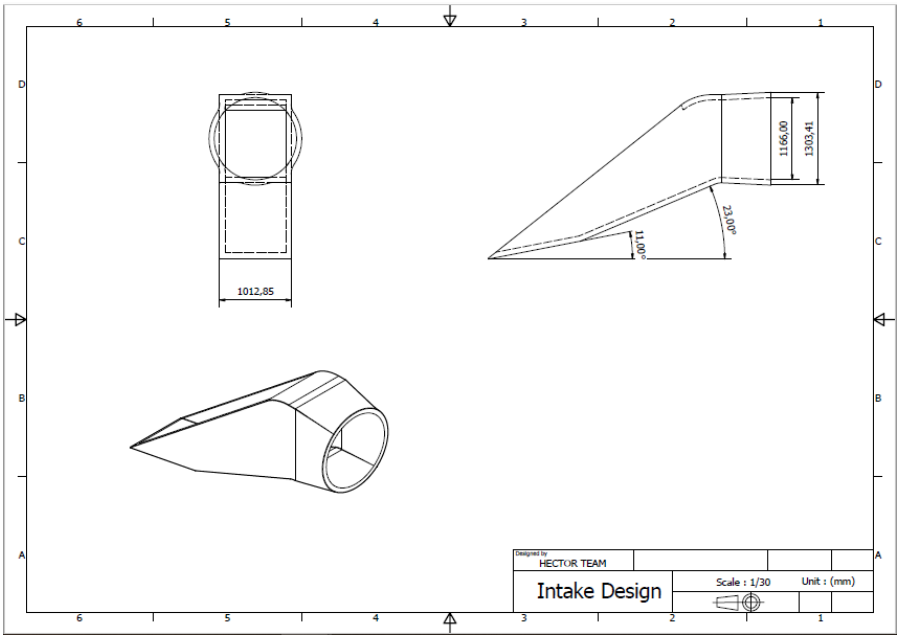

Appendix E2: Combustion Chamber Design

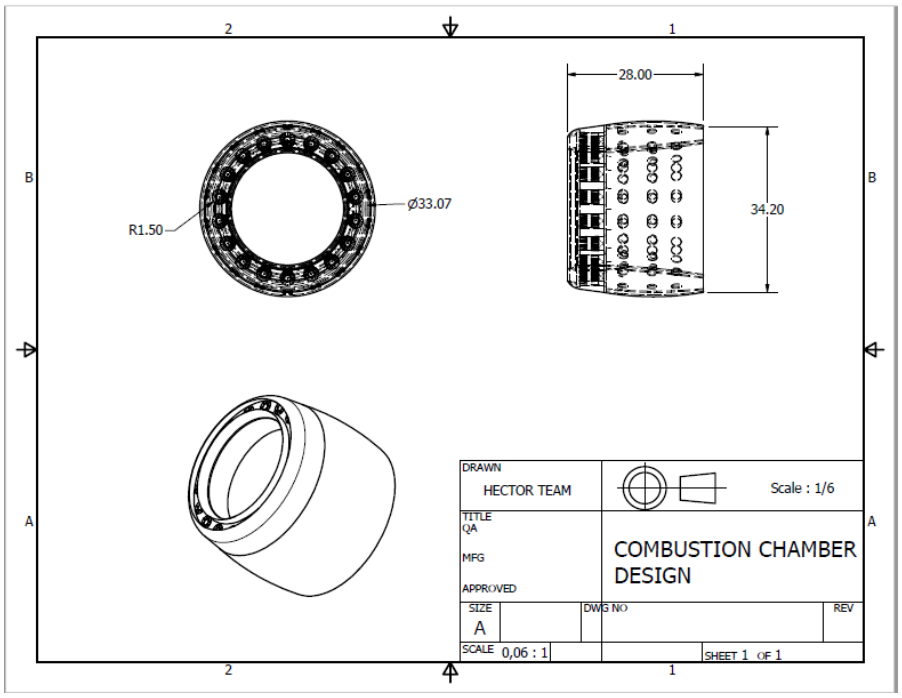

Appendix E3: Mixer Design

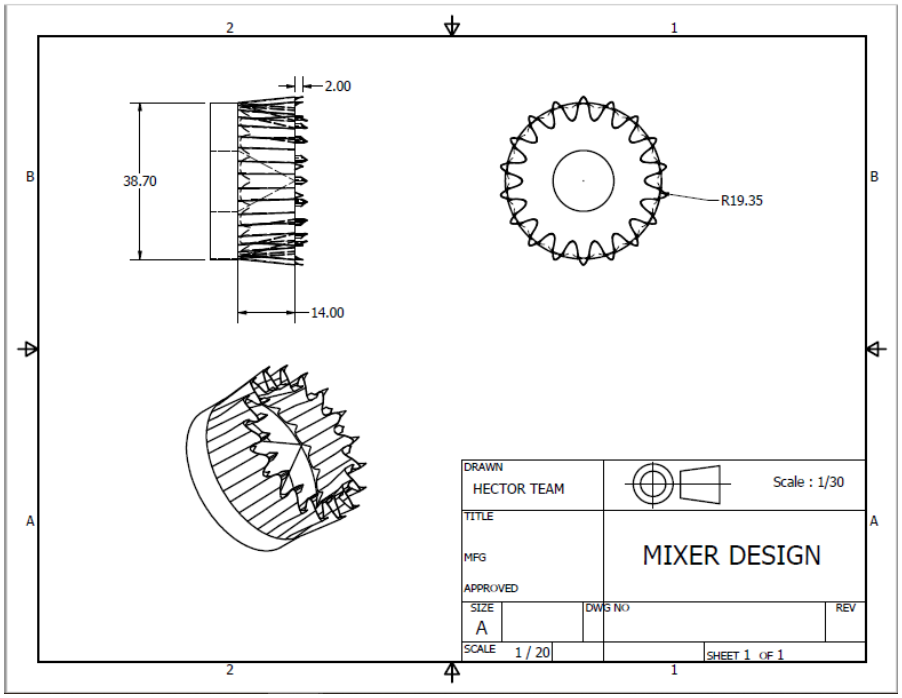

Appendix E4: Nozzle Design